The Thesis Committee for Evan Daniel Gilmore Certifies that this is the approved version of the following thesis:

Gravimetric Measurement of Spontaneous Imbibition of Water in Organic-Rich Shales

APPROVED BY
SUPERVISING COMMITTEE:

Supervisor:

Mukul M. Sharma

Martin E. Chenevert

Gravimetric Measurement of Spontaneous Imbibition of Water in Organic-Rich Shales

by

Evan Daniel Gilmore, BSME

Thesis

Presented to the Faculty of the Graduate School of

The University of Texas at Austin

in Partial Fulfillment

of the Requirements

for the Degree of

Master of Science in Engineering

The University of Texas at Austin

December 2013

Dedication

To my teachers and loved ones.

Acknowledgements

I am very grateful to the research sponsors that financially supported this research.

I would like to express my sincere gratitude towards Dr. Mukul Sharma and Dr. Martin Chenevert for the essential support and guidance provided in this project. I would also like to thank JP Gips, Rod Russell, Junhao Zhou, Changmin Jung and Weiwei Wu for their guidance and support in my experiments. I would also like to thank Jin Lee and Frankie Hart for the administrative support that helped me keep organized and improved my experience in the department.

Abstract

Gravimetric Measurement of Spontaneous Imbibition of Water in Organic-Rich Shales

Evan Daniel Gilmore, M.S.E.

The University of Texas at Austin, 2013

Supervisor: Mukul M. Sharma

Organic-rich shales in the last decade have become a focus of the oil and gas industry, and currently are the primary source of oil and gas production from Unconventional resources. These resources will be in need of a method of enhanced recovery to maximize lifetime production from each well. Spontaneous imbibition, or the adsorption of a fluid into a porous media due to capillary forces and consequent displacement of non-wetting fluids is a good potential enhanced recovery method. Measuring the amount of spontaneous imbibition in an organic-rich shale is complicated by several challenges compared to traditional oil reservoir rocks, such as the ultra-low permeability and the high clay content. This clay content can often lead to swelling, which can affect imbibition measurements.

In this study, a new gravimetric method for measuring spontaneous imbibition is developed that can measure the rate, and volume of spontaneous imbibition as well as the degree of shale swelling. Two organic-rich shales, the Bakken and the Utica were examined and compared to establish the viability of the experimental method. The results of this work suggest that this method is a promising and viable method for measuring the volume and rate of spontaneous imbibition in organic-rich shale.

The exposure of organic-rich shales to atmospheric conditions can significantly modify the properties of the shale through drying or hydration of the samples. All of the shales used in experiments in the following study were carefully maintained at their native state before exposure to the imbibition fluids. Additionally, the shale samples were exposed to several surfactant mixtures to measure the effect of these surfactants on the rate of imbibition.

Table of Contents

List of Tables xii

List of Figures xiv

Chapter 1: Introduction 1

1.1 Unconventional Hydrocarbon Resources 1

1.3 Shale 3

1.3 Motivation for Imbibition Study 7

1.4 Scope 10

1.5 Review of Chapters 12

Chapter 2: Background and Literature Review 13

2.1 Introduction 13

2.2 Organic Rich Shale Background and Physical Properties 13

2.2.1 Mineralogy of Resource Shale 16

2.2.2 Native Shale Water Activity and Swelling 24

2.2.3 Porosity, Permeability and Saturation 26

2.3 Wettability 35

2.3.1 Spontaneous Imbibition 38

2.3.2 Spontaneous Imbibition in Shale and Archimedes Method..... 42

Chapter 3 – Experimental Design and Procedure 45

3.1 Experimental Setup: 45

3.11 Measurement module 46

3.1.2 Imbibition assembly 48

3.2 Experimental Setup Preparation 50

3.2.1 Shale sample preparation 50

3.2.2 Measurement module preparation 54

3.2.3 Imbibition vessel preparation 55

3.2.4 Imbibition fluid preparation 55

3.3 Experimental Measurement Procedure 57

3.3.1 Primary fluid measurements 57

3.3.2 Routine Experimental procedure 58

Chapter 4: Theory 60

4.1 Theory 60

4.2 Initial sample and fluid measurements 60

4.3 Imbibition sample weight measurements 62

4.4 Volume of Imbibition calculated from fluid measurements 66

Chapter 5: Results and Discussion 70

5.1 Evaluation of Theory 71

5.1.1 Initial sample and fluid measurements 71

5.1.2 Comparing Air and Fluid Measurements 72

5.1.3 Examining Volume Change 78

5.1.4 Volume of Fluid Adhering to Surface of sample: Archimedes Air Weight 79

5.2 Metrics for Evaluation of Assumptions, and Measurement Precision ... 85

5.2.1 Air Weight Measurement Precision and Variance of Adhered Fluid Film 85

5.2.2 Fluid Weight Precision and Volume Change of Sample 91

5.2.4 Spontaneous Imbibition: Volume of Displaced Pore Fluid 95

5.3 Analysis of Experimental Results 100

5.3.1 Bakken Shale Spontaneous Imbibition Experiments 101

5.3.1.1 Bakken Experiment 1 102

5.3.1.2 Bakken Experiment 2 113

5.3.2 Utica Spontaneous Imbibition Experiment 121

Chapter 6: Conclusions and Future Work 130

6.1 Conclusions 130

6.2 Future Work 136

Appendix 138

A.1 Measured Air and Fluid Weights 138

Glossary 144

References 148

List of Tables

Table 2.1: Mineralogical Analysis of hydrocarbon bearing Shale formations (Carman 2010). 18

Table 2.2: Surface area of common clay minerals (and fine grain sandstone) (Passey, 2010) 22

Table 2.3: Super saturated Salt Solutions and Corresponding Water Activities (Winston, 1960). 25

Table 2.4: Relationship between contact angle and wettability (Anderson 1986b) 36

Table 5.1: Initial sample and Fluid 2 measurements of example Bakken shale sample. 72

Table 5.2: Average values of weight and volume of fluid adhering to surface of the example Bakken sample during air weight measurements. 83

Table 5.3: Individual effects of different types of error upon coupled error analysis figures. 94

Table 5.4: Surfactant designations and formulations. 101

Table 5.5: Produced Bakken brine fluid properties, 7.2 pH. 102

Table 5.6: Bakken experiment 1— Shale sample and fluid properties. 103

Table 5.7: Bakken experiment 1—Estimated amounts and error of fluid adhering to surface of shale sample during air weight measurements. 109

Table 5.8: Bakken Experiment 2—Shale sample and fluid properties. 113

Table 5.9: Bakken Experiment 2— Estimated amounts and error of fluid adhering to surface of shale sample during air weight measurements 114

Table 5.10: Utica experiment— Utica Brine (6.07 pH)..... 121
Table 5.11: Utica experiment—Shale sample and fluid properties. 122
Table 5.12: Utica experiment—Estimated amounts and error of fluid adhering to surface of shale sample during air weight measurements..... 124
Table A.1: Bakken Experiment 1 Measured Data: Imbibition Fluids A and B.138
Table A.2: Bakken Experiment 1 Measured Data: Imbibition Fluids C and Brine. 139
Table A.3: Bakken Experiment 2 Measured Data: Imbibition Fluids A and B.140
Table A.4: Bakken Experiment 2 Measured Data: Imbibition Fluids C and Brine. 141
Table A.5: Utica Experiment Measured Data: Imbibition Fluids A and B..... 142
Table A.6: Utica Experiment Measured Data: Imbibition Fluids C and Brine.143

List of Figures

Figure 1.1: 1-2 meter Parasequences in Green River Shale Outcrop (Passey, 2010) 4

Figure 1.2: Ternary plot of classification for organic rich mudstones / shales containing five classifications of mudstones and the average composition of the shale resource plays currently in production (Allix et al, 2010). 6

Figure 2.1: Cross section of formations in Bakken (West et al., 2013) 14

Figure 2.2: Utica Shale Extent and TOC (Warner et al., 2013) 15

Figure 2.3: Compositional diagram for understanding resource shale mineralogy ternary diagrams (Loucks, 2012) 16

Figure 2.4: Mineralogy of the Barnett and Eagleford shale gas reservoirs (Passey, 2010) 17

Figure 2.5: Mineralogy of the Utica shale (after Harper, 2011 and Nyahay, 2011) 17

Figure 2.6: Change in cumulative composition as a function of depth measured by XRD of a single well. (after Sondergeld, 2010). 19

Figure 2.7: Crystal structure of smectite (after Passey, 2010) 20

Figure 2.8: Common clay minerals found in organic rich shales (Passey, 2010)21

Figure 2.9: Illustration of adsorbed clay surface and double-layer water on surface of clays, and schematics, and SEM images of kaolinite and smectite illustrating surface areas. (after Passey, 2010)..... 22

Figure 2.10: Change in yield strength due fluid exposure (Chenevert, 1970) 23

Figure 2.11: Shale samples stored in constant humidity desiccators (Jung, 2013)25
Figure 2.12: Water activity measurement of Eagleford Shale (Jung, 2013) 26
Figure 2.13: Plot of whole core helium porosity vs. GRI porosity (after Spears et al., 2011) 28
Figure 2.14: Relationship between preservation and measured porosity (after Passey, 2010) 30
Figure 2.15: Relationship between TOC (Total organic content weight %) and measured porosity (after Passey, 2010) 30
Figure 2.17: Schematic of organic rich and clay rich shale with water and hydrocarbons (Passey, 2010) 33
Figure 2.18: Contact angle and interfacial tension equilibrium in a water-oil-solid system (after Abdallah, 2007). 36
Figure 2.19: Pore scale distribution of fluid in porous media with different wetness (after Abdallah, 2007) 37
Figure 2.20: Pore scale visualization of oil displacement due to imbibition with inlet and outlet boundaries marked with dashed lines. (after Al-Menjeni, 2011). 39
Figure 3.1 - Gravimetric Spontaneous Imbibition Setup. 46
Figure 3.2 - Sartorius liquid density kit. 47
Figure 3.3 - Imbibition vessel covered and uncovered. 49
Figure 3.4 - Imbibition oven containing imbibition vessels 50
Figure 3.5- Knot tying jig 52
Figure 3.6 – Monofilament line with overhand loop on right and two half hitches on left 53

Figure 3.7 - Sample attached to monofilament line 54
Figure 5.1: Measured fluid and air weights of the example Bakken sample. 73
Figure 5.2: Change in measured air and fluid weights of the example Bakken sample. 74
Figure 5.2: Percent change in measured air and fluid weight of initial air weight of the example Bakken sample..... 75
Figure 5.3: Percent difference between change in measured air and fluid weights, , of the example Bakken sample. 77
Figure 5.4: Relative change of the volume of the example Bakken sample where.79
Figure 5.5: Measured air weights and Archimedes calculated air weight of the Bakken brine shale sample..... 81
Figure 5.6: Percent weight of adhered surface fluid film of example Bakken sample. 82
Figure 5.7: Change in Weight of Fluid Film Adhered to example Bakken Sample. 87
Figure 5.8: Variance of thickness of adhered thin fluid film relative of example Bakken sample. 88
Figure 5.9: Contour plot of percent Volume of pore volume of fluid film as function of thickness of film and length of 1-inch diameter by 1-inch long core plug. 90
Figure 5.10: Percent change of thin fluid film relative to pore volume of example Bakken sample. 93
Figure 5.11: Error in displaced pore volume due to variance in thickness of fluid film on the example Bakken sample..... 93

Figure 5.12: Volume of displaced pore fluid in the example Bakken sample. 96
Figure 5.13: Displaced pore fluid as percent of total pore volume of the example Bakken sample. 97
Figure 5.14: Displaced pore fluid as percent of total pore volume of the example Bakken sample in characteristic time. 98
Figure 5.15: Bakken Experiment 1—Change in measured air and fluid weight for Bakken shale samples A and brine. 105
Figure 5.16: Bakken Experiment 1—Change in measured air and fluid weight for Bakken shale samples B and C. 105
Figure 5.17: Bakken experiment 1— Variance in displaced pore volume between air and fluid measurements resulting from variance in thickness of fluid film and/or swelling from Equation 5.20. 107
Figure 5.18: Bakken experiment 1—Percent displaced pore fluid of total pore fluid of shale samples calculated only from air weight measurements. 110
Figure 5.19: Bakken experiment 1—Percent displaced pore fluid of total pore fluid of shale samples calculated only from air weight measurements in characteristic time. 110
Figure 5.20: Bakken experiment 1—Percent displaced pore fluid of total pore fluid of shale samples calculated only from fluid weight measurements.. 111
Figure 5.21: Bakken experiment 1—Percent displaced pore fluid of total pore fluid of shale samples calculated only from fluid weight measurements in characteristic time. 111
Figure 5.22: Bakken Experiment 2—Change in measured air and fluid weight for Bakken shale samples A and Brine..... 115

Figure 5.23: Bakken Experiment 2—Change in measured air and fluid weight for Bakken shale samples B and C. 116
Figure 5.24: Bakken Experiment 2— Variance in displaced pore volume between air and fluid measurements due to variance in thickness of fluid film and/or swelling from Equation 5.20. 116
Figure 5.25: Bakken Experiment 2—Percent displaced pore fluid of total pore fluid shale samples calculated only from air weight measurements. 118
Figure 5.26: Bakken Experiment 2—Percent displaced pore fluid of total pore fluid of shale samples calculated only from fluid weight measurements.118
Figure 5.27: Bakken Experiment 2—Percent displaced pore fluid of total pore fluid of shale samples calculated only from fluid weight measurements.119
Figure 5.28: Utica experiment—Change in measured air and fluid weight of Utica shale samples A and B. 123
Figure 5.29: Utica experiment—Change in measured air and fluid weight of Utica shale samples C and Brine. 124
Figure 5.30: Utica experiment —Variance in displaced pore volume between air and fluid measurements due to variance in thickness of fluid film and/or swelling from Equation 5.20. 126
Figure 5.31: Percent displaced pore fluid of total pore fluid of Utica experiment shale samples calculated only from fluid weight measurements. 127
Figure 5.32: Percent displaced pore fluid of total pore fluid of Utica experiment shale samples calculated only from air weight measurements. 128
Figure 5.33: Percent displaced pore fluid of total pore fluid of Utica experiment shale samples calculated only from air weight measurements. 128

Figure 6.1: Volume of adsorbed fluid of samples versus Increase in Bulk Volume. 131

Figure 6.2: Contour plot of relative weight of 0.05 mm thin fluid layer of density 1.0 g/cc adhered to surface of cylindrical shale sample with a bulk density of 2.65 g/cc. 132

Figure 6.3: Change in measured weight of sample as a function of pore volume and difference between saturation fluid density and imbibition fluid density. 133

Chapter 1: Introduction

1.1 Unconventional Hydrocarbon Resources

The global demand for energy is ever increasing and unconventional hydrocarbons resources once overlooked as technologically and economically infeasible are have become a staple of the oil and gas industry, and now are included in world oil and gas reserves calculations (NPC 2007). With the anticipation of world energy demand increasing by at least 33% by 2035, unconventional oil and gas resources such as shale will help fuel our ever increasing demand (OECD 2013).

Unconventional hydrocarbon resources are defined as resources that only produce oil and gas at profitable production rates and volumes after massive reservoir stimulation methods that increase and maximize contact between the surface area of a reservoir rock and the wellbore above traditional drilling and completion techniques (NPC 2007a). Such methods include: horizontal drilling, multilateral wellbores, and large-scale stimulation techniques such as multistage hydraulic fracturing (fracing).

Fracing is a well treatment technique originally developed in the 1950s (Flores 2011) and enhances the level of production of hydrocarbon bearing formations through increasing the surface area of the reservoir in contact with the wellbore. Fracing is accomplished by pumping fluids into a formation at pressures high enough to cause tensile failure within the rock. Once the initial fracture is opened, it is propagated through continuing to pump a fluid and often proppant, which causes growth of the fracture

(Economides). The proppant, often well-sorted sand or a stress resistant man-made spherical material, is added to the fluid mixture to hold open the fracture once the pressure at the surface is relieved and to create a high permeability pathway to the wellbore. In hydrocarbon bearing shale plays, fracing is combined with horizontal drilling and as many as 40 fracture treatments can be pumped per horizontal well. Horizontal drilling and hydraulic fracturing increase the area of contact by several orders of magnitude, enabling the economic production of unconventional resources including hydrocarbon bearing shale formations, as the reservoir matrix permeability is far too low otherwise (King 2010).

While this paper is mainly concerned with shale gas and oil-bearing shale (also referred to as tight oil reservoirs), the term unconventional reservoir can be used to describe hydrocarbon-bearing formations including but not limited to Shale Gas, Gas Hydrates Heavy Oil Sandstones, Oil Shale formations, and Tight-Gas Sandstones. It is worth noting that horizontal drilling and fracing expose the shale to large volumes of water, often ranging between 2 and 4 million gallons of water per well, which can have positive and negative effects upon the formation (Ground Water Protection Council, 2009). Unconventional resources such as tight oil, oil-bearing shale, and shale gas have now been in production closing in on a decade and as such that a form of increased oil recovery or enhanced oil recovery is desired to maximize the total production over the lifetime of the wells. Though shale oil typically refers to kerogen saturated shales, the term will be used in this paper in reference to tight oil plays such as the Bakken which

have fully matured and are producible. Shale oil will also be used interchangeably with organic rich oil shale, and resource shale.

1.3 SHALE

Shale by definition is "a fine-grained detrital sedimentary rock, formed by the compaction of clay, silt, or mud" (Bates 1984). Shale is also referred to as mudrocks or mudstones, and is composed of the sedimentation of tiny particles less than 4 microns in diameter. Occasionally shale may contain larger particles up, 62.5 microns or the size of silt (Bates 1984). Many different types minerals and organic particles can make up shale including but not limited to quartz, phosphate, carbonate, feldspar, clays and organic matter (Ruppel 2012).

Hydrocarbon bearing shale formations are often black to dark grey in color and are found the window for oil-generation. Resource shales can form if the organic rich mud deposited in a lake, a swamp, or marine environment then encounters the correct sequence of geologic events. In order to deposit enough organic material to form a organic rich shale, the depositional rate of minerals and organic content must remain at a specific ratio. The shale is formed once is exposed to a pressure and temperature due to burial and subsequent compaction (Passey, 2010).

Due to the very specific order of events that must occur over geologic time the hydrocarbon source rock formations often exhibit enormous stratigraphic heterogeneity, vertically over distances less than one meter even when the shale is hundreds of meters thick. The stratigraphic heterogeneity continues to vary horizontally over scales ranging

from a millimeter to hundreds of meters (Bohacs et al., 2005). It is important to recall that shale is deposited at a relatively slow rate even in geologic time, a single meter in a shale could take a one thousand years to a over one million years to be created depending upon the rate of deposition.

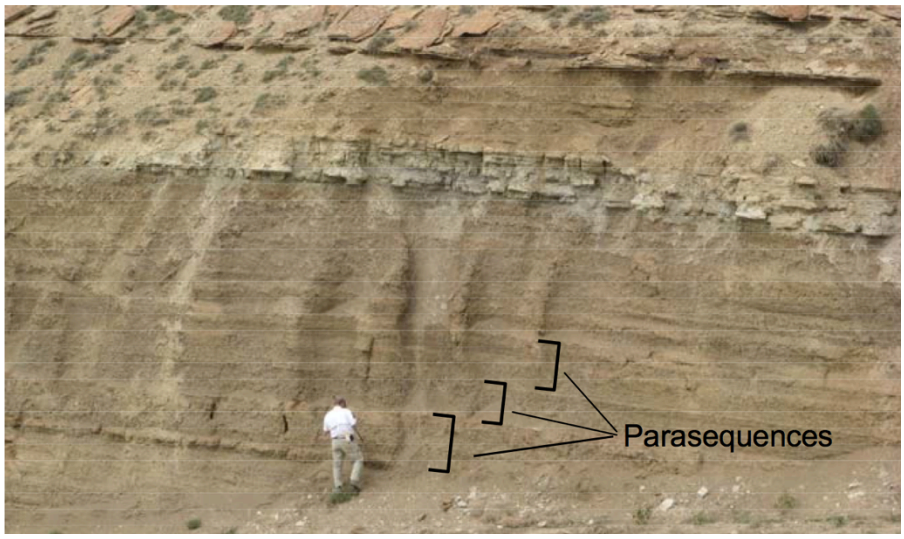

Figure 1.1: 1-2 meter Parasequences in Green River Shale Outcrop (Passey, 2010)

During this slow process of deposition significant compaction occurs, and transforms vast amounts of silt particles deposited over very long periods of time into just a few feet of rock. The depositional environment of the resource shale controls much of the heterogeneity, and even within a favorable environment the stratigraphic heterogeneity can still vary substantially. Despite both the frequent small-scale vertical heterogeneity and stratigraphic heterogeneity repeating patterns or parasequences develop

(seen in figure 1.1) which allows for geological characterization of the shale (Passey, 2010).

The resulting type of fossil fuel generated in the source rock formation is dependent upon the type of organic material deposited. The total organic richness is characterized by total organic carbon (TOC), the depth of burial, and its age or maturity level. As TOC is related saturation and porosity in shale oil and gas rocks, a high TOC is ideal for hydrocarbon production from shale with a cut off point around 2-3% (Gamero-Diaz, 2013; Agboada 2013).

The production of shale gas from resource shale dates back over 190 years, only became profitable through the use of hydraulic fracturing and horizontal drilling in the last decade. These technologies allow for the high gas flow rates required profitability, and have increased the amount of shale gas recovery from 2% to 50% (King 2010). To optimize shale gas and oil production, the shale reservoirs must be effectively characterized through an understanding of the geology, lithology, mineralogy, and petrophysical parameters. Petrophysical characterization techniques for shale are being developed at the University of Texas to optimize production and understanding of shale reservoirs.

All organic rich hydrocarbon shales consist of differing fraction of clays, and minerals. This relative concentration of the various minerals varies widely between formations as seen in figure 1.2. This variation is not unexpected expected as nearly every depositional environment of resource shale varies in some manner. However the

stratigraphic heterogeneity discussed previously, continues to be observable in the shale mineralogy. Resource shales vary widely in mineral and clay composition both internally and between different resource shales.

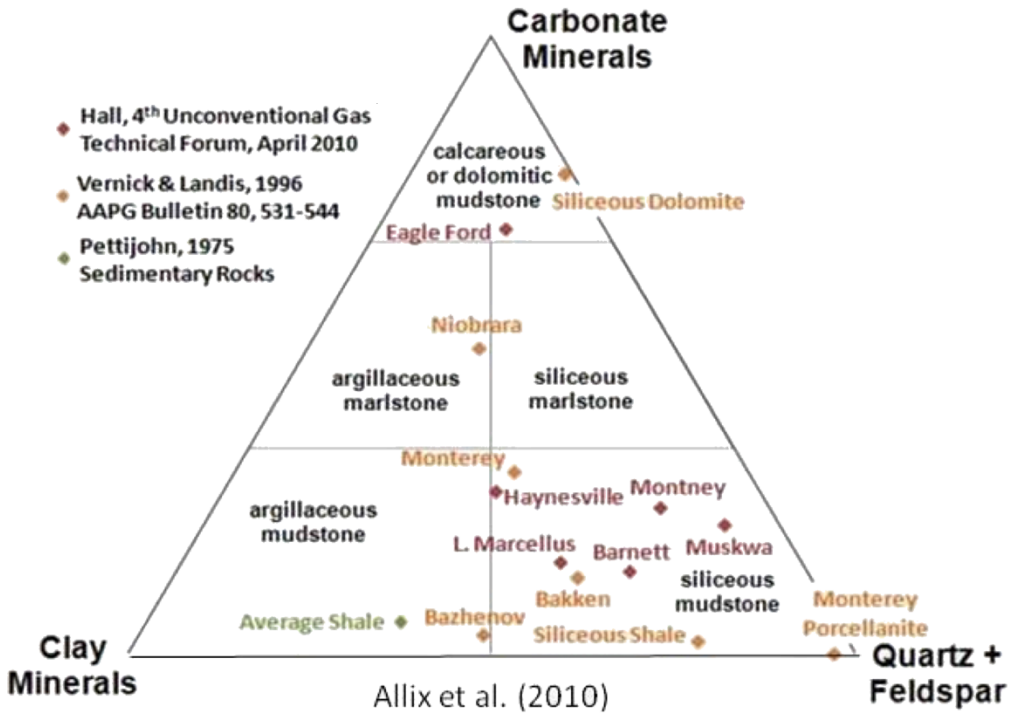

Figure 1.2: Ternary plot of classification for organic rich mudstones / shales containing five classifications of mudstones and the average composition of the shale resource plays currently in production (Allix et al, 2010).

The clays within the resource shale contain water molecules that are integral to the both clay's structure, and the overall structure organic rich shale itself. For this reason the method handling of shale samples is of utmost importance as the shale is highly sensitive to dehydration, and exposure to water based fluids (Sharma, 2004). After exposure to water based fluids, the shale softens and sometimes swells, and cannot return to its original hydration state once it is altered (Chenevert, 2001). For these reasons, any

petrophysical tests on shale must be preformed at its native state water activity (Jung et al, 2013, Chenevert, 1970). The techniques for shale sample handling and preservation will be discussed later at length.

1.3 Motivation for Imbibition Study

The focus of resource shale exploration and production has shifted from gas shale to oil bearing resource shales over the last 5 years (Birger, 2011). Over the next 30 years, the United States of America is projected to produce 38 billion barrels of oil from shale resource oil-bearing formations such as the Bakken (EIA, 2013b). The USGS has estimated that 7.4 billion barrels of undiscovered recoverable oil is in the Bakken shale formation alone (Gaswirth et al, 2013).

With such a large volume of oil in place and estimated production, there is a large incentive to enhance recovery above current levels, as even an increase in oil recovery as small as a half of a percent boost in total oil recovery would significantly increase the total production. Past estimated recovery factors for the Bakken have ranged from 0.7% to 50%, but the true recovery factor most likely lies between 9.2 and 16% (Dechongkit and Prasad, 2011). The variation of recovery factor is likely to be highly dependent upon the effectiveness of hydraulic fracturing treatment, and connection to natural fractures within the reservoir if present.

Traditionally, the recovery of oil and gas is broken up into three phases in conventional reservoirs: primary, secondary, and tertiary recovery. Primary recovery is the production of oil and gas using the internal reservoir forces such as the overburden

pressure, solution gas, or a natural water drive. The effectiveness of primary recovery depends upon reservoir architecture, geology, and fluid properties. Typical recovery for primary recovery factors range between 5 and 20% of original oil in place (OOIP). The values of oil recovery in the Bakken shale are reasonable recovery values for primary recovery for formations with overburden pressure and solution gas drive.

Waterflooding is the process of injecting fluids back into the reservoir to boost reservoir pressure once the differential pressure between the formation and the surface is no longer sufficient for production. Waterflooding is a proven and effective conventional secondary recovery (also referred to as increased oil recovery (IOR)) process that has been in use for decades. Waterflooding, and other forms of IOR, boost recovery factors up to 40-60% of OOIP by adding energy into the reservoir system to assist in production.

To recover oil in place, above secondary recovery, tertiary recovery techniques (also known as enhanced oil recovery (EOR)) must be applied to displace the oil that was left behind due to wettability conditions, natural fracture networks or hydrocarbons trapped through capillary forces.

EOR techniques can be broken into four major groups: chemical EOR, thermal EOR, gas EOR and other EOR methods that don't fall within the previously listed categories. Each type of EOR has advantages and disadvantages, and must be paired appropriately with the reservoir conditions, fluid and rock properties to achieve maximum oil recovery from a formation.

IOR and EOR have not yet been widely applied to tight oil shale systems. Traditional waterflooding techniques would not be an ideal for all tight shale oil formations as the permeability of organic-rich shale ranges between 100 nD and 30 mD (King, 2010, Wang 2012), and could require very large pressures would be required to create the water drive. Additionally, the highly fluid sensitive nature of some shales make traditional waterflooding an even poorer choice as the fluid sensitivity of these organic rich shales would most likely lead to significant problems with injection. Many organic-rich shale reservoirs contain significant amounts of natural fractures. In the case of highly fractured reservoirs, the injected fluid can bypass the matrix and travel through natural fracture networks if the wells are interconnected.

Large-scale production of unconventional tight shale oil plays such as the Bakken began in the early 2000s with the Bakken boom beginning in 2006 (Clark, 2009). As a result, some wells are over 7 years old and have reached very low levels of productivity compared to new wells. In the South Antelope Field, the first year decline alone is 83% with a 6% terminal decline. Over a 7 year time period the production in the South Antelope Field drops to 11.7% of its original value (West, 2013). While Cressent Point Energy is currently preforming a selective waterflood field test in the Bakken of conclusive results have yet to be found (Wood and Milne, 2001). Cressent Point Energy only provided limited production about the waterflood which makes it nearly impossible to make any meaningful conclusions.

The ground is primed for a novel method for the increase in oil production in tight oil organic shale formations. In tight oil reservoirs, spontaneous imbibition and wettability modification can be an effective chemical EOR treatment. This form of EOR is particularly effective in fractured reservoirs. Spontaneous imbibition at it is most basic level is the diffusion and displacement of one fluid by another in a porous medium and is a function of capillary pressure. Wettability can be best described as a bulk description of the intermolecular interactions between the interfacial tension between two liquid phases or a solid and a liquid phase. The wetting fluid will spread out on the solid surface in the presence of other immiscible fluids. The interactions between the adhesive and surface forces described by wettability can be modified through the use of surfactants and can aid in imbibition through modification of the interfacial tension (Peters, 2009). Wettability modification and the subsequent countercurrent spontaneous imbibition into a formation can provide an effective displacement of oil as the wettability modification changes the capillary pressure within the formation from negative to positive.

1.4 SCOPE

The goal of this paper is to establish a method for measuring spontaneous imbibition in organic rich shale samples, specifically Bakken and Utica Shale. When measuring spontaneous imbibition in organic rich shale, the fluid sensitivity of the shale introduces a number of complicating factors to the experimental measurement as the sample may swell. To gather a full understanding of the physical phenomena when a

preserved shale sample undergoes spontaneous imbibition, a novel technique was required that allowed for the measurement weight change and swelling.

As preserved organic rich shale samples are quite expensive and finite in quantity, an experimental technique that required the minimum amount of shale was ideal to maximize the amount of characterization that can be preformed. As the volume sample of sample is reduced, the physical volumes of imbibition can become quite small due to the often-small values of effective pore space for resource plays.

Laboratory measured porosities for organic rich mudstones typically range between 2% and 15%. An experimental technique was required with high resolution capable of measuring than with more accurately than traditional imbibition cells provided was desired as the volume of imbibition may have not been recordable with preserved samples. The pore space for a 1-inch by 1-inch diameter core plug with a 2% porosity (low end of the measured range) is for a then the pore space of the sample, and the maximum volume imbibition is 0.26 mL, which is well below the normal measurement range for traditional imbibition cells.

The motivation for the following paper was to establish and evaluate a procedure for Gravimetric Spontaneous Imbibition for preserved shale samples using Archimedes principle. While using Archimedes principal to measure the relative weight change in a porous media is not a novel concept, it has not yet been applied to shale in the attempt to measure both the volume of fluid displaced due to spontaneous imbibition to the relative increase in volume of the shale sample due to swelling. The surfactant formulations and

concentrations used in the following paper are not part of the scope of this experimental investigation, as the research sponsor provided the formulation and concentrations of the surfactants. The primary objective of this thesis was to evaluate the use of a gravimetric method for measuring both the rate and magnitude of spontaneous imbibition and swelling due to fluid exposure.

1.5 Review of Chapters

Chapter Two of this thesis contains a background and literature review of shale petrophysical properties, wettability and imbibition..

Chapter Three covers the experimental setup and all experimental procedures followed used in the gravimetric spontaneous imbibition experiments.

Chapter Four presents the fundamental equations behind the gravimetric spontaneous imbibition.

Chapter Five presents a number of metrics upon which to examine if the results of a shale results of the experiment are valid and examines the results of the measurement of gravimetric imbibition.

Chapter Six presents a summary of results and primary conclusions based upon the research and suggestions for future work to expand upon this research.

Chapter 2: Background and Literature Review

2.1 Introduction

Both general petrophysical properties and the petrophysical properties specific to organic rich shale must be understood before an appreciation of the experimental setup and design of gravimetric spontaneous imbibition can be had. In the following chapter the following properties of shale will be examined: geological background, mineralogy, native shale water activity, are discussed in the following section as well as previous work on the subject. Additionally an overview of the concept of wettability and its measurement, spontaneous imbibition, and the properties that affect spontaneous imbibition will be covered and the previous work of these concepts with a focus on imbibition in shale will be briefly reviewed.

2.2 Organic Rich Shale Background and Physical Properties

Two organic rich shale formations were examined in this paper, the Bakken and the Utica. The geologic background, the mineralogy shown in table 2.1 and are both quite different from each other, though both the Utica and Bakken are organic-rich shale formations.

The Devonian and Mississippian Bakken cover an area of 24,600,000 acres and are located in the Williston Basin of North Dakota and Montana. The current estimate of technically recoverable hydrocarbons in the Bakken are 7.383 billion barrels of oil, 6,726 billion cubic feet of gas and 527 million barrels of natural gas liquids (Gaswirth, 2013).

Though the Bakken shale formation is commonly referred to as a single unit, it consists of four separate members: the Pronghorn Member, the lower Bakken member, middle Bakken member, the upper Bakken member. The Bakken formation has bottom hole temperatures ranging between 90 and 120 degrees centigrade with relatively high salinity that ranges from 150 to 300 g/L (Wang et al., 2012).

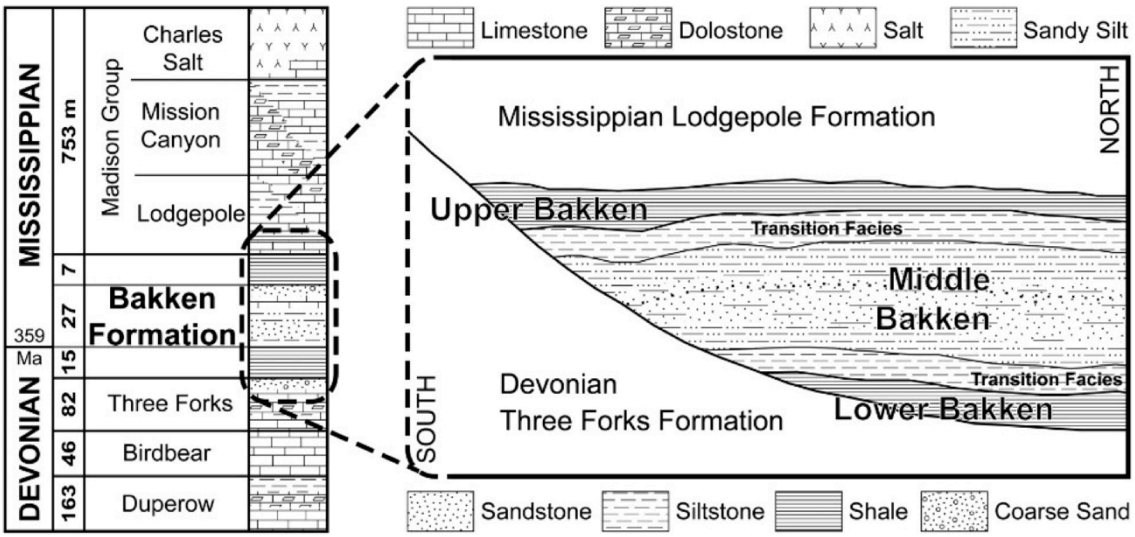

Figure 2.1: Cross section of formations in Bakken (West et al., 2013)

The Ordovian Utica is a black organic rich shale formation that found at depths that spans the hydrocarbon maturation window covering a geographic area of 46,600,000 acres ranging from western Pennsylvania to eastern Ohio (Kischbaum et al, 2012). The Utica lies atop the Point Pleasant formation, which is an interbedded limestone and calcareous shale. The Utica has a significant amount of organic content, while in other areas the Point Pleasant formation is the better target formation due to its higher organic content and porosity (Warner et al., 2013).

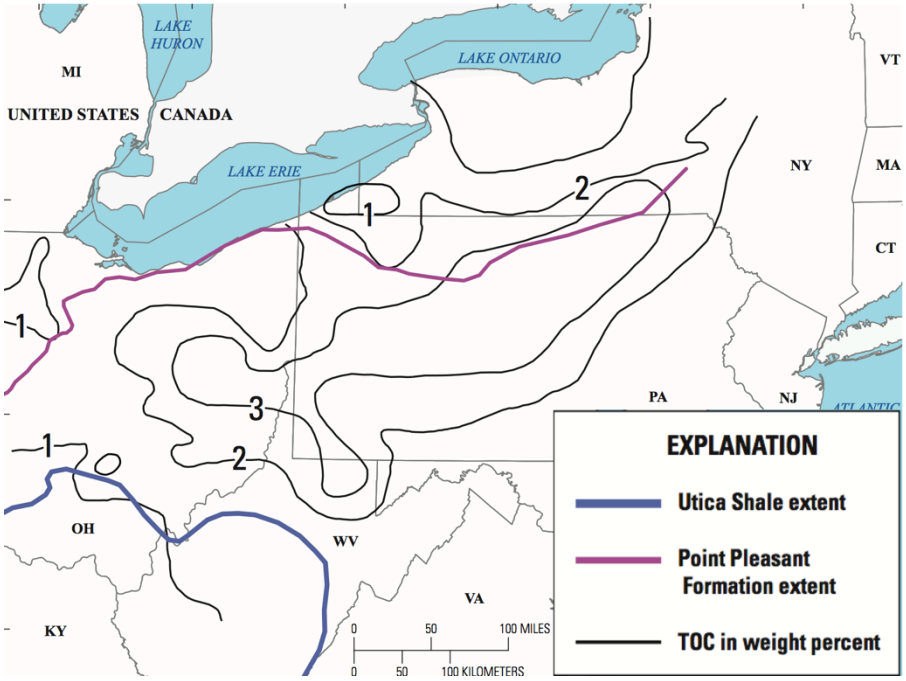

Figure 2.2: Utica Shale Extent and TOC (Warner et al., 2013)

However the Utica, was the focus of the experimental investigation in this paper. The Utica shale is the primary source rock in the petroleum system with a TOC commonly higher than 1% with selected a oil "sweet spot" with a higher TOC of 2-3% seen above in figure 2.2. The Utica is up to 700 feet thick in some areas and 150-350 feet thick on averages. Though limited production data exists for the Utica, the USGS has estimated that there are 940 million barrels of oil, 38.2 trillion cubic feet of gas and 208 million barrels of natural gas liquids technically recoverable. The oil window of the Utica Shale is only 15,000,000 acres and sweet spot for production (Warner et al., 2013).

2.2.1 Mineralogy of Resource Shale

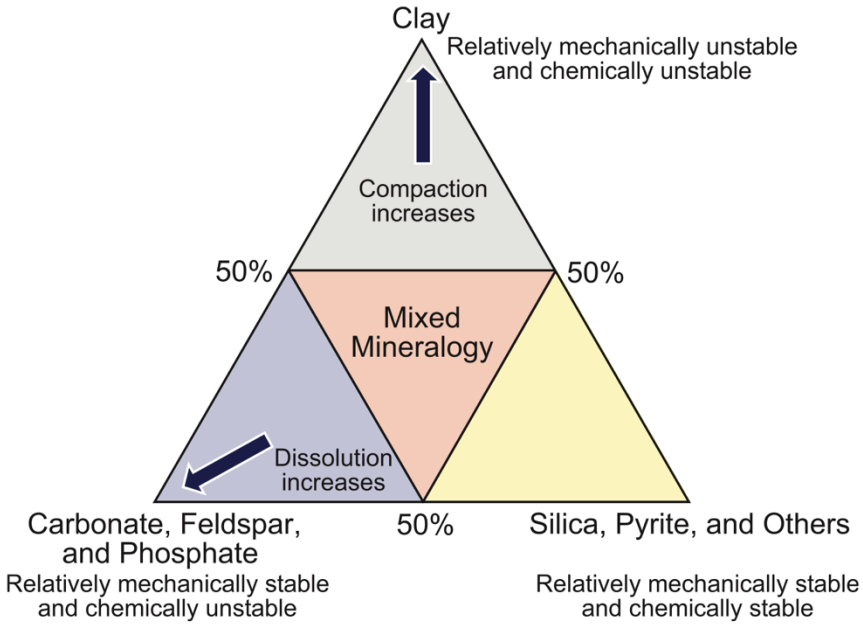

Figure 2.3: Compositional diagram for understanding resource shale mineralogy ternary diagrams (Loucks, 2012)

As previously mentioned, the mineralogy of organic-rich shale spans a wide range between types resource shales (figure 1.1 and table 2.1), and within the same formation (figure 2.4 and figure 2.5). The classical definition of shale is "A laminated, indurated rock with greater than 67% clay-sized minerals" (Neuendorf, 2005); however, productive hydrocarbon bearing resource shales are often greater than 50% carbonate or quartz by weight and less than 50% clay by weight. Resource shales are more brittle and respond better to hydraulic fracturing and other current well stimulation techniques, a guid to understanding the ternary mineral plots can be found in figure 2.3 (Gamero-Diaz, 2013 and Passey, 2010).

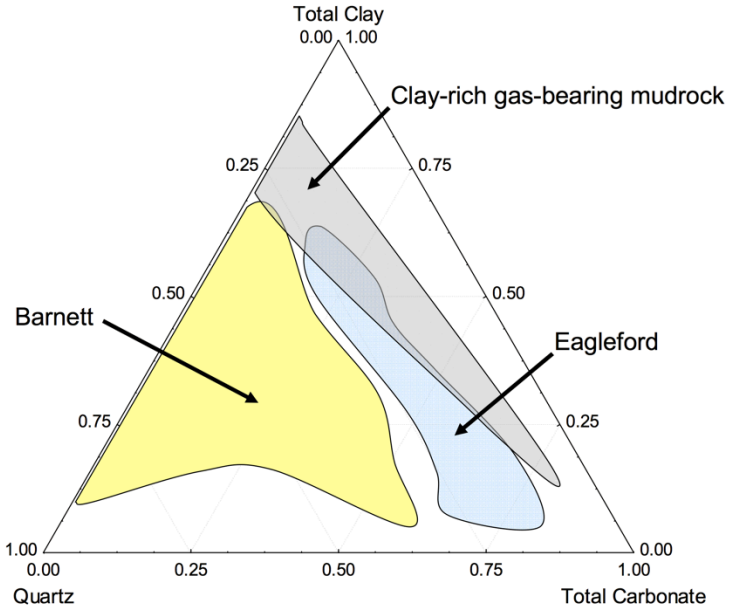

Figure 2.4: Mineralogy of the Barnett and Eagleford shale gas reservoirs (Passey, 2010)

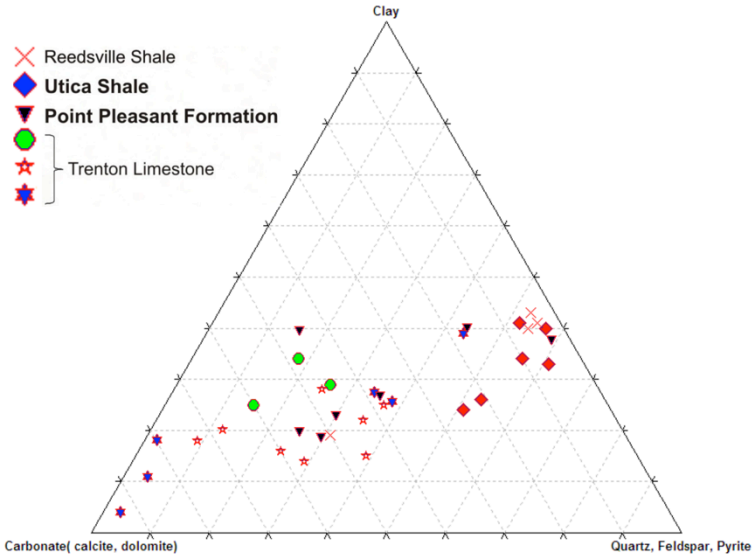

Figure 2.5: Mineralogy of the Utica shale (after Harper, 2011 and Nyahay, 2011)

Table 2.1: Mineralogical Analysis of hydrocarbon bearing Shale formations (Carman 2010).

Mineral Phases	Eagle Ford	Utica	Bakken	Marcellus	Lower Lorraine	Haynesville
	13260-13280 ft	5476 - 5495 ft	13260 - 13280 ft	7051 - 7062 ft	4344 - 4393 ft	12050 - 12104 ft
Quartz (SiO2)	9	11	52	31	31	31
Plagioclase Feldspar	1	3	7	4	7	7
Potassium Feldspar		nd	7	nd	nd	1
Calcite (CaCO3)	85	48	8	6	2	34
Fe-Dolomite (Ca[Fe,Mg][CO3]2)		7	8	nd	2	nd
Dolomite (CaMg[CO3]2)	tr	nd	8	3	nd	1
Siderite (FeCO3)	nd	nd	nd	nd	nd	nd
Apatite [Ca5(PO4)3F]	nd	nd	nd	nd	nd	1
Pyrite (FeS2)	tr	1	tr	5	3	3
Marcasite (FeS2)	nd	nd	1	nd	nd	nd
Chlorite	nd	2	1	5	4	tr
Kaolinite	tr	nd	nd	nd	nd	nd
Mica and/or Illite	nd	28	8	43	51	22
Mixed-Layer Illite85 / Smectite15	4	nd	nd	nd	nd	nd
C-rich material	nd	nd	nd	3	nd	nd
TOTALS	100%	100%	100%	100%	100%	100%

The high lateral heterogeneity in resource shale (figures 2.4 and 2.5) as the mineral composition of the resource shale reservoirs cover nearly the entire compositional range of shale. While the Barnet and Eagleford resource shale are not examined in this paper, highly variable mineralogy within a single reservoir shale reservoir is property all resource shales share. The scale of the vertical and horizontal heterogeneity of mineralogy can varies between different resource shales (Boyer, 2006).

The scale of vertical heterogeneity can be seen in figure 2.6 The lateral and vertical heterogeneity within a resource shale reservoir is due to the depositional environment of the resource shale, it's stacking patterns and can be related to sequence stratigraphic framework (Macquaker et al., 2003, Passey, 2010).

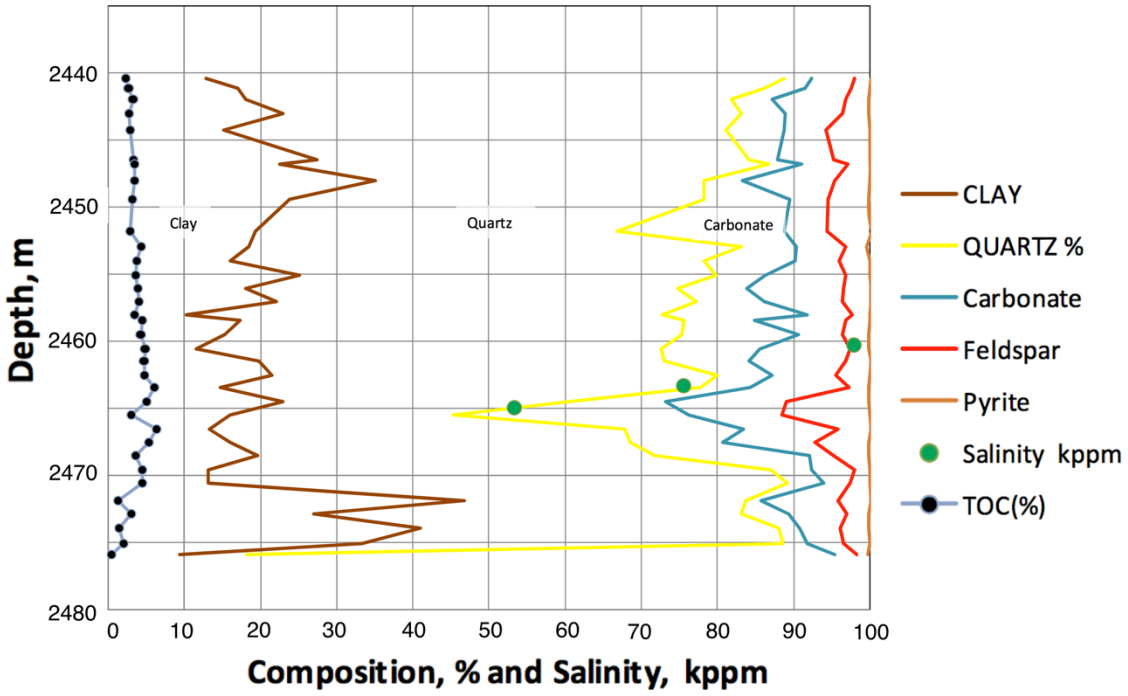

Figure 2.6: Change in cumulative composition as a function of depth measured by XRD of a single well. (after Sondergeld, 2010).

Mineralogy can be measured using a number of techniques including but not limited to optical microscopy, and forms of electron microscopy (Ruppel, 2012), XRD remains the most common measurement of mineralogy. XRD measurements are preformed by a directing an x-ray beam at onto the at a core sample, upon contact with the core sample the x-rays are scattered and diffracted by the various minerals and the

resulting pattern of reflection is caused by the crystal lattices of the minerals present in the sample. The diffraction of the x-ray beam can then be analyzed to infer the crystal lattices of the minerals present and the concentrations in the core sample (Hurlbut, 1998). Quartz and calcite are easily detailed through XRD but clays are not always easily detectible through with XRD as they are complex structures as seen below in figure 2.7 and 2.8 (Srondon). The clay content of resource shale can be a good indicator of its productivity as it can dictate the response to well stimulation treatments such as hydraulic fracturing as well as its fluid sensitivity. Geologically clays are defined as particle size that is smaller than 4 microns or (Neuendorf, 2005).

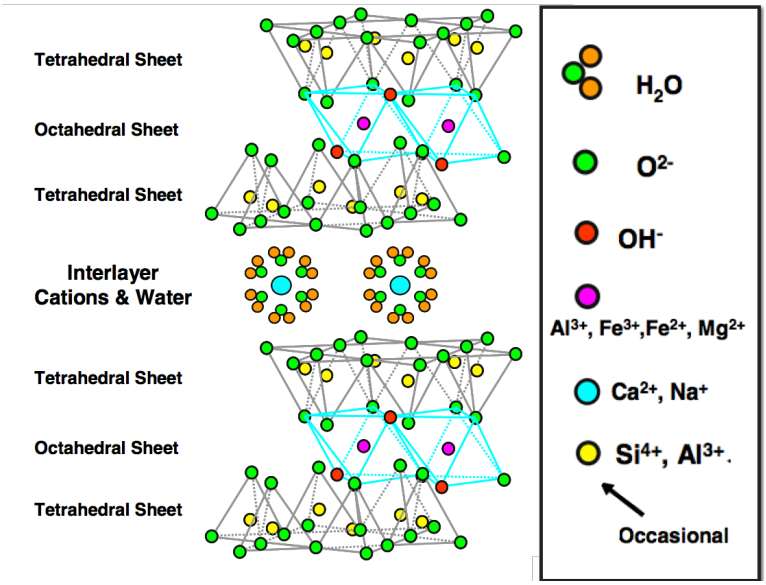

Figure 2.7: Crystal structure of smectite (after Passey, 2010)

All clays have ah hydroxyls as part of their crystalline structure as shown in figure 2.7. The most common clays in the subsurface are chlorite, illite, kaolinite,

montmorillonite, smectite and mixed layer illite-smectite. Four of these common clays are presented in Figure 2.8. Clays can cause formation damage and production issues in two ways: their small size plugs up pore throats and reduces permeability, and swelling from fluid exposure. All clays are susceptible to swelling when exposed to solutions containing water. The magnitude of clay swelling due to exposure to an aqueous solution is primarily dependent upon the solution to which the clay comes in contact (Zhou, 1995).

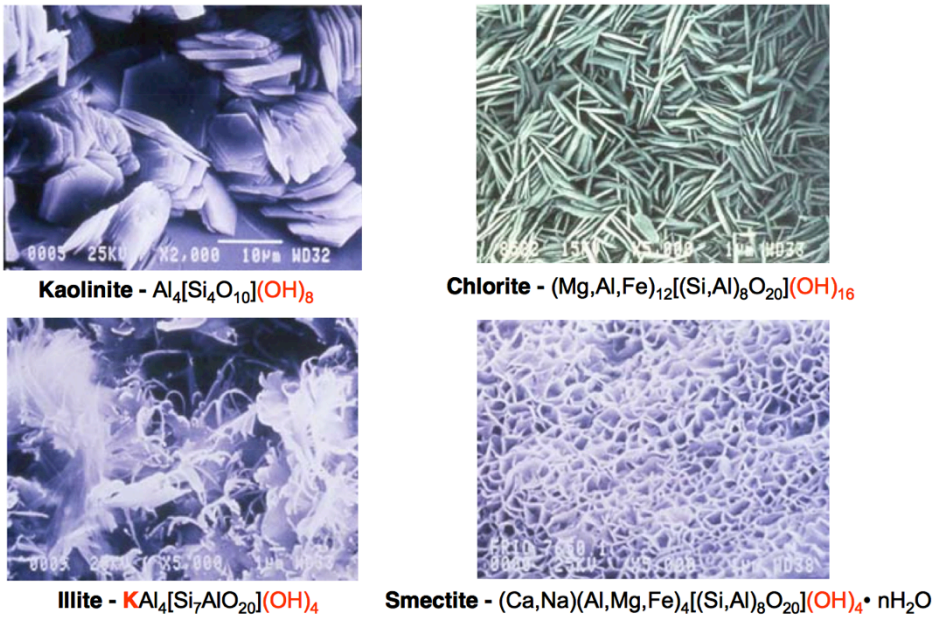

Figure 2.8: Common clay minerals found in organic rich shales (Passey, 2010)

Most siliciclastic grains are water-wet, which implies that there is a very thin layer or double layer of water in contact with the grains surface. In traditional porous media this volume of surface water is trivial compared to the total pore volume of the rock, however as porosity and the size of the pores and decrease the ratio between the

surface water increases. The surface area of the clays is orders of magnitude larger than quartz as seen in table 2.2.

Table 2.2: Surface area of common clay minerals (and fine grain sandstone) (Passey, 2010)

Clay Type	Internal Surface Area (m^2/g)	External Surface Area (m^2/g)	Total Surface Area (m^2/g)
Smectite	750	50	800
Illite	0	30	30
Chlorite	0	15	15
Kaolinite	0	15	15
Fine Quartz Sand	0	0.02	0.02

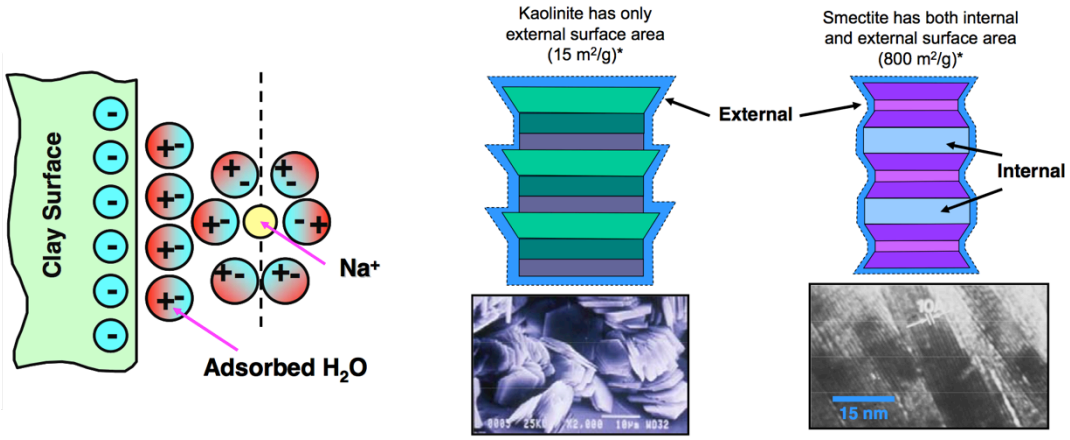

Figure 2.9: Illustration of adsorbed clay surface and double-layer water on surface of clays, and schematics, and SEM images of kaolinite and smectite illustrating surface areas. (after Passey, 2010)

In clay rich formations such as resource shales, the single or double layer surface clay water can be a significant portion of physical pore volume, though this volume is not considered by all to be part of the total porosity system of a shale (Passey, 2010). There is

an associated internal surface area that can adsorb water in smectite and montmorillonite; seen in figure 2.9. The ions in the aqueous solutions can also cause both crystalline swelling and osmotic swelling of the shale (Zhou, 1995 and 1997).

Expansion of clays due to ion and water adsorption onto the electrically charged surface of the clay translates into expansion of the laminated layers of shale, and consequently alters its physical volume (van Olfen, 1953). As little as a 3% weight gain due to adsorption of fresh water can change physical properties significantly, Chenevert (1970) demonstrated a decrease in compressive yield strength by nearly 70% with only 20% by weight shown below in figure 2.10.

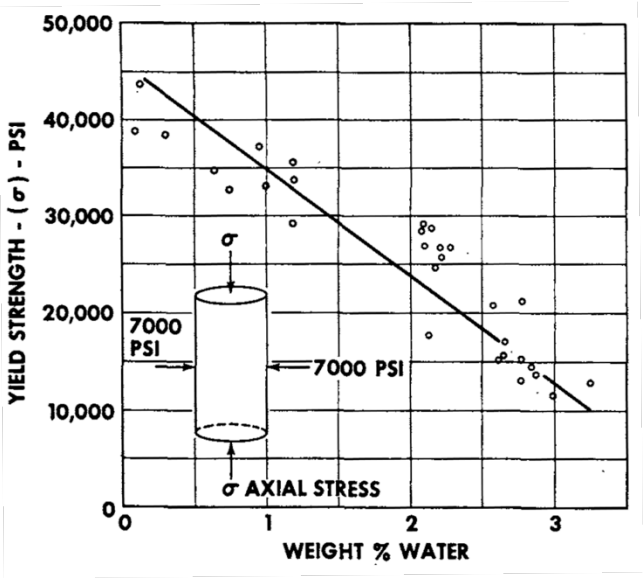

Figure 2.10: Change in yield strength due fluid exposure (Chenevert, 1970)

2.2.2 Native Shale Water Activity and Swelling

The preservation of shale is one of the most fundamental components of quality shale research. Over the previous 50 years a great deal of research has been performed on non-oil bearing shales with regards to fluid sensitivity. It has been shown by Chenevert (1970; 1992; 2001) that unpreserved shale does not have the same mechanical and chemical properties as preserved shale as previously mentioned.

In the preservation of shale, maintaining the native state water content is fundamental. The water activity (a_w) of a shale is on of the most fundamental properties when it comes to shale preservation and is the ratio of the vapor pressure of a fluid or a fluid-solid system to that of pure water at the same temperature. Water activity is directly related relative humidity but is expressed as a unitless ratio rather than a percentage. If shale is not stored in an atmosphere with the same water activity, the shale either adsorbs or loses water depending if the water activity is higher or lower than its own. Water activity can also be converted to a measure of salinity of aqueous solutions, though it is temperature dependent (Chenevert, 1975). Pure water has an activity of one and the activity of the solution decreases as the ion concentration increases.

Considering the fluid sensitivity of shale is paramount when preserved sidewall core samples are taking from an organic-rich shale formation. Shale samples are taken using oil based mud to minimize fluid interaction and immediately sealed at the surface. While exposure to the oil based may contaminate the core it cannot be avoided. If the core sample is received unopened and still sealed it is considered well preserved.

Table 2.3: Super saturated Salt Solutions and Corresponding Water Activities (Winston, 1960).

Salt	a_w	Salt	a_w
$K_2Cr_2O_7$	0.98	$(NH_4)_2SO_4$	0.80
KH_2PO_4	0.96	NaCl	0.75
Na Tartrate	0.92	$Ca(NO_3)_2$	0.505
$MgSO_4$	0.90	$MgCl_2*6H2O$	0.33
KCl	0.85	$ZnCl_2$	0.10

Figure 2.11: Shale samples stored in constant humidity desiccators (Jung, 2013)

Once a preserved core sample is received from the field, it is carefully unsealed and small pieces are cut and placed in different desiccators under vacuum at differing relative humidity as shown in figure 2.11. The supersaturated salt solutions used in the desiccators create a constant relative humidity or water activities under a vacuum and the solutions and activities are shown in table 2.3 (Winston, 1960).

The relative weight change of each shale sample in its respective desiccator is monitored and recorded once the value stabilizes. This relative weight change is then plotted against relative humidity as seen in figure 2.12. The intersection of the weight

change and water activity is equal to the organic rich shales native water activity. Shale samples can be sored safely without fear of property change, as additional hydration will not occur either in the appropriate water activity desiccator or immersed in mineral oil in a sealed opaque vessel (Chenevert, 2001).

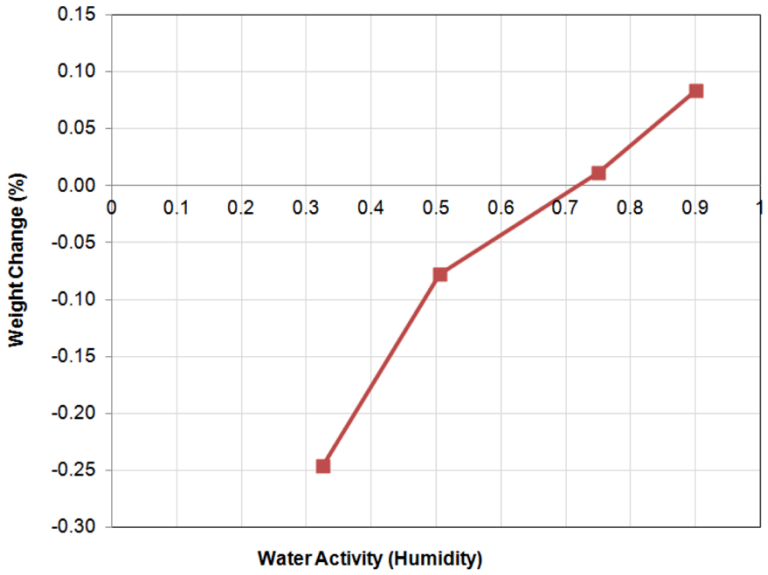

Figure 2.12: Water activity measurement of Eagleford Shale (Jung, 2013)

2.2.3 Porosity, Permeability and Saturation

Organic-rich mudrocks or resource shales have a pore space composed of nanometer to micrometer sized pores. The shale has a four of different types of porosity contributing to the total value: interparticle porosity (intraP), intraparticle porosity (interP), organic porosity (OM), and fracture porosity (Loucks, 2012). InterP and intraP porosities are associated with the matrix. InterP porosity and intraP porosity are defined

as “pores found within the particles and pores found between particles and crystals” respectively (Loucks, 2012). The different types of porosity all contribute to the total or absolute porosity in differing fractions, but may not all contribute to the effective porosity. An accurate value of porosity is very important for measuring the relative amount of imbibition and for accurate estimations of reserves however, obtaining such an accurate value is a non-trivial task for organic-rich resource shale. The following section will discuss some of the most commonly used methods of measuring the porosity and permeability of organic rich and the various factors that affect the measured porosity and permeability values.

Laboratory measurements for porosity and permeability of organic rich shale are extremely important to correlate against the log-based values measured in the field and establish a realistic reservoir model. A reservoir model allows for the estimation of reserves and estimated ultimate recovery. Many laboratory measurements of porosity and permeability values rely upon crushing the shale sample using the Gas Research Institute (GRI) method.

The GRI method of measuring resource shale, first introduced by Luffel et al. (1992) is the current industry standard for measuring porosity. This method involves crushing shale sample from a core and sieving the samples to a standard size (Luffel, 1992), allowing for faster measurements for both porosity and saturation over conventional measurement techniques. The crushing and physical modification of the core is likely introducing an unknown amount of error into porosity, permeability,

saturation measurement or any petrophysical measurement relying upon the GRI method. Though GRI is supported by proven uncertainty associated with traditional porosity measurement techniques applied to organic-rich shale (Spears, 2009).

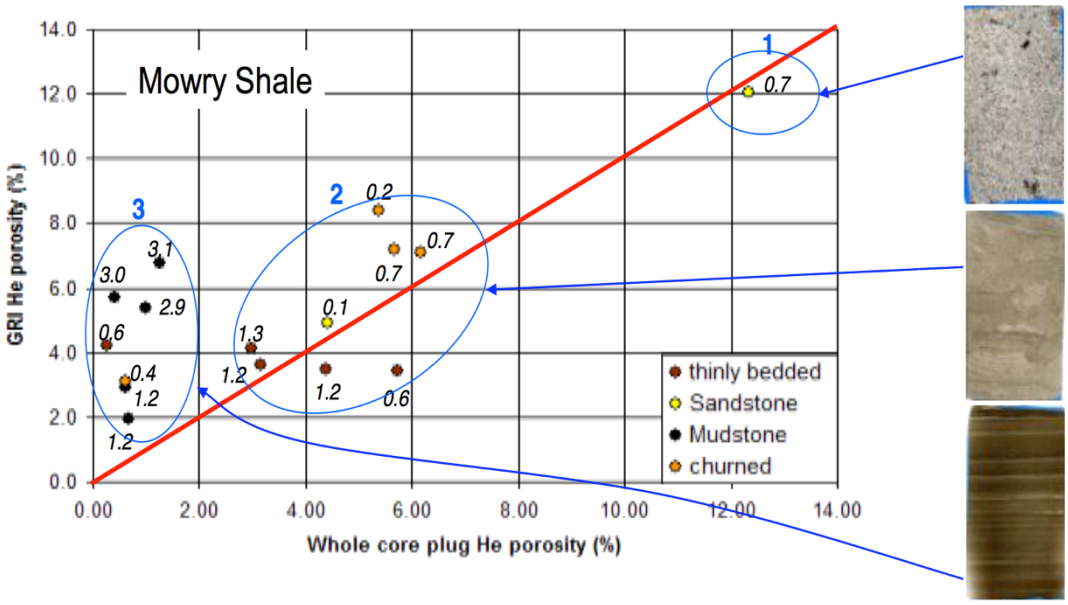

Figure 2.13: Plot of whole core helium porosity vs. GRI porosity (after Spears et al., 2011)

Petrophysical measurements that rely upon crushing resource shale samples are a considerable source of debate. As the crushing and sieving process of the shale does not guarantee the native distribution of both pore size or the distribution of the micro-facies within the rock will be equivalent to the crushed sample (Spears, 2011). Additionally, there is a well-documented difference in the measurement porosity using the GRI method between different laboratories as seen in figure 2.13 (Passey, 2010; Spears, 2011). While Spears and his collages (2011) were able to develop a method to correlate measurements of porosity between different laboratories using a correlation based upon the clay bound

water, the error introduced through the crushing of resource shale samples is still not well known.

In conventional rocks permeability measurements are made using steady state or pulse decay methods on plug samples under reservoir stress. Similar methods have been used with relative success in low permeability rocks (Yang, 2009). Often with organic-rich shales permeability is measured using a method similar to the GRI method (Guidry, 1996; Luffel, 1992). The permeability of the rock matrix is measured by first crushing and sieving the shale as described previously, and a pressure decay test is preformed upon the crushed sample. Much like the porosity measurements, permeably is not measured under reservoir conditions, nor is there is there high agreement of the permeability measurements as they can vary by up to 300% between laboratories (Sondergeld, 2010).

Another technique used to measure permeability on preserved shales is preformed at the University of Texas at Austin, is the pressure penetration test or PPT (Al-Bazali, 2005). In this test a fluid, often brine, is flowed across the surface of a shale sample at a constant pressure and the buildup of pressure on the bottom of the sample that is connected to a sealed chamber of known volume is monitored. This measurement provides significantly different values than a crushed rock sample and can be preformed upon on intact preserved shale samples.

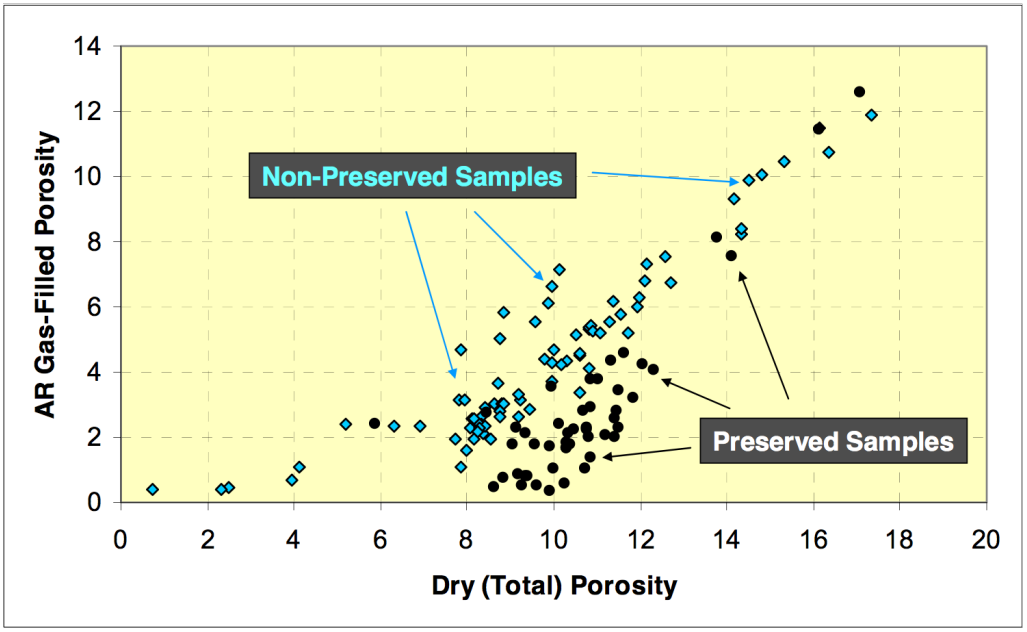

Figure 2.14: Relationship between preservation and measured porosity (after Passey, 2010)

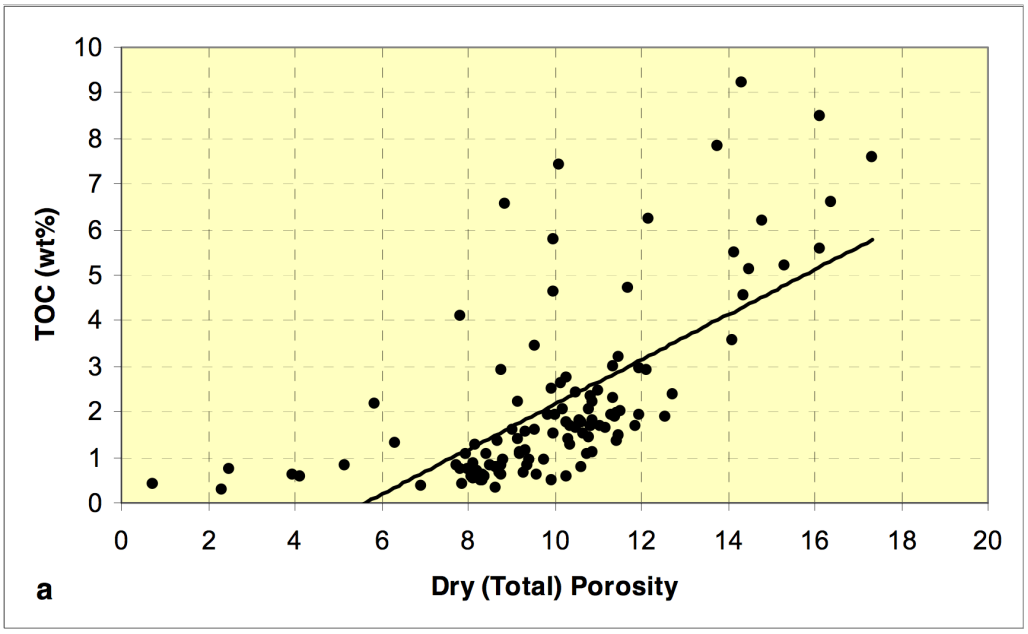

Figure 2.15: Relationship between TOC (Total organic content weight %) and measured porosity (after Passey, 2010)

Shale preservation has an significant impact upon the results of petrophysical measurements such as porosity and permeability (Passey, 2010; Spears, 2011; Jung, 2013; Zhou 2013). As seen in figure 2.14, the porosity values measured for preserved and unpreserved shales do not agree. Additionally it has been shown by Jung (2013), that permeability measurements made using the PPT by up to 300% when comparing preserved and unpreserved cores of organic rich shale (Jung, 2013).

There is a positive correlation between porosity and TOC (Passey, 2010 and 2012) as shown above in figure 2.15. This positive correlation is due to both the total organic content's association with the depositional environment, and the generation of organic pores (OM) during hydrocarbon maturation.

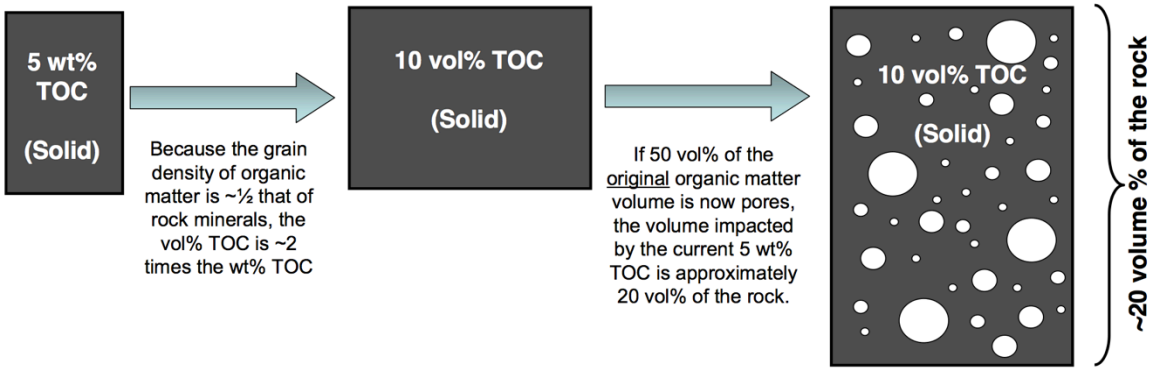

Figure 2.16: Evolution of 5% TOC to 20% porosity when all organic matter is converted to pores. (Passey, 2010)

As the organic material matures into hydrocarbon in the oil window, new pores are formed through the expulsion of maturing hydrocarbons out of the space the organic material once occupied (Sarg, 2012). These pores are often considered oil-wet. Figure

2.16 demonstrates a specialized case of this process where all of the organic matter, matures into hydrocarbons creating organic pores.

The typical literature values for porosities of the shale formations examined in this paper (Bakken and Utica shale) are between 2% to 12% with an average 5% for the Utica (Murphy et al., 2013), and between 1% and 16% with an average of 9% for Bakken (Wang et al, 2012). Though the method of measurement for any of these values is not known so there is an unknown amount of error.

Often with organic rich shale, the effective porosity is much lower than the measured porosity due to clay bound water, irreducible water, and organic matter shown in figure 2.17 (Passey et al., 2010). The effective pore space by definition is sum of all interconnected pore space that contains mobile water, capillary bound water, or hydrocarbons, where as the total pore space also includes clay bound water.

In conventional reservoir rock, the effective pore volume is not significantly affected by clay bound water as the relative volume of clay minerals to non-clay minerals is very low, but as the relative volume of clays increase so does the volume of clay bound water. As discussed previously, the clay bound water is divided into two categories: internal or structural clay bound water and external or surface bound clay water.

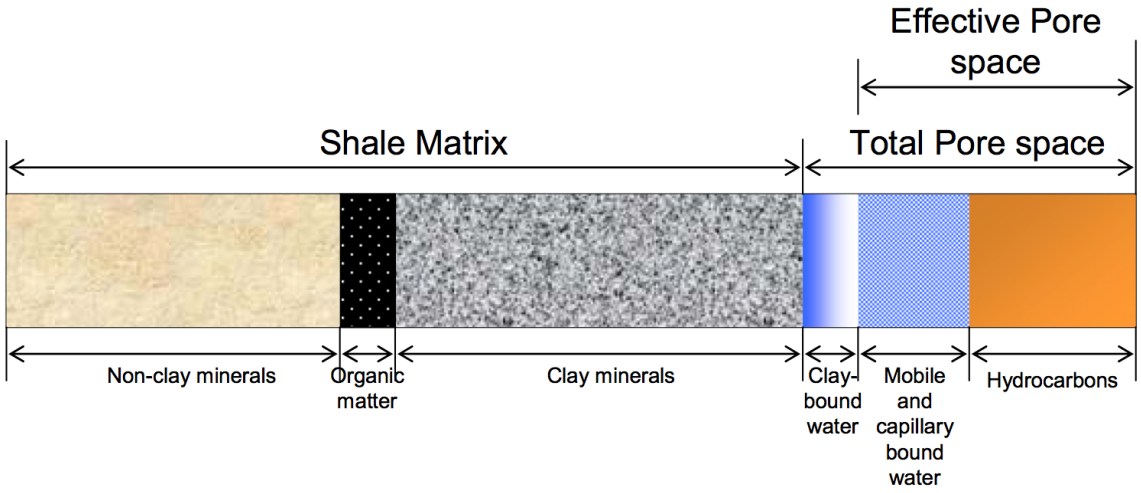

Figure 2.17: Schematic of organic rich and clay rich shale with water and hydrocarbons (Passey, 2010)

The structural or internal clay bound water both does not significantly affect the physical volume effective porosity significantly as long as significant swelling does not occur. The single or bilayer bound to the surface of the clays can significantly impact the effective porosity, as the pores in organic rich shale are extremely small, so the relative volume occupied by clay bound water is much larger than in conventional rocks (Passey, 2012).

The relative hydrocarbon saturation has been linked to the TOC of organic-rich shales and is a proven indicator of hydrocarbon saturation in resource shales (Passey, 2010 and 2012). Though a measure of TOC does correlate to an accurate measure of the relative volumes the fluid contained within the pore space of the shale.

Traditionally, saturation is measured through retorting a sample. In a retort measurement, a saturated rock is heated to temperatures ranging from 100 to 850 degrees

Celsius at discrete temperature steps. The vapor formed through this process is condensed and measured at each temperature step. From this measurement and the use of a correction curve, the saturation of the core sample can be measured. The relative volumes of clay bound water and inter-crystalline clay water also can be determined depending upon the temperature range chosen.

Porosity and saturation of resource shale can also be measured indirectly through the use of nuclear magnetic resonance or NMR techniques, as described in Borysenko (2009). Borysenko (2009) made use of the techniques developed by Hirasaki (2000) and Toumelin (2004). Nuclear magnetic resonance measurements are made through exposing a core sample to electromagnetic radiation. The nuclei of the sample and fluids in the pore space adsorb the magnetic radiation and then remit the electronic magnetic radiation. By measuring the relaxation times of the remission of the magnetic fields, the porosity, types of fluids, and relative volumes of the fluids can be measured.

NMR measurements, measure all of the fluids within a given sample, including the clay bound water. This can lead to errors in the measurement of porosity, as often the NMR measured porosities are not equivalent of the effective pore volume of the sample as previously discussed. Despite this flaw, NMR measurements are useful for not only measuring the porosity and saturation of shale samples, but can also be combined with experimental procedures as Borysenko (2009), Hiraskai (2000), and Tourmelin (2004) describe to measure the wettability of the sample, and quantify imbibition. The initial or final saturations of the samples used in the following paper were not measured.

2.3 WETTABILITY

In the case of a porous media saturated with two more immiscible phases, the interaction of the immiscible phases, capillary forces and intermolecular forces between the fluids and the rock and the fluids often result in an observable affinity between a single fluid phase and the rock fabric of the porous media. This affinity, or observable preference of one phase to adhere to the surface of the rock is characterized by the concept of wettability. In the following section the concepts of wettability and spontaneous imbibition will be introduced and previous work on spontaneous imbibition in organic rich shales will be discussed. It is worth noting that though the technical definition of imbibition is dependent upon the wettability of the porous media. In the context of this paper any spontaneous water uptake by a porous media into the pore space will be considered imbibition.

Wettability is defined as "the tendency of one fluid to spread on or adhere to a solid surface in the presence of other immiscible fluids" (Anderson, 1986a). The most apparent and easily measurable of wettability is the interaction between a smooth surface of uniform chemical composition, and two immiscible phases at equilibrium. The equilibrium of the interfacial tensions of each phase results in an observable angle at the point where the two immiscible fluid phases and the surface intersect. This angle is known as the contact angle (θ), and by convention the contact angle is measured through the denser phase. Figure 2.18, illustrates three equilibrium contact angles in a oil-water-solid system where the light grey rectangle is the solid, the oil phase is black and the

water phase is present, but not illustrated. At equilibrium the interfacial tensions are related by the Young-Dupre equation shown in equation 2.1.

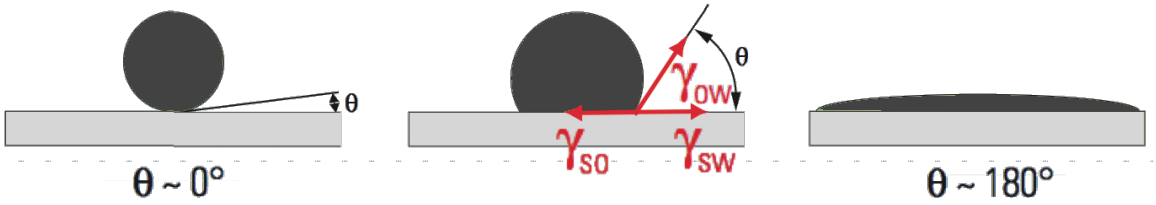

Figure 2.18: Contact angle and interfacial tension equilibrium in a water-oil-solid system (after Abdallah, 2007).

$$\gamma_{so} = \gamma_{sw} + \gamma_{ow}\cos\theta \quad \text{..... (2.1)}$$

where,

γ_{so} — Interfacial tension between the solid and oil, units of N/m.

γ_{sw} — Interfacial tension between the solid and water, units of N/m.

γ_{ow} — Interfacial tension between the oil and water, units of N/m.

θ — Contact angle between immiscible fluid phases and surface, units of degrees.

Table 2.4: Relationship between contact angle and wettability (Anderson 1986b)

Contact Angle	Water-Wet	Neutral-Wet	Oil-Wet
Minimum	0°	60° to 75°	105° to 120°
Maximum	60° to 75°	105° to 120°	180°

The concept of wettability is key in the production of hydrocarbons, as it has a strong influence on the flow and distribution of the oil and water in the reservoir (Morrow, 1990; Cuiec, 1991). Figure 2.19 illustrate the change in oil and water distribution in a porous media when the wetness is changed holding all other properties constant. In a water-wet rock, the oil has little contact with the surface of the rock, the oil remains in the center of the pores, and the reverse is true in the case of an oil-wet rock seen on the far right. Mixed wettability is a blending of the oil-wet and water-wet cases, only oil is in contact with the grains at some points and only the water is in contact with the grains at others.

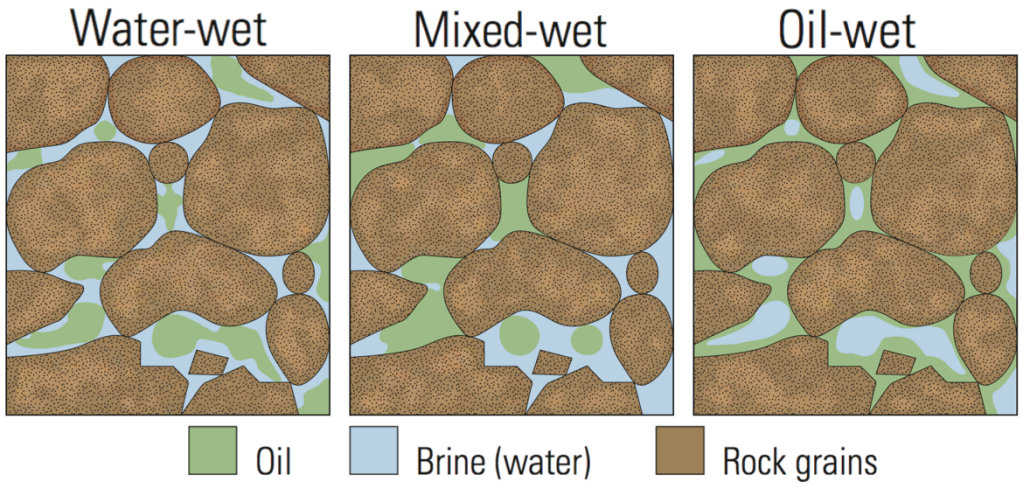

Figure 2.19: Pore scale distribution of fluid in porous media with different wetness (after Abdallah, 2007)

While the wettability of a uniform surface can easily be defined and measured, the quantification of wettability of a reservoir is a non-trivial problem. Wettability much like permeability and porosity while fundamental theory is elementary, when scaled up and applied porous media becomes extremely complex. There are many different ways to

measure the wettability of a core sample. Anderson (1986b) in his review of wettability reviewed several quantitative measurement techniques and their strengths and weaknesses. These quantitative experimental techniques are still use in today and are contact angle, Amott Index and the USBM method. Additionally, since Andersons's review in 1986 a number of other techniques have been developed to qualitatively measure wettability including spontaneous imbibition and NMR techniques as discussed previously and used by Borysenko (2009), Basu and Sharma (1993), Hirasaki (2000) and Toumelin (2004).

2.3.1 Spontaneous Imbibition

Spontaneous imbibition occurs when a wetting fluid imbibes into the core, displacing an immiscible non-wetting fluid illustrated in figure 2.22 and occurs due to capillary pressure and/or gravity. Capillary pressure is a function of contact angle and interfacial tension as shown below in equation 2.2.

$$P_c = \frac{2\gamma \cos\theta}{r} \quad \text{..... (2.2)}$$

where,

P_c —Capillary pressure, units of Pa.

γ —Interfacial tension, units of N/m.

θ —Contact angle, unites of degrees.

r —radius of capillary tube, units of meters.

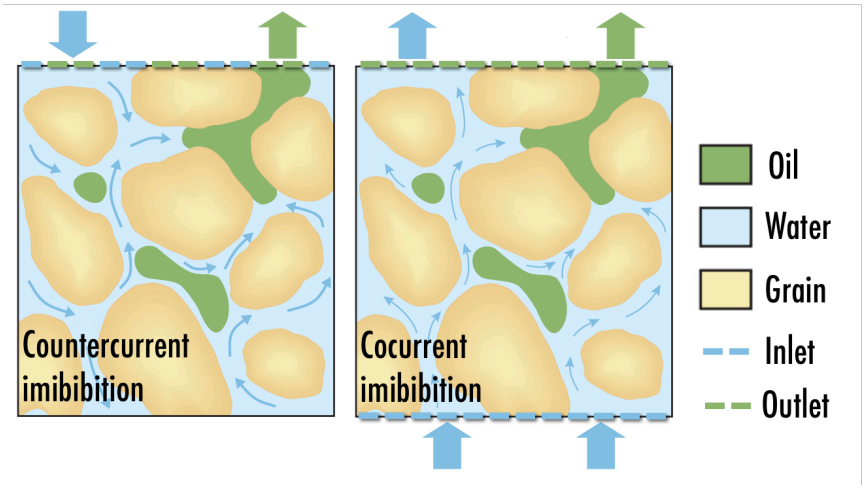

Figure 2.20: Pore scale visualization of oil displacement due to imbibition with inlet and outlet boundaries marked with dashed lines. (after Al-Menjeni, 2011).

Spontaneous imbibition can be classified into two major categories: cocurrent and countercurrent imbibition illustrated in figure 2.20 where the dashed green lines are the outlets and the dashed blue lines are the outlets. Cocurrent imbibition occurs when there is a predominate direction of travel of the imbibition in the sample, and is analogous to a water flood. In 1-D cocurrent imbibition, one boundary of the rock sample functions as an inlet and is exposed to the wetting fluid, and the oil is displaced at the outlet boundary directly opposite to the inlet. Countercurrent imbibition is analogous to the displacement of oil that occurs in highly fractured reservoirs, and where the same boundary of the rock serves as both the inlet and the outlet. Countercurrent imbibition can be measured in 1-D, 2-D or 3D, depending upon the number of boundaries open to imbibition. 3-D

countercurrent imbibition (where all surfaces of a sample are boundaries for imbibition) is studied in the following chapters.

There are a number of parameters that influence the rate and volume of imbibition which include but are not limited to: permeability, heterogeneity, initial water saturation, fluid density and viscosity, interfacial tension and as previously mentioned the boundary conditions. As imbibition is a function of capillary pressure which in turn is a function of wettability, as the wettability of a sample increases so does its rate of imbibition (Zhou, 2000). While this logic follows theoretically it is difficult to experimentally link capillary pressure of a homogenous sample to ones formed over geologic time due to the sheer quantity of heterogeneity (Harmon, 1986).

Permeability has notable effects upon spontaneous imbibition. The permeability of the core is directly related to the rate of imbibition, and as would be expected, higher rates of imbibition occur in cores with higher permeability (Mattax, 1962). Additionally, while imbibition has been known to be an important recovery mechanism in low permeability reservoirs, Cuiec (1994) demonstrated the efficiency and speed at which spontaneous imbibition can function as a recovery mechanism in strongly water wet cores.

The fluids involved in the process of spontaneous imbibition also have a notable effect upon the rate and total volume of displacement. The fluids that interact in spontaneous imbibition are the saturating fluids within the core sample, which include oil, brine and occasionally gas and the fluid being imbibed. The rate of imbibition is

effected by the by the respective densities and viscosities of both the saturation fluids and the imbibition, and specifically the relationship between the density and viscosities of the immiscible fluids (Ma, 1996; Zhou 2002). The chemical composition of the imbibition fluid can also significantly impact the imbibition (Iffy 1972).

The interfacial tensions (IFT) between the various fluids involved in spontaneous imbibition also affects the rate of imbibition. When the oil-water IFT is reduced, the rate of imbibition decreases significantly, as this IFT is part of the drive mechanism of spontaneous imbibition (Austad, 1997). The wettability of the rock, can be altered through the use of surfactants in the imbibition fluid (Austad, 2000)

Finally the boundary conditions as alluded to earlier effect the rate of imbibition, as the surface area open to imbibition fluids is related to the rate of imbibition (Cil, 1998). Additionally the surface condition or wettability of the grains is a controlling factor in imbibition as described by the scaling factor introduced by Ma (1996) in equation 2.3. Where, t_D is dimensionless time, t is the actual time of imbibition, φ is porosity, k is permeability, σ is the interfacial tension, μ_w is the viscosity of the displacing fluid, μ_o is the viscosity of the displaced fluid, and L_c is the characteristic length. L_c is equal to equation 2.4 in the case of a cylindrical core, where d is the diameter and L is the length of the core.

$$t_D = \frac{\sigma\sqrt{\frac{k}{\varphi}}}{L_c^2\sqrt{\mu_o \times \mu_w}}t \quad \text{..... (2.3)}$$

$$L_c = \frac{Ld}{\sqrt{d^2 + 2L^2}} \quad \text{..... (2.4)}$$

2.3.2 Spontaneous Imbibition in Shale and Archimedes Method

Conventional spontaneous imbibition measurements are made with an imbibition cell, which is a sealed glass vessel that has space for a core at one end and a form of graduated cylinder at the other to measure the volume of displaced fluid. This measurement technique works well with samples of where the total pore fluid displacement is on the order of several milliliters or more. This measurement method is not ideal in shale due to its inability to account for the swelling of the shale sample, and due to the typical volume of preserved shale used in petrophysical measurements. The bulk volume of preserved organic-rich shale used in petrophysical measurments is usually less 16 mL. This bulk volume used for characterization is an order of magnitude lower than the sample size used in an imbibition cell. The total volume of fluid displaced from a typical bulk volume of organic-rich shale for petrophysical measurement is on the order of tenths of a milliliter which is far to small to be ideal for use in imbibition cells.

Archimedes principle states that the measured loss in weight of a sample immersed in a fluid is equal to the weight of the fluid that the sample displaces. As long as the volume of the sample remains constant during the measurement of the relative weight change, the weight change of a sample immersed in fluid is equal to the weight change of the sample in air.

Archimedes principle has been used over 60 years in the measurement the bulk volume of samples (Lewelling, 1952), but it has also been adapted to measure countercurrent spontaneous imbibition (Cil, 1998; Wang 2010 and 2012). There are two possible ways to measure spontaneous imbibition, the volume of fluid displaced, and the relative weight gain or loss in the sample due to the difference in the densities of the fluid saturating the core and the imbibition fluid (Cil, 1998; Wang 2010 and 2012).

Spontaneous imbibition in organic-rich shale is still not well understood and is still being researched and as a result a significant amount experimental literature does not yet exist. Though swelling and water adsorption of clay rich shale has been researched for many years. At the time of this research, Elijah (2011), Sulucarnian (2012), Morsy (2013), Wang (2011 and 2012), and Zhang (2013) have investigated spontaneous imbibition and wettability in organic rich shale.

Overall the wettability of organic rich shales have been found to be oil-wet to mixed-wet using both traditional techniques such as spontaneous imbibition and the Ammot-Harvey index and NMR techniques (Elijah,2011 ;Sulucarnian, 2012; Wang 2011 and 2012).

Wang (2011 and 2012) has studied the flow rate behavior and imbibition in Bakken and Pierre shale. Wang (2011 and 2012) performed imbibition experiments using the Archimedes method as well as modified Ammott-Harvey tests. Spontaneous imbibition was enhanced using through wettability modification of the rock by surfactants by 6 to 10.2% over only brine imbibition. The overall recovery of the oil in

place ranged from 15.6 to 25.4%. Though the Archimedes method was used, they did not measure the air weight, and as such the amount of swelling is unknown.

The overall results of Wang's research show that imbibition in shale is measurable and is a highly promising method of EOR for organic-rich shale rocks and this claim is supported by both Takahashi (2009) and Morsy (2013) though Morsy investigated the use of alkali rather than surfactants. However, all the results neglect the effects of swelling in regards specifically to shale and or the resulting condition of the internal stresses of the organic-rich shale due to fluid exposure. This will lead to a significant overestimation of the oil recovery (or water imbibition) in shales.

Chapter 3 – Experimental Design and Procedure

3.1 Experimental Setup:

The gravimetric spontaneous imbibition experimental setup was designed to measure the small changes in mass as imbibition occurs within a shale sample. The volumes of oil and water moving are very small in shales, and as a result a novel method was needed in order to minimize the error in these measurements. The total amount of preserved shale used in the experiments also needs to be reasonable, as obtaining and preserving shale samples is both expensive and time-consuming. In the ideal case of a 1-inch diameter by 1-inch long core plug with a 5% effective porosity and a 100% oil saturation, the maximum amount of oil that could be measured would be on the order of 0.64 milliliters. This is far below the resolution of standard imbibition cells. Using more shale would not only minimize the total number of tests that one could perform (as the preserved shale supply is limited) but would also slow the results of the experiments as any imbibition based process is a function of the surface area exposed to volume.

Because of the limitations of traditional imbibition experimental methods, a novel method was required. If the volumes of the oil and water are not accurately measurable, then it is possible to measure the mass change of the sample. However, measuring the mass of a sample in a fluid is a non-trivial problem. The experimental setup is designed to minimize as many variables with regards to this problem. The gravimetric spontaneous

imbibition experimental setup can be broken into two discrete subgroups of components: the measurement module and the imbibition assembly.

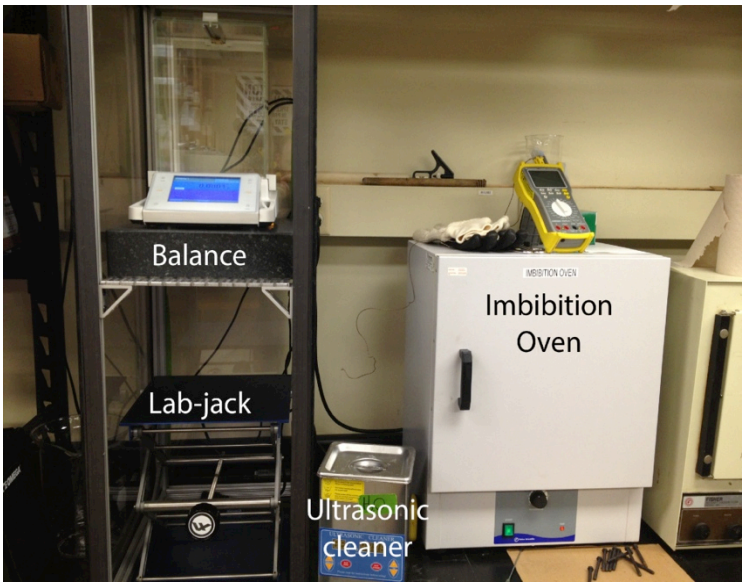

Figure 3.1 - Gravimetric Spontaneous Imbibition Setup.

3.11 Measurement module

The measurement module contains the following components: a bottom loading balance elevated on an enclosed frame, a lab-jack, and an ultrasonic cleaner as seen above in Figure 3.1.

The balance is a Sartorius Cubis MSA with a maximum capacity of 220 grams and a gradation of 0.0001 grams ± 0.00005 grams. The balance can be setup in both top- and bottom-loading configurations. A top-loading balance is used in the traditional method, where the sample is placed in the glass isolation chamber and weighed on the

weighing platform. Bottom-loading balances measure the weight of suspended samples on a hook on the base of the balance. In this setup, the balance is on an 80/20 frame with clear polycarbonate panels magnetically attached to all sides to minimize weighing errors caused by air movement around the sample. The balance is set atop a 36 kg granite slab in which a 1-inch hole has been bored to allow the bottom-loading sample hook to pass through. This granite slab is merely a large mass to provide some inertia-based shock insulation from the surrounding workstation. The balance is also used to measure fluid densities when paired with the Sartorius density kit, which can be seen below in Figure 3.2. The Sartorius density kit includes a 10-milliliter argon glass pendulum, which allows for the measurement of densities with an accuracy of 0.001 grams per milliliter ± 0.0005 grams per milliliter.

Figure 3.2 - Sartorius liquid density kit.

To change the relative height of the shale sample in relation of the imbibition fluid being tested, a lab-jack is used to raise and lower the imbibition vessel. This allows a precise measurement of the sample's weight in fluid and in air. The lab-jack is a Fisherbrand lab-jack, with a 12-inch by 12-inch platform and a 6 to 20 inch vertical lift.

Finally, an ultrasonic cleaner is very important in the measurement assembly if visible oil droplets form on the surface of the shale sample during spontaneous imbibition. In order to ensure an accurate weight measurement in the fluid, the surface oil droplets must be minimized or removed. The ultrasonic cleaner does this efficiently and with minimal fines generation. This ultrasonic cleaner is somewhat unique in that it allows the user to control the heat of the fluid in the cleaner and the cleaning action independently. The cleaner can be heated to a maximum of 80 degrees centigrade and the user-set timer controls duration of the cleaning function.

3.1.2 Imbibition assembly

The imbibition assembly is made up of an oven for temperature control and the individual imbibition vessels. Spontaneous imbibition occurs in the imbibition vessel and contains the shale sample being tested, and the fluid being tested. The imbibition vessels are stored in the oven to control the temperature at which imbibition occurs.

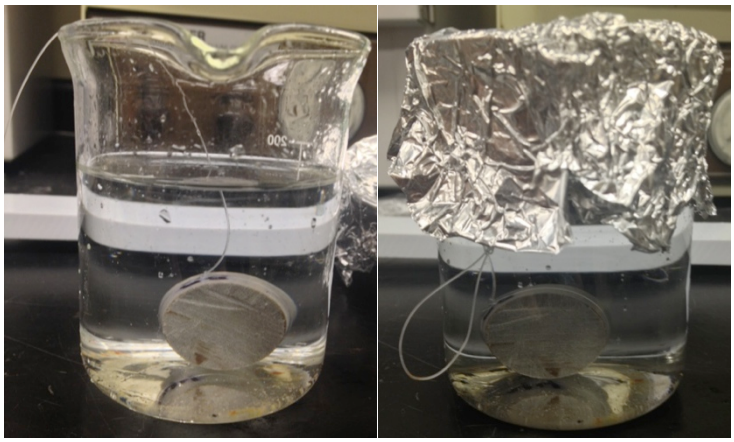

Figure 3.3 - Imbibition vessel covered and uncovered.

Multiple fluid and shale samples can be tested at the same time with this experimental design simply by using as many imbibition vessels as needed. Each imbibition vessel consists of a covered beaker, which contains the shale sample, the fluid being tested, and a monofilament line attached to the sample with a loop at the opposite end to allow for measurement. The beaker may be covered with aluminum foil to minimize fluid loss due to evaporation in the oven. The monofilament line is a 0.016-inch diameter nylon line. A loop at the end of the line allows for easy attachment to the weighing hook on the balance and the opposite end of the line is secured around the sample. Both the fluid and the shale samples in the vessel vary depending upon what is being studied.

Figure 3.4 - Imbibition oven containing imbibition vessels

A Fisherbrand oven is used for thermal control and isolation. The oven is an important component, but for the purposes of this thesis, all tests were performed at room temperature to confirm the novel experimental method.

3.2 Experimental Setup Preparation

3.2.1 Shale sample preparation

After a preserved core sample is received from an industry supplier in the form of preserved plugs (1-inch or 1.5-inch diameter and half an inch to 3 inches long) or a whole core (4 inches in diameter and approximately 10 inches long where one side may or may not be slabbed to examine bedding planes). The samples for the gravimetric spontaneous

imbibition must be prepared. If the core is well preserved, then it is wrapped in aluminum foil and wax to maintain the native state humidity of the shale minimizing dehydration of the sample during transport and storage.

The core received is then stored in at room temperature in sealed boxes as received until gravimetric spontaneous samples need to be prepared.

If a whole preserved core is received, first the foil and wax are removed, then 1-inch core plugs are cut in the direction of the bedding planes using a mineral oil-cooled drill press with a 1-inch diamond coring bit. If a preserved plug is received from the industry supplier, then the foil and wax are removed as with the whole core. Once these core plugs are cut or the foil and wax are removed from a preserved core plug, the sample is cut using a mineral oil-cooled saw into the appropriate thickness for the gravimetric imbibition testing experiment, a length ranging from one quarter of an inch to 1 inch. This process is repeated until the total number of samples required is prepared. These samples are then stored in a paint can filled with mineral oil and sealed to maintain the humidity of the sample, while the rest of the procedure is completed.

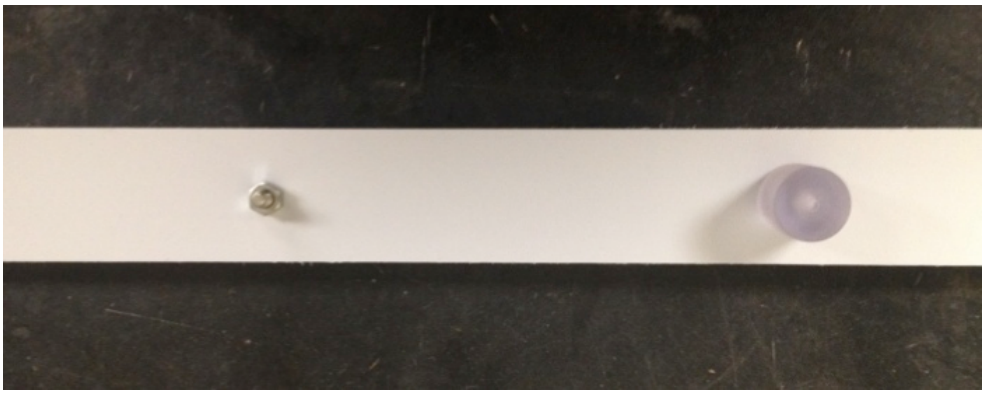

Figure 3.5- Knot tying jig

The monofilament lines are tied using a custom jig. The lines have a total length of approximately 8-inches. To create a line to secure around the sample, first a overhand loop is tied and secured around the bolt in the jig as seen in Figure 3.5, then the line is cut to a length of approximately 14-inches and an two half hitches are tied around the 1-inch diameter polycarbonate jig. A picture guide to the knot tying process can be found in Appendix (LINK). The working end of the overhand loop is trimmed to approximately 2mm and the line is then slipped off the jig and placed aside. This procedure is repeated for however many imbibition vessels need to be prepared and can be seen in Figure 3.6.

Figure 3.6 – Monofilament line with overhand loop on right and two half hitches on left

When all other components of the imbibition vessel are prepared, the shale sample is removed from the mineral oil and its length and diameter are measured and recorded three times for each dimension. The shale sample is then rinsed with hexanes to remove the surface mineral oil. The hexanes are allowed to evaporate and the mass of the sample is recorded three times.

After the samples are weighed and measured, the monofilament lines are attached to the two half hitch loop and the working end of the half hitches is trimmed to ~2 mm. The mass of the shale sample and monofilament line combined is then recorded three times. The shale samples with monofilament lines attached are then ready to be placed into the imbibition vessels and perform the initial fluid measurements as seen below in Figure 3.7. This process is repeated for each shale sample that is to be tested.

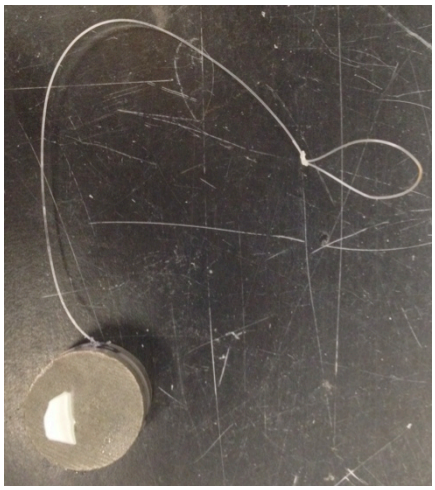

Figure 3.7 - Sample attached to monofilament line

3.2.2 Measurement module preparation

Before any imbibition measurements can be made, the measurement module must be prepared. If the experiment is going to be carried out at a temperature higher than ambient conditions then the oven must be set. The oven has a simple temperature control by means of a graded knob. To maintain a constant temperature, several large pieces of steel and sandstone were placed in the oven as thermal mass to help maintain a constant temperature in the oven even when the door is opened and closed during the experiment. The oven's temperature is set, monitored and adjusted until is it is the correct value using thermocouples, before any imbibition vessels were placed inside. The ultrasonic cleaner is used selectively only in the case of oil droplets attached to the surface of the shale sample. To use the ultrasonic cleaner, the unit is plugged in, turned on, and allowed to heat to the appropriate temperature. Once the unit is at the appropriate heat an imbibition vessel is placed inside and the cleaning function is activated. The imbibition vessel is

then removed and inspected every 30 seconds until the surface oil droplets are no longer visible.

3.2.3 Imbibition vessel preparation

The imbibition preparation can be broken into several discrete steps: equipment cleaning, fluid analysis and preparation, primary fluid and sample measurements and oven temperature calibration.

All components of the imbibition vessel must be cleaned before the start of the experiment. The beakers are the only component of the experiment that are reused, and must be cleaned to prevent contamination and endure a good experiment. The beakers are all thoroughly washed using laboratory soap and rinsed using deionized water. After a thorough rinsing, the beakers are dried off using chem wipes and set aside to await assembly of the other components of the imbibition vessel.

3.2.4 Imbibition fluid preparation

The fluid being tested is as fundamental to the rate of imbibition as the shale sample. The concentration and types of ions in the fluid that are going to be investigated are provided by the industry sponsor, in the form of either an ion report or a field brine sample. To minimize effects from unknown chemicals in the field, artificial brine is used in the imbibition vessel. If the industry sponsor provides an ion report, then the artificial brine procedure is followed and the following field brine preparation procedure is skipped.

The field brine is first unsealed, opened, and recovered, but not resealed. The unsealed field brine is placed in a fume hood for a period of 24 hours to ensure that any volatiles disperse. Once the volatiles have escaped, the field brine is vacuum filtered through a series progressively smaller of paper filters until it is passed through a 0.22-micron filter. The brine is then packaged and sent to an external lab for ion analysis.

The artificial field brine is mixed to the correct ion concentrations using the research sponsor provided ion report or the external lab ion report. To prepare the artificial brine, a clean Erlenmeyer flask is weighed dry and then filled with an amount of deionized water so that the water weight is known. The appropriate amounts of ions are then added in their chloride form and the brine is then vacuum filtered through a 0.22-micron paper filter to remove any particles. A beaker's dry weight is then recorded and approximately 200 milliliters of artificial brine is then poured into the beakers that will become the imbibition vessels.

After the brine is poured into the appropriate number of beakers for the number of imbibition vessels needing to be assembled, various surfactants and combinations of surfactants at given concentrations are added to all beakers with the exception of one, which will be the artificial field brine control. The beakers are then labeled with the surfactant combination and type of brine that they contain. To ensure that the surfactant is thoroughly dissolved in the brine, the beakers are then placed upon a stir plate until the surfactant is completely dissolved. The imbibition vessels are ready for the addition of their respective samples after dissolution of the surfactant mixture is achieved.

It is important to experimentally determine the density of the fluids used in the imbibition vessels, so that the rate of imbibition can be calculated accurately. The Sartorius Cubis balance can measure the density of fluids when combined with Sartorius density kit. The user simply assembles the density kit inside of the balance on the top-loading portion of the balance and hangs the 10-milliliter argon glass pendulum from the kit according to the included instructions. The user then selects the liquid density measurement program from the balance program menu and follows the instructions in the liquid density measurement program. The densities of all the brine and surfactant mixtures to be used in the experiment are then measured and recorded 3 times for each mixture.

3.3 Experimental Measurement Procedure

3.3.1 Primary fluid measurements

The shale sample is ready to be placed into the liquid of the imbibition vessel after the brine solution densities have been measured for each unique solution. The imbibition vessel is then placed on the lab-jack, and the shale sample is hung from the bottom-loading balance hook. The lab-jack is then raised until the suspended sample is completely covered by the brine. The lab-jack is adjusted until the fluid level of the imbibition vessel is even with the highest portion of the knot either the knot itself or the working end. The lab-jack control knob is then raised one-quarter turn more. The weight is then recorded and this process is repeated a total of 3 times. This measurement can also

be used to determine the volume of the sample more accurately than through the simple physical measurement using Archimedes principle.

3.3.2 Routine Experimental procedure

Once the primary measurements are made, the procedure becomes a routine process. Measurements are taken at the following time increments after primary exposure to the brine surfactant mixture: 2 hours, 12 hours, and then every 24 hours for 1 week. The processes can be broken into two measurements: air measurements and fluid measurements. Each measurement type is performed a total of three times. The imbibition vessel is removed from the oven, uncovered, and inspected for oil droplets on the surface of the shale sample. If there are no oil droplets present on the surface of the sample, the following step is bypassed.

If oil droplets are present on the surface of the sample then the imbibition vessel is recovered and replaced in the oven and the ultrasonic cleaner is prepped for use. The ultrasonic cleaner is prepared and the procedure as described in the measurement module preparation procedure previously is followed, until the oil, droplets are removed.

The surface oil droplet-free imbibition vessel is then placed upon the lab-jack and adjusted until the overhand loop can be attached to the bottom-loading balance hook. The lab-jack is then adjusted until the fluid level is even with the highest portion of the knot around the shale sample, either the knot itself or the working end. The lab-jack is then raised one-quarter turn more. The weight is then allowed to stabilize and then the measurement is taken and recorded.

The lab-jack is then lowered with the shale sample still attached to the balance until the shale sample is hanging approximately 2 inches above the rim of the beaker. A prepared paper towel is then placed atop the rim of the beaker and the lab jack is then raised so that the shale sample rests atop the paper towel. The paper towel folding procedure can be found in the Appendix. The shale sample is allowed to rest for a total of 15 seconds before it is lifted off the paper towel, the weight is allowed to stabilize for a total of 5 seconds, and then the mass is recorded. The paper towel is then removed and the shale sample is lowered into the fluid once more. The fluid and air measurement procedures are repeated 3 times each. The imbibition vessel is then recovered and replaced in the oven. This procedure is then repeated for each imbibition vessel that measurements are needed.

Chapter 4: Theory

4.1 THEORY

The fundamental basis for this experimental design was Archimedes principle, which relates the density, and volume of a sample through the measurement of a sample in two different density fluids. In the case of this experiment air and a brine surfactant mixture are the two fluids in which the shale sample is measured. This principle is used to measure the change of density of a shale sample as it undergoes spontaneous imbibition. It is important to understand the fundamental equations used to measure the volume of imbibition in this novel experiment in order to appreciate the results. The measurements made in this novel experiment can be broken up into three discrete groups: initial shale sample measurements, fluid density measurements, and shale sample measurements during spontaneous imbibition. From these fundamental measurements, the volume of oil or fluid saturating the pores displaced and the rate of imbibition can be calculated. The mathematical terms used in the theory section are defined as they are used and are additionally defined in the glossary.

4.2 INITIAL SAMPLE AND FLUID MEASUREMENTS

The initial measurements made on the prepared shale sample as described in the procedure are made before any contact with the brine solution. These initial measurements are the initial volume of the shale sample, $V_{\text{sample}}^{\text{initial}}$, and the initial measured

air weight, $W_{air}^{initial}$. The volume of the sample is measured physically with calipers as described in the procedure. This physical measurement is a good estimation of the volume, but it is not accurate measure of the true volume of the shale sample, as sometimes the cuts are not always parallel or symmetrical. Fortunately, it is possible to measure the volume of the sample using Archimedes principle, as shown below in Equation 1.

$$\rho_{fluid} * V_{sample}^{initial} = W_{air}^{initial} - W_{fluid}^{initial} \quad \text{.....(4.1)}$$

Where,

$W_{air}^{initial}$ — Measured initial air weight of shale sample

$W_{fluid}^{initial}$ — Measured initial weight of shale sample in the imbibition fluid

ρ_{fluid} — Measured density of imbibition fluid

$V_{sample}^{initial}$ — Initial volume of the shale sample

With some algebraic manipulation, the volume of the shale sample can be calculated from the shale sample's air weight measurement and its apparent weight immersed in the imbibition fluid as shown in equation 2.

$$V_{sample}^{initial} = \frac{W_{air}^{initial} - W_{fluid}^{initial}}{\rho_{fluid}} \quad \text{.....(4.2)}$$

This calculated volume value assumes that the fluid does not imbibe into the sample over short periods of time. It is more accurate than the caliper measured value as it accounts for any irregularities in the shale sample, as often the faces of the sample are

not parallel. Once the volume of the sample is known, it is relatively trivial to calculate the initial density, $\rho_{\text{sample}}^{\text{intial}}$, of the sample as shown below in equation 3.

$$\rho_{\text{sample}}^{\text{intial}} = \frac{W_{\text{air}}^{\text{intial}}}{V_{\text{sample}}^{\text{intial}}} \quad \rho_{\text{sample}}^{\text{intial}} = \frac{W_{\text{air}}^{\text{intial}}}{V_{\text{sample}}^{\text{intial}}} \quad \text{.....(4.3)}$$

This initial density calculation is paramount as Archimedes principle relates the measured weight difference of an object between two different fluids, which in this case are air, and a brine mixture. The apparent weight difference due to buoyancy allows for the calculation of the density of a sample. When a sample of known volume is measured, the density of the object can be measured from the measurements of the sample immersed in the fluid alone. This is shown in equation 4 and can be solved for by rearranging equation 1 and using the definition of $\rho_{\text{sample}}^{\text{intial}}$ in equation 3.

$$\rho_{\text{sample}}^{\text{intial}} = \frac{W_{\text{fluid}}^{\text{intial}}}{V_{\text{sample}}^{\text{intial}}} + \rho_{\text{fluid}} \quad \text{.....(4.4)}$$

4.3 IMBIBITION SAMPLE WEIGHT MEASUREMENTS

While Archimedes principle is rather well defined and straightforward as shown above in the theory and equations, some variation and complexity is introduced when measuring a sample of changing density as in the case of a sample undergoing spontaneous imbibition. The density of the sample changes with time as spontaneous imbibition progresses and one fluid displaces the other. As this displacement occurs, a

different density fluid displaces the fluid saturating the pore space, which causes an increase in weight as shown in equation 5.

$$\Delta W_{\text{air}}(t) = W_{\text{air}}(t) - W_{\text{air}}^{\text{initial}} \quad \text{.....(4.5)}$$

where,

t — The amount of time the sample has been exposed to imbibition fluid

$\Delta W_{\text{air}}(t)$ —Change in measured air weight of shale sample at time t

$W_{\text{air}}(t)$ —Measured weight of sample at time t

At any time, t, the measured weight of the shale sample immersed in the fluid, $W_{\text{fluid}}(t)$ is given by,

$$W_{\text{fluid}}(t) = W_{\text{air}}(t) - V_{\text{sample}}(t) * \rho_{\text{fluid}} \quad \text{.....(4.6)}$$

Preforming this method with shale also introduces a number of additional challenges beyond a sample of changing density, as the apparent fluid volume displaced by the shale sample is also subject to change if proper experimental practices are not followed. The change in the displaced fluid volume of the sample, $V_{\text{sample}}(t)$, is a function of the change of the volume from swelling of the shale sample due to fluid exposure, $\Delta V_{\text{swell}}(t)$, and is also a function of the volume of any droplets of oil stuck to the surface of the shale sample, $\Delta V_{\text{drops}}(t)$, which augment the apparent volume of displaced fluid. The relationship between $V_{\text{sample}}(t)$, $\Delta V_{\text{swell}}(t)$, and $\Delta V_{\text{drops}}(t)$ is shown

in equation 7. While $\Delta V_{\text{swell}}(t)$, and $\Delta V_{\text{drops}}(t)$ found in equation 7 are not easily measured in the experimental setting, it is possible to minimize these values through proper experimental procedure as described in chapter 2. It is important to note that $\Delta V_{\text{drops}}(t)$ is equal to zero when the sample is not immersed in the brine mixture, but the volume of the shale sample is still augmented by any swelling regardless of immersion or not.

$$V_{\text{sample}}(t) = V_{\text{sample}}^{\text{initial}} + \Delta V_{\text{swell}}(t) + \Delta V_{\text{drops}}(t) \quad \text{..... (4.7)}$$

Once $V_{\text{sample}}(t)$ is defined, it is possible to redefine the density of the shale sample as a function of time, $\rho_{\text{sample}}(t)$, as shown in equation 8, and in equation 9. Equation 8 and equation 9 each rely solely on air or fluid measurements respectively for the calculation of the density of the sample. Similarly, it is possible to define the change in density over time, $\Delta\rho_{\text{sample}}(t)$, can be redefined, and is shown below in equation 10, and in equation 11. Equation 10 and equation 11, like equation 8 and equation 9, also only rely on air or fluid measurements for the calculation of the change in density of the sample.

$$\rho_{\text{sample}}(t) = \frac{W_{\text{air}}(t)}{V_{\text{sample}}(t)} \quad \text{.....(4.8)}$$

$$\rho_{\text{sample}}(t) = \frac{W_{\text{fluid}}(t)}{V_{\text{sample}}(t)} + \rho_{\text{fluid}} \quad \text{.....(4.9)}$$

$$\Delta\rho_{\text{sample}}(t) = \frac{W_{\text{air}}(t)}{V_{\text{sample}}(t)} - \frac{W_{\text{air}}^{\text{intial}}}{V_{\text{sample}}^{\text{intial}}} \quad \text{.....(4.10)}$$

$$\Delta\rho_{\text{sample}}(t) = \frac{W_{\text{fluid}}(t)}{V_{\text{sample}}(t)} - \frac{W_{\text{fluid}}^{\text{initial}}}{V_{\text{sample}}^{\text{initial}}} \quad \text{..... (4.11)}$$

This change in density of the sample as a function of time can is attributed the exchange of fluids of differing densities in the pore space of the shale sample. The volume of the fluid saturating the pore space displaced, $V_{\text{pore fluid}}^{\text{displaced}}(t)$, by spontaneous imbibition is equal to the volume of the brine solution imbibed into the shale. This relationship is shown in equation 12, where the change of the measured weight of the shale sample in air is directly proportional to the difference in density between the two fluids times the volume of oil or pore fluid being displaced. In the case of this study, the preserved shale sample is assumed to be completely oil saturated and thus the density of the pore fluid is equal to the density of the produced oil. Additionally this implies that all the displaced pore fluid is oil.

$$\Delta W_{\text{air}}(t) = \left(\rho_{\text{fluid}} - \rho_{\text{pore fluid}}\right) * V_{\text{pore fluid}}^{\text{displaced}}(t) \quad \text{.....(4.13)}$$

where,

ρ_{fluid} —Measured density of imbibed brine solution

$\rho_{\text{pore fluid}}$ — Density of the pore fluid saturating the shale sample

$V_{\text{pore fluid}}^{\text{displaced}}(t)$ — The volume of displaced pore fluid due to spontaneous imbibition

The above equation, demonstrates the ability to empirically measure the volume of pore fluid or oil that is displaced by spontaneous imbibition through air weight measurements alone. However, in its current form it is not useful until it is solved for $V_{\text{pore fluid}}^{\text{displaced}}(t)$ as shown below in equation 13.

$$V_{\text{pore fluid}}^{\text{displaced}}(t) = \frac{\Delta W_{\text{air}}(t)}{\left(\rho_{\text{fluid}} - \rho_{\text{pore fluid}}\right)} \quad \text{.....(4.13)}$$

4.4 VOLUME OF IMBIBITION CALCULATED FROM FLUID MEASUREMENTS

While this is a valid solution to measure the volume of displaced pore fluid due to spontaneous imbibition, it is not the ideal solution in practice. The air weight measurements, $W_{\text{air}}(t)$, after exposure to the brine solution have a small and highly variable volume of brine solution adhered to the surface of the shale sample. This volume of brine solution can introduce a large amount error despite best experimental practices. However, the weight measurements made in the fluid are very repeatable, and accurate. Due to the higher accuracy of the fluid weight measurements, a method for calculating $V_{\text{pore fluid}}^{\text{displaced}}(t)$ using only weight measurements made in the brine solution or prior to exposure to the brine is required to minimize error. To achieve such a solution, an understanding of the relationship between the shale sample density, $\rho_{\text{sample}}(t)$, and $V_{\text{pore fluid}}^{\text{displaced}}(t)$ is needed. To develop this relationship, equation 12 can be divided through

by $V_{\text{sample}}(t)$ to develop the expression, equation 14, after some simplification and using the definition of $\rho_{\text{sample}}(t)$, and $\Delta W_{\text{air}}(t)$ from equation 8 and equation 5 respectively.

$$\rho_{\text{sample}}(t) = \frac{V_{\text{pore fluid}}^{\text{displaced}}(t) * \left(\rho_{\text{fluid}} - \rho_{\text{pore fluid}}\right) + W_{\text{air}}^{\text{initial}}}{V_{\text{sample}}(t)} \quad \text{.....(4.14)}$$

The density of the shale sample, $\rho_{\text{sample}}(t)$, can be measured as a function of only the fluid measurements and is defined in such terms in equation 9. When the definition of $\rho_{\text{sample}}(t)$ from equation 9 is substituted into equation 14, $V_{\text{pore fluid}}^{\text{displaced}}(t)$ becomes a function of only initial weight measurements and immersed fluid weight measurements. This relationship as shown in equation 15 introduces the smallest amount of error experimental error into the final calculations. Equation 15 can then be solved for $V_{\text{pore fluid}}^{\text{displaced}}(t)$ as shown below in equation 16.

$$\frac{W_{\text{fluid}}(t)}{V_{\text{sample}}(t)} + \rho_{\text{fluid}} = \frac{\left(\rho_{\text{fluid}} - \rho_{\text{pore fluid}}\right) * V_{\text{pore fluid}}^{\text{displaced}}(t) + W_{\text{air}}^{\text{initial}}}{V_{\text{sample}}(t)} \quad \text{.....(4.15)}$$

$$V_{\text{pore fluid}}^{\text{displaced}}(t) = \frac{\left(W_{\text{fluid}}(t) + \rho_{\text{fluid}} * V_{\text{sample}}(t) - W_{\text{air}}^{\text{initial}}\right)}{\left(\rho_{\text{fluid}} - \rho_{\text{sat fluid}}\right)} \quad \text{.....(4.16)}$$

The displaced volume of fluid by the shale sample is described in equation 7, and can be further simplified with the use of best experimental practices. For the purposes of establishing this novel experimental method the assumption was made that minimal swelling of the shale occurred such that $\Delta V_{\text{swell}}(t) \ll V_{\text{sample}}^{\text{initial}}$. The amount of swelling

depends upon the type of shale and varies upon the content of the brine solution. The assumption that the amount of swelling is much smaller than the volume of the sample allows for the neglection of this swelling term. Additionally, proper experimental practices allow for the neglection of $\Delta V_{\text{drops}}(t)$ due to the use of an ultrasonic cleaner which removes any surface droplets. When these terms are negligible, equation 7 reduces into the following definition.

$$V_{\text{sample}}(t) = V_{\text{sample}}^{\text{intial}} \quad \text{.....(4.17)}$$

The simplification of equation 7 allows for a redefinition of the density of the shale sample as defined in equation 9.

$$\rho_{\text{sample}}(t) = \frac{W_{\text{fluid}}(t)}{V_{\text{sample}}^{\text{intial}}} + \rho_{\text{fluid}} \quad \text{.....(4.18)}$$

Using this new definition of density of the shale sample, as shown in equation 18, allows for a different solution for $V_{\text{pore fluid}}^{\text{displaced}}(t)$ when combined with equation 14. While the significance of this is not visible at first, using the Archimedes principle from equation 1 in equation 19 simplifies the solution of $V_{\text{pore fluid}}^{\text{displaced}}(t)$ significantly, as shown in equation 20.

$$V_{\text{pore fluid}}^{\text{displaced}}(t) = \frac{\left(W_{\text{fluid}}(t) + \rho_{\text{fluid}} * V_{\text{sample}}^{\text{initial}} - W_{\text{air}}^{\text{initial}}\right)}{\left(\rho_{\text{fluid}} - \rho_{\text{sat fluid}}\right)} \quad \text{.....(4.19)}$$

$$V_{\text{pore fluid}}^{\text{displaced}}\left(t\right)=\frac{W_{\text{fluid}}\left(t\right)-W_{\text{fluid}}^{\text{initial}}}{\left(\rho_{\text{fluid}}-\rho_{\text{sat fluid}}\right)} \quad \text{.....(4.20)}$$

Equation 20 demonstrates that using Archimedes principle is a valid theoretical approach for measuring spontaneous imbibition in a shale sample when the fluids are of differing densities. This theoretical approach allows for a solution of the volume of the displaced pore fluid using only measurements made in the fluid, which are highly accurate and repeatable as shown in the following chapter.

Chapter 5: Results and Discussion

As shown in the previous Chapter, the theory behind this experimental method relies upon a few key assumptions, it is important to validate the theory with verifiable experimental results. This process is somewhat complicated as the experimental method was designed to measure spontaneous imbibition. The following Chapter evaluates the experimental results, the quality of the experimental setup, experimental procedure with an error analysis, checks to see if the results fall within expected bounds, and establishes metrics for to evaluate the validity of the assumptions made.

The first key assumption is that the density of the imbibition fluid in the imbibition vessel does not change significantly over the course of the experiment. To maximize the validity of this assumption the imbibition vessels are kept covered at all times, except when the measurement is performed. Another key assumption is that the fluid saturating the pore space is at residual water saturation (or at a lower water saturation), and that the density of that fluid consequently is equal to density of produced oil. This assumption could be made better if the saturation of the sample was known; unfortunately determining the saturation of a shale sample is a non-trivial problem. As a result of not having an established method for determining the initial saturation of preserved shale, a constant value was assumed. The final key assumption that is inherent to this experimental design is that during the course of the experiment no significant amount of fines are lost from the sample. The sample must stay intact during the course

of the experiment in order for the mass measurements to remain consistent. This can be checked visually by looking for any evidence of fines in the imbibition cell.

All of the Figures in this Chapter have error bars and if they are not visible then they are smaller than the marker size, and lines have been added to connect the data points for clarity unless otherwise stated. An error analysis for our methods namely Archimedes method is not novel (Power, 1996), but has additional complications in the context of measuring imbibition in shale. A comparative analysis of the experimental results from all the samples and comparison of the Bakken and Utica will be discussed in Chapter 6.

5.1 Evaluation of Theory

5.1.1 Initial sample and fluid measurements

The following section will evaluate the theory discussed in the previous Chapter through the examination of the measured data from a single Bakken shale sample undergoing spontaneous imbibition in simulated reservoir brine. This data set is part of the data collected in the second Bakken experiment that is discussed in length later on in the Chapter. As described in the procedure in Chapter 3 and in the theory in Chapter 4, the experiment begins with establishing the fundamental physical properties of the different fluids and the shale sample or samples.

These quantities for the example Bakken Shale sample can be found in Table 5.1. These measurements and calculations must be made before any analysis of the data can

be preformed. Table 5.1, has all the relevant initial measurements for the data set examined to evaluate the theory described in the previous Chapter.

Table 5.1: Initial sample and Fluid 2 measurements of example Bakken shale sample.

Parameter	Symbol	Source of parameter	Units	Value
Initial air weight	$W_{\text{air}}^{\text{initial}}$	Measured with Balance	Grams	26.9534 g ± 5.00E-5 g
Initial fluid weight	$W_{\text{fluid}}^{\text{initial}}$	Measured with Balance	Grams	15.6299 g ± 5.00E-5 g
Density of imbibition fluid	ρ_{fluid}	Measured with Balance	Grams per Cubic Centimeter	1.110 g/cc ± 5.00E-4 g/cc
Density of pore saturating fluid	$\rho_{\text{pore fluid}}$	Measured or Assumed	Grams per Cubic Centimeter	0.823 g/cc ± 5.00E-4 g/cc
Archimedes bulk volume	$V_{\text{sample}}^{\text{initial}}$	Calculated using equation 4.2	Cubic Centimeters	10.212 cc ± 4.60E-3 cc
Total porosity	ϕ_{Total}	Measured or literature value	Percent of Bulk Volume	10.07% ± 0.005%
Total pore volume	$V_{\text{Pore Total}}$	Calculated using equation A.1	Cubic Centimeters	1.0284 cc ± 1.49E-3 cc
Diameter	d	Measured	Centimeters	2.41 cm ± 5.00E-5 cm
Length	L	Measured	Centimeters	2.240 cm ± 5.00E-5 cm
Characteristic Length	L_c	Calculated using equation (2.4)	Unitless	0.294 ± 1.36E-5

5.1.2 Comparing Air and Fluid Measurements

After the shale sample and fluids are characterized through the initial measurements, only weight measurements are made of the sample at defined time steps.

Two types of weight measurements are made at any time after fluid contact: air weight measurements of the shale sample and the apparent weight of the sample immersed in the imbibition fluid. The fluid weight measurements are lighter than the air measurements due to buoyancy caused by the displaced volume of the sample.

As discussed in the previous chapter, the goal of these measurements is to measure the weight gain of the sample as a result of spontaneous imbibition. Both the fluid or air weight measurements can be used to accomplish this goal given a sample that does not undergo swelling. To confirm the presence or absence of swelling and consequently the misrepresentation of the weight gain due to spontaneous imbibition in the fluid measurements both air and fluid weight measurements must be made at each time step.

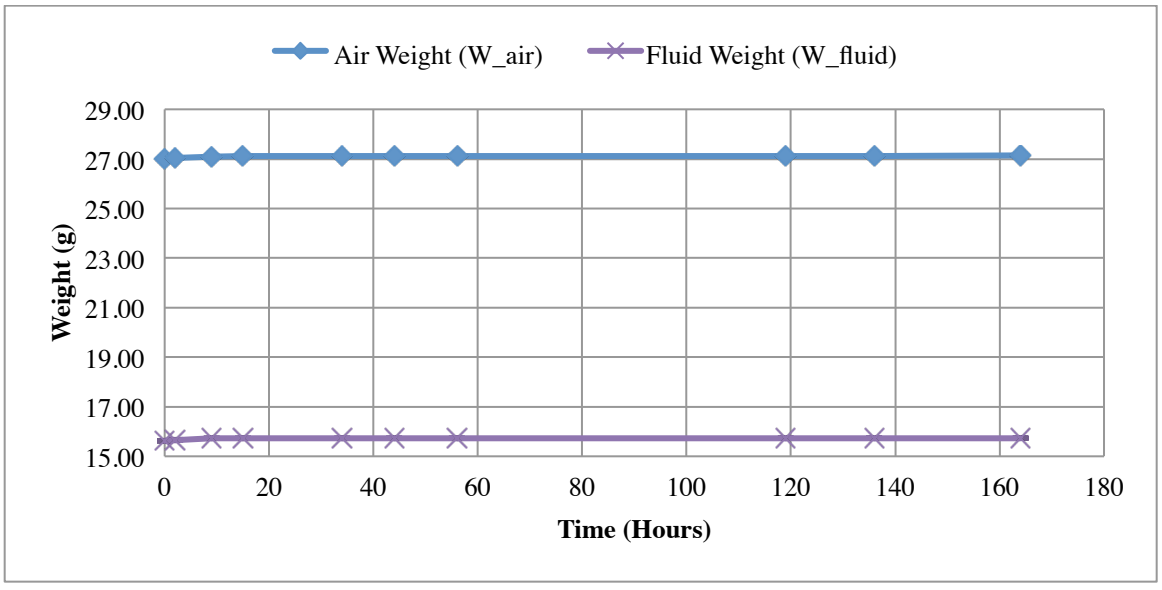

Figure 5.1: Measured fluid and air weights of the example Bakken sample.

Figure 5.1 plots the values of the fluid and air weight measurements as function of time for the example Bakken shale sample. At first glance these two measurements seem to undergo very little change as a function of time; however, this is not the case if we look at the mass change as a function of time, rather than absolute mass. Figure 5.2 plots the change in weight of the air weight and fluid weight measurements respectively.

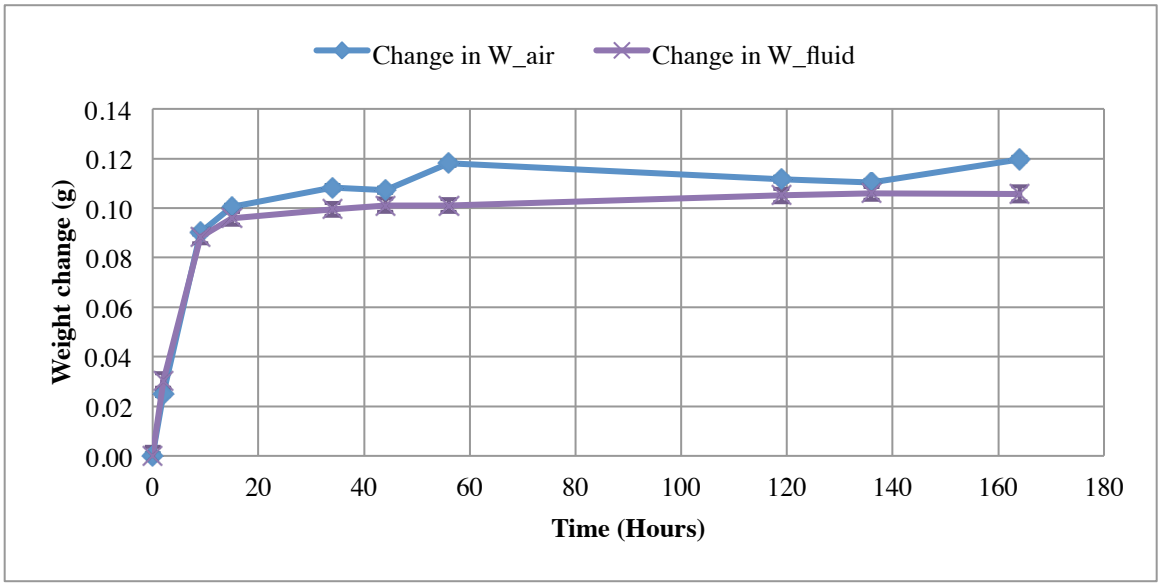

Figure 5.2: Change in measured air and fluid weights of the example Bakken sample.

By examining Figure 5.2 it is immediately apparent that the air weight and fluid weight measurements are not equal at every time step. The second observation made is that the air weight measurements seem to be noisy or the sample gained and lost weight rapidly, which is inconsistent with expected effects of imbibition or swelling. As the trend is not also observed in the fluid weight measurements this lack of equivalence is most likely error due to some factor other than imbibition or swelling.

While Figure 5.2 is of more interest than Figure 5.1 as the change in mass is due to fluid imbibition, the analysis must be sample size independent. The percent weight change compared to the original air weight is important when multiple samples are compared, as the initial mass will likely not be equivalent. The percent change in mass of the sample is presented in Figure 5.3. Both the fluid and air weight measurements are compared to the original air weight, as any weight change should be equal in constant volume case.

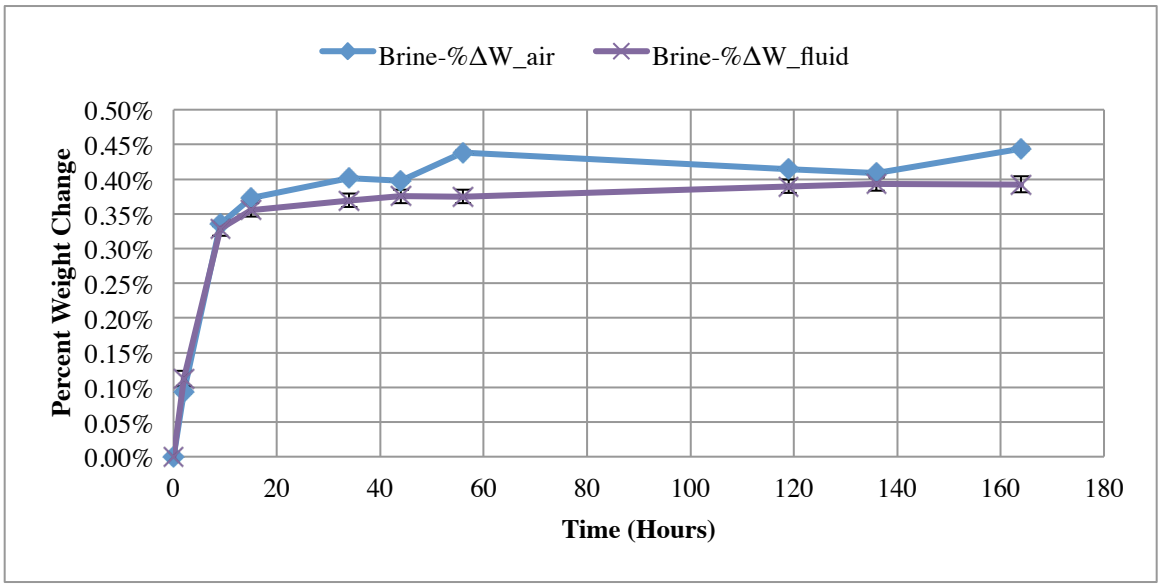

Figure 5.2: Percent change in measured air and fluid weight of initial air weight of the example Bakken sample.

However, the percent change in measured fluid and air weights are not equivalent. The percent change in measured air weight follows an increasing time dependent trend as anticipated with imbibition, but fluctuates up and down between measurements. This oscillatory behavior is most likely not due to swelling or imbibition. An increase in

volume of the sample due to swelling should only affect fluid measurement, and would be observed as decrease in the measured fluid weight. Imbibition of a denser fluid should not cause a decrease in sample weight at any time. As imbibition often occurs at a steady time dependent rate and only the air weight measurements are affected, the oscillatory behavior observed is most likely not due to either of these phenomena.

When the sample is removed from the imbibition a thin film of imbibition fluid is adhered to the surface of the sample. The experimental procedure attempts to minimize the volume of this thin film adhered to the surface by allowing the sample to rest on a paper towel. The paper towel succeeds in reducing the total volume of fluid adhered to the surface, but it does not always remove the same amount of water from the surface of the shale sample. As a result the variation in the air weight measurements is likely due to the variations in this film of surface fluid.

Despite the small fluctuations in the air weight measurements due to the variance in volume of the thin fluid film, another trend is apparent. Both the fluid and the air measurements follow nearly identical trends. This equivalence in the relative weight gain between the two measurements agrees with the theory for a constant volume sample. The difference between the two measurements is can be seen in Figure 5.3.

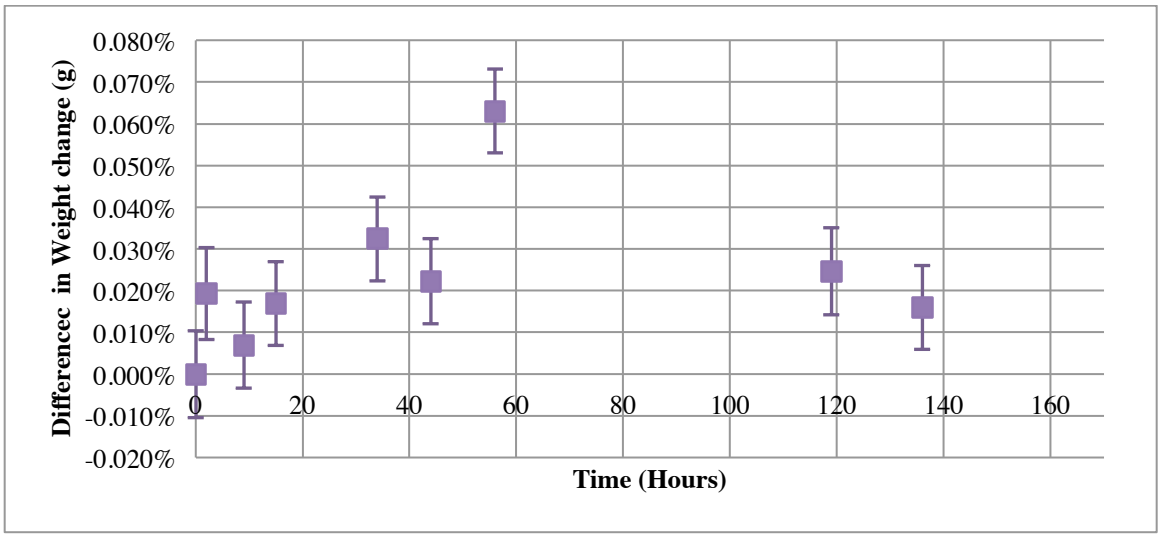

Figure 5.3: Percent difference between change in measured air and fluid weights, $\left|\%\Delta W_{\text{air}}(t) - \%\Delta W_{\text{fluid}}(t)\right|$, of the example Bakken sample.

When a sample does not undergo any significant change in volume due to fluid exposure, the relative weight change should be identical in both the fluid and air weight measurements and it nearly is identical in this case as seen in Figure 5.3. The average difference between the two measurements is less than 10 milligrams or 0.05% of the sample weight. This variance will later be shown to fall well within the realm of the variability due to the changing amount of imbibition fluid adhering to the surface of the shale sample.

The relationship between the relative changes in weight is best demonstrated by through the examination of Equations 4.10 and 4.11. These equations define the relationship between the change in density of the sample, $\Delta\rho_{\text{sample}}(t)$, and air or fluid weight measurements respectively. The change in density of the sample should be

equivalent regardless of the measurement used to calculate the change. The equivalence between equations 4.10 and 4.11 in the case of a constant volume sample $\left(\text{i.e. } V_{\text{sample}}(t) = V_{\text{sample}}^{\text{intial}}\right)$ simplify to $\Delta W_{\text{air}}(t) = \Delta W_{\text{fluid}}(t)$. To make this equivalence sample size independent, it becomes $\%\Delta W_{\text{air}}(t) = \%\Delta W_{\text{fluid}}(t)$ by dividing both sides by the original air weight. This validity of this equivalence and its implications will be further demonstrated in the following section.

5.1.3 Examining Volume Change

The volume of the sample can be calculated using Archimedes principle (equation 4.6), and the initial measured fluid and sample properties (shown in table 5.1). This volume $\left(V_{\text{sample}}(t)\right)$ can be calculated before fluid exposure, and at any other time where both fluid and air weight measurements are made concurrently. However examining absolute volume of the sample is not as useful for examining the percent change in volume as shown in Figure 5.4.

The percent change of $V_{\text{sample}}(t)$ relative to the original volume changes very little over the course of the experiment and follows no clear trend. The change in volume of the sample varies slightly between negative 0.05% and positive 0.10%. This volume of swelling is rather small and is made potentially insignificant once error is considered as will be shown later. The main source of error in this calculation is the inclusion of the air weight measurements, which are affected by the variance in the weight in the volume of

thin fluid film adhered to the surface. Any fluctuations in the thin film of surface fluid adhering to the sample during the air weight measurements would also propagate into the change in volume calculation. This apparent change in volume is most likely the cause of the variations in volume of the shale sample.

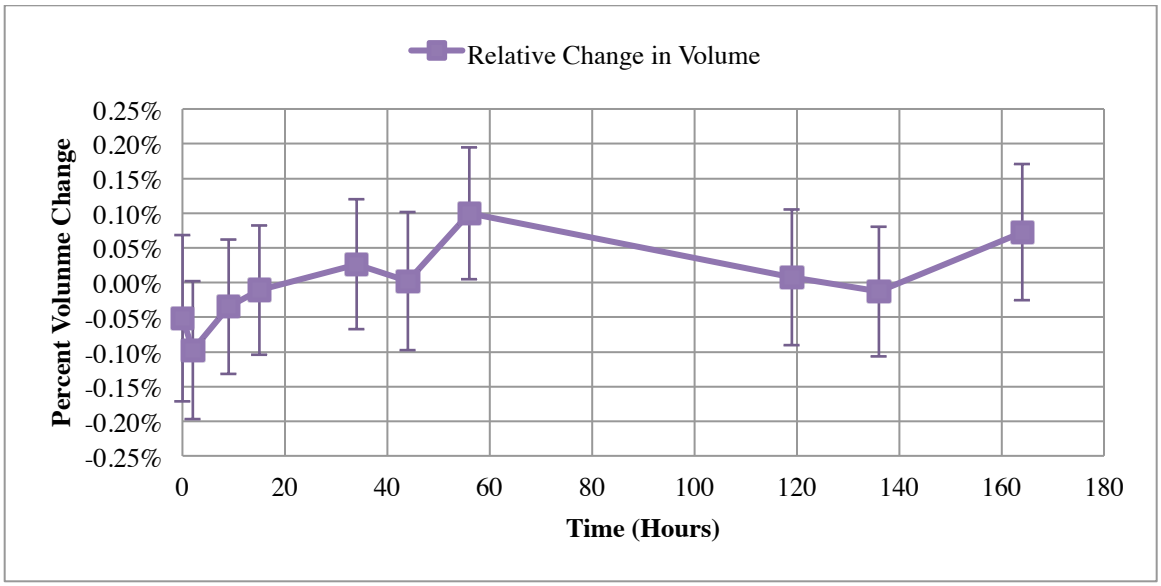

Figure 5.4: Relative change of the volume of the example Bakken sample where $\%V_{\text{sample}}(t) = \frac{\Delta V_{\text{sample}}(t)}{V_{\text{sample}}^{\text{intial}}}$.

5.1.4 Volume of Fluid Adhering to Surface of sample: Archimedes Air Weight

Thin to thick fluid surface adhesion is a phenomenon exploited in other industries to apply liquid coatings to solid substances (Qu, 2002). However, this phenomenon is potentially one of the largest sources of error in this experimental measurement. The thickness of the fluid film adhering to a solid surface is a function of the shear viscosity of the fluid, the density of the fluid, the velocity of removal, interfacial, or surface tension

(Landau, 1942; Morey 1940; Qu, 2002; Krechetnikov, 2006). As surfactants change the surface tension, different film thicknesses and thus different total volumes of adhering fluid on the surface would most likely be expected (Krechetnikov, 2006). The controlling factor most likely in this experiment is the withdrawal speed from the fluid and the subsequent exposure to the paper towel.

The paper towel adsorbs a portion of the fluid film off of the sample, and reduces the overall error. Though the volume of fluid adhered to the surface of the sample cannot be measured it can be calculated using Archimedes principle when the sample volume remains constant $\left(V_{\text{sample}}\left(t\right)=V_{\text{sample}}^{\text{intial}}\right)$. The measured air weight values should be equivalent to values calculated using Archimedes principle (Equation 5.1). This calculated air weight will be henceforth referred to as the Archimedes air weight.

$$W_{\text{Archimedes air}}\left(t\right)=W_{\text{fluid}}\left(t\right)+V_{\text{sample}}\left(t\right)*\rho_{\text{fluid}} \quad \text{.....(5.1)}$$

Equation 5.1 demonstrates the relationship between the measured fluid weight and the Archimedes air weight, $W_{\text{Archimedes air}}\left(t\right)$. Though this relationship is logical theoretically, due to the fluid adhering to the surface of the shale sample the Archimedes air weight is not equivalent to the measured air weight of the sample as seen in Figure 5.5. The following figures, table, and equations will quantify the variability due to the weight of the adhering surface fluid, $W_{\text{surface fluid}}\left(t\right)$.

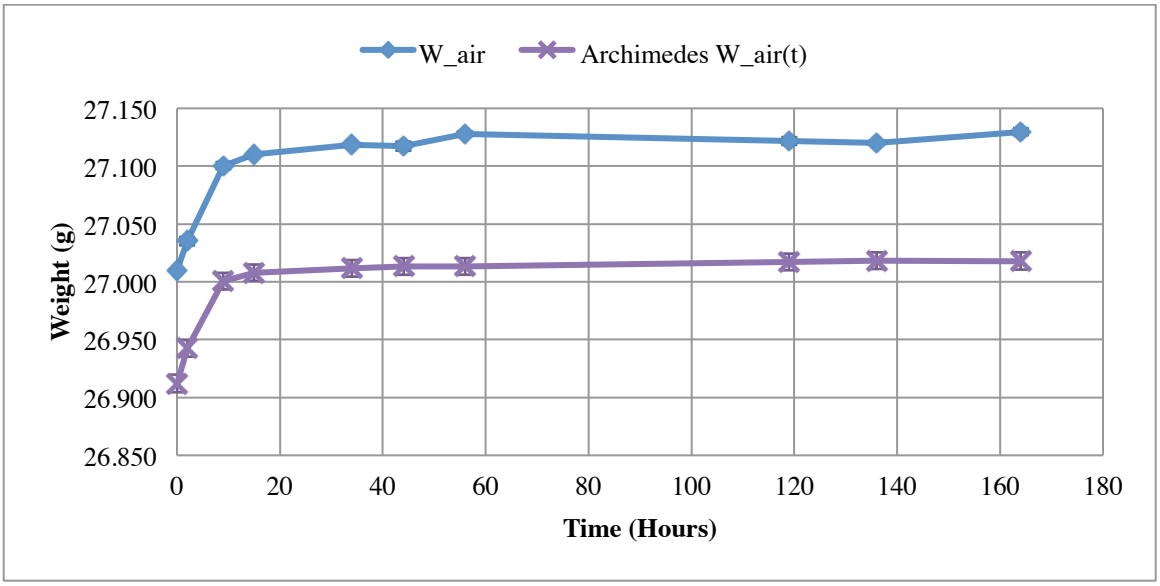

Figure 5.5: Measured air weights and Archimedes calculated air weight of the Bakken brine shale sample.

$$W_{air}(t) = W_{surface\ fluid}(t) + W_{Archimedes\ air}(t) \quad \text{(5.2)}$$

The difference between $W_{Archimedes\ air}(t)$ and $W_{air}(t)$ defined as $W_{surface\ fluid}(t)$ (Equation 5.2) is shown below in Figure 5.6 as percent $W_{surface\ fluid}(t)$ of original air weight. As previously hypothesized, there is not a constant amount of fluid adhering to the surface of the shale sample. The weight of the fluid adhering to the surface falls within a limited range of 0.14% to 0.23% of original dry weight (40 to 60 milligrams), but there is not a distinct trend. This calculation relies upon the constant volume assumption, and if there was a prevalent trend, then this assumption is most likely invalid as swelling is a time dependent phenomena. Equation 5.3 shows the relationship between the surface fluid, the Archimedes air weight, and the measured air weight. $W_{surface\ fluid}(t)$.

As Equation 5.3 demonstrates, the change in the air weight measurements is due to both the mass change due to spontaneous imbibition, and the mass of the fluid adhering to the surface of the sample. The values plotted in Figure 5.6, are calculated using equations 5.1 and 5.3. The surface fluid density is assumed to be the imbibition fluid as the ultrasonic cleaner removes any oil layer. With a known density of the surface determining the volume of the fluid on the surface is straightforward and shown in equation 5.4.

$$W_{\text{surface fluid}}(t) = W_{\text{Archimedes air}}(t) - W_{\text{air}}(t) \quad \text{.....(5.3)}$$

$$V_{\text{Surface fluid}}(t) = \frac{W_{\text{surface fluid}}(t)}{\rho_{\text{fluid}}} \quad \text{.....(5.4)}$$

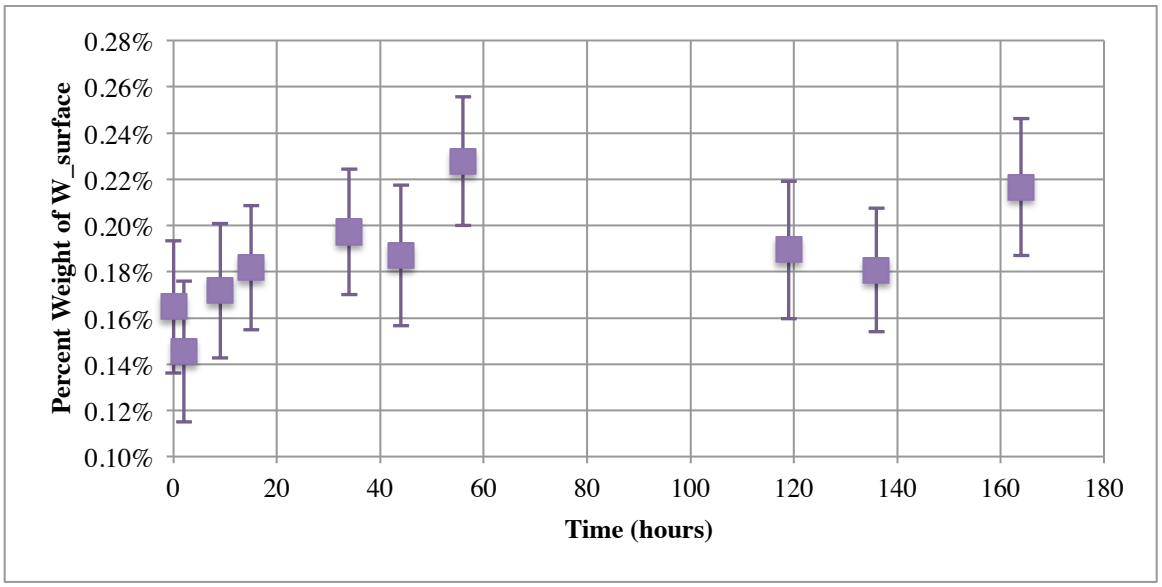

Figure 5.6: Percent weight of adhered surface fluid film of example Bakken sample.

$$\Delta W_{air}(t) = \Delta W_{Archimedes\ air}(t) + \Delta W_{surface\ fluid}(t) \quad (5.5)$$

While the ability to calculate an estimate of the mass of adhered fluid film measured during the air measurements is useful, the change in weight of the adhered film of surface fluid is more useful in this experimental analysis. The change in the Archimedes calculated air weight ($\Delta W_{Archimedes\ air}(t)$, Equation 5.5) should be considered the ideal value of change in measured air weight for a sample with no adhered fluid film. As $W_{surface\ fluid}(t)$ is not constant, the measured values of $\Delta W_{air}(t)$ differ from this ideal value by $\Delta W_{surface\ fluid}(t)$ as shown in Equation 5.6 and 5.7.

$$\Delta W_{air}(t) = \Delta W_{fluid}(t) + \Delta W_{surface\ fluid}(t) \quad (5.6)$$

$$\Delta W_{surface\ fluid}(t) = \Delta W_{air}(t) - \Delta W_{fluid}(t) \quad (5.7)$$

Table 5.2: Average values of weight and volume of fluid adhering to surface of the example Bakken sample during air weight measurements.

$\overline{W_{surface\ fluid}(t)}$	$\overline{\frac{W_{surface\ fluid}(t)}{W_{air}^{intial}}}$	$\overline{V_{Surface\ fluid}(t)}$	$\overline{\left(\frac{V_{Surface\ fluid}(t)}{V_{sample}^{intial}}\right)}$	**Thicknes of Fluid Film**
0.0502 g ± 0.0077 g	0.19% ± 0.029%	0.0452 cc ± 0.0070 cc	0.443% ± 0.0681%	0.0191 mm ± 0.0930 mm

As shown in Table 5.2, average values for the adhered surface fluid and error in these values can easily be calculated using the above equations. The error in the weight of

adhered surface fluid is the larger value of the standard deviation of the calculated values of the mass of the surface fluid or the error propagation through the calculations.

The values presented in Table 5.2 are useful for understanding the relative volume and mass of fluid adhering to the surface of the shale sample. These average values of the surface fluid do provide a full picture or evaluate of the precision of the experimental measurements. A few metrics for analysis of the quality of the results are needed as this experimental method relies upon such a number of assumptions namely minimal shale swelling.Shale swelling is formation and mineralogy dependent as discussed in Chapter 2. When the shale sample swells additional error is added, as now the fluid measurements are no longer accurate. This complicates the calculation of the volume of surface fluid as shown in equation 5.8. Additionally while swelling occurs as described in Chapter 4, the difference in air and fluid weight measurements are no longer equal, leaving two unknowns.

$$\Delta W_{\text{surface fluid}}\left(t\right)=\Delta W_{\text{air}}\left(t\right)-\Delta W_{\text{fluid}}\left(t\right)-\Delta V_{\text{sample}}\left(t\right)\rho_{\text{fluid}} \quad \text{.....(5.8)}$$

$$\Delta W_{\text{air}}\left(t\right)=V_{\text{pore fluid}}^{\text{displaced}}\left(\rho_{\text{fluid}}-\rho_{\text{pore fluid}}\right)+\Delta W_{\text{surface fluid}}\left(t\right) \quad \text{.....(5.9)}$$

$$\Delta W_{\text{fluid}}\left(t\right)=V_{\text{pore fluid}}^{\text{displaced}}\left(\rho_{\text{fluid}}-\rho_{\text{pore fluid}}\right)-\Delta V_{\text{sample}}\left(t\right)\rho_{\text{fluid}} \quad \text{.....(5.10)}$$

where,

$$V_{\text{pore fluid}}^{\text{displaced}}=V_{\text{fluid}}^{\text{imbibed}}$$

Unfortunately, there is no way to decouple the air weight measurement of the sample and the adhered fluid film nor is there a way to decouple the fluid weight

measurement from swelling as shown in Equations 5.9 and 5.10 respectively. The following metrics will assist in determining the source of variance from theoretical values, the validity of the constant volume assumption, and consequently what is the best source of measurements for calculating the volume of pore fluid displaced: Either the noisy air measurements, or the repeatable fluid based measurements. This addition of error in both sources of measurements requires a method for quantifying the relative amount of error to the measurements made. In the following section, two metrics are proposed to determine the measurement source with the lowest error, and examine the validity of the assumptions discussed previously. The following metrics rely on the use of both the fluid and air weight measurements, but through the use of the two graphical methods in conjunction a conclusion on the precision of each respective measurement can be inferred.

5.2 Metrics for Evaluation of Assumptions, and Measurement Precision

5.2.1 Air Weight Measurement Precision and Variance of Adhered Fluid Film

The air weight measurements are noisy and lack precision over the duration over the experiment due to the changing volume of fluid film. This first metric consists of graphical methods for examining the relative change, and volume of this fluid film. It is important to recall that the calculation of the volume of the surface film is dependent upon the use of the fluid weight measurements. As such the relative amount of error added due to swelling is not known, but any error added should present itself as a time dependent shift of the data. The first metric consists of two components: the weight, and

change in weight of the thin film of surface fluid relative to the weight of the sample, and the existence of a strong correlation between $\Delta W_{\text{surface fluid}}(t)$ and time.

If the constant volume assumption is true, then the percent changes in measured weight should be equal in both the fluid and air weight measurements if the air weight measurements have been corrected by accounting for the weight of the of adhered surface fluid. Consequently the variation from equivalence in measured weight change is described by the following expression in Equation 5.11. This equation expresses that any deviation from equivalence is due to a variation in the mass of the thin film of fluid adhered to the surface of the shale sample.

$$\frac{\Delta W_{\text{surface fluid}}(t)}{W^{\text{intial}}_{\text{air(dry)}}}\% = \left| \frac{\Delta W_{\text{air}}(t)}{W^{\text{intial}}_{\text{air(dry)}}}\% - \frac{\Delta W_{\text{fluid}}(t)}{W^{\text{intial}}_{\text{air(dry)}}}\% \right| \quad \text{.....(5.11)}$$

$$\frac{\Delta W_{\text{surface fluid}}(t)}{W^{\text{intial}}_{\text{air(dry)}}}\% = \left| \frac{\Delta W_{\text{air}}(t)}{W^{\text{intial}}_{\text{air(dry)}}}\% - \frac{\Delta W_{\text{fluid}}(t)}{W^{\text{intial}}_{\text{air(dry)}}}\% + \Delta V_{\text{sample}}(t)\rho_{\text{fluid}} \right| \quad \text{.....(5.12)}$$

While Equation 5.11, relies upon the constant volume assumption as previously described, the change in measured fluid weight from swelling would show up as a time dependent increase as described in Equation 5.12. Though a time dependent increase in adhered fluid volume could be due to wettability modification of the surface from surfactant as dip coating equations are a function of contact angle. As the wettability modification of the shale samples due to aging in an aqueous surfactant mixture has not been examined, any consistent time dependent increase in the volume of fluid volume

adhered to the surface will be attributed to swelling rather than an increase due to wettability modification of the exposed surface of the shale sample.

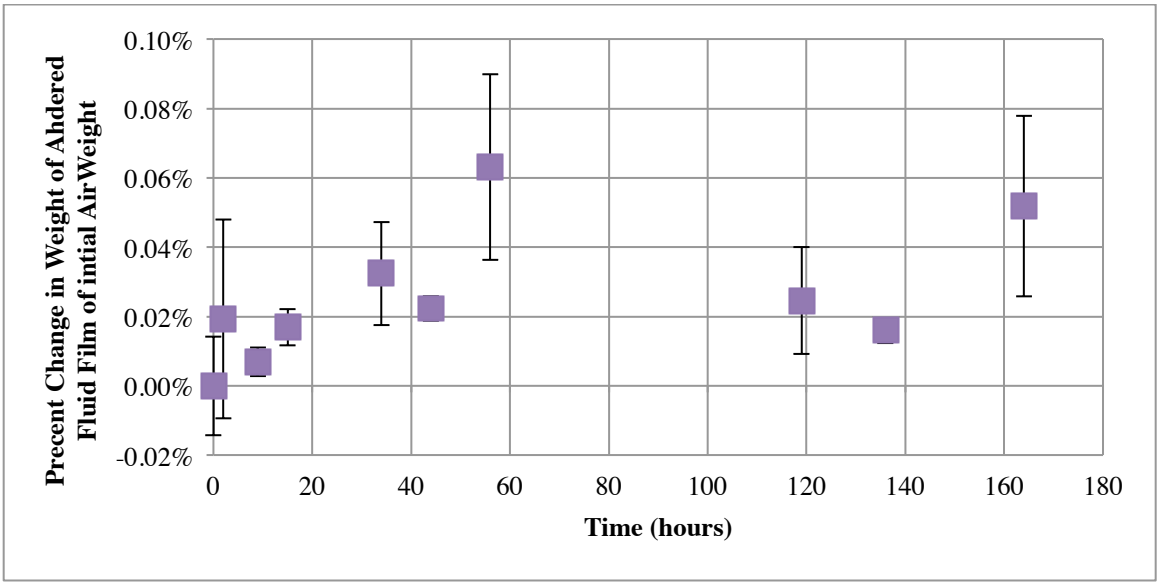

Figure 5.7: Change in Weight of Fluid Film Adhered to example Bakken Sample.

The calculated values of $\Delta W_{\text{surface fluid}}(t)$ from Equation 5.11 are presented in Figure 5.7. While this figure clearly shows that relative change in measured weight is rather small and not time dependent, this is not the most useful figure for determining if the change in volume of adhered thin surface fluid is a realistic value. The real measure of this quantity is best measured by the change in thickness of the surface fluid film, which can be calculated using Equation 5.13, and shown in Figure 5.8.

$$\Delta h(t) = \frac{\Delta W_{\text{surface fluid}}(t)}{\rho_{\text{fluid}} A_{\text{surface}}^{\text{intial}}} \quad \text{.....(5.13)}$$

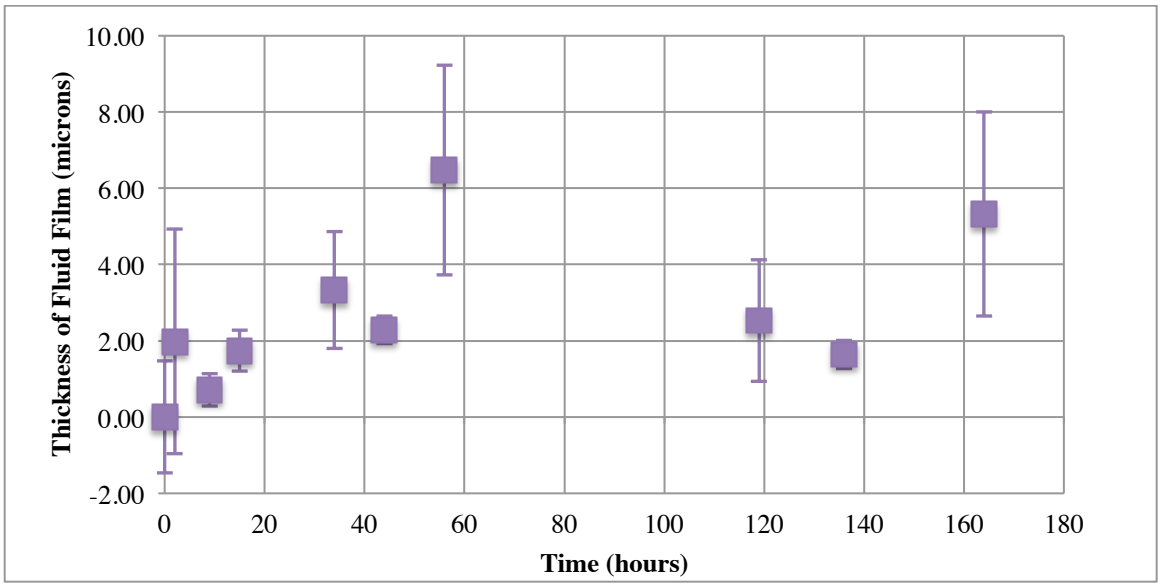

Figure 5.8: Variance of thickness of adhered thin fluid film relative of example Bakken sample.

Figure 5.8, presents the change in thickness of the fluid of thin film adhered to the sample assuming a constant distribution as defined in Equation 5.13. While this assumption does not account for gravity, it is reasonable as the total change in thickness of fluid film adhered to the surface of the sample is just a few microns. The calculated value of fluid thickness is small to the overall thickness of the overall sample, but varies by up to 40% from the average value presented in table 5.2. This change of the relative thickness of the adhered surface fluid is quit significant, compared to its overall value. This plot demonstrates that less than an 8-micron change in thickness of the fluid layer adhered to the surface can be a major contributing factor to the error of the air weight measurements.

The sample size is an important consideration when it comes to comparing the relative thickness of the adhered surface fluid film to the both the bulk volume and pore volume of the sample. As the sample size increases, the bulk volume and consequently the pore volume of the sample increases the relative volume of fluid film decreases. The thickness of the fluid film does not increase in proportion to the increase in bulk volume. This property should imply using a sample size as large as possible, but this is not ideal as the surface area to volume ratio controls imbibition rate.

As the ratio of surface area is a function of sample size, as sample size is increased the total time required for imbibition increases, and number of tests that can be preformed upon preserved shale decreases as there is a limited quantity of preserved samples. Consequently there is there is a limiting rate of return in exchange for gained accuracy, as the total quantity of tests will decrease. The goal must be to properly choose a sample size that minimizes the relative volume of the adhered fluid film to the pore volume.

$$\%V_{\text{surface fluid}}\left(t\right)=\frac{W_{\text{surface fluid}}\left(t\right)}{\rho_{\text{fluid}}V_{\text{pore}}} \quad \text{.....(5.14)}$$

$$\%\Delta V_{\text{surface fluid}}\left(t\right)=\frac{\Delta W_{\text{surface fluid}}\left(t\right)}{\rho_{\text{fluid}}V_{\text{pore}}} \quad \text{.....(5.15)}$$

The fluid film thickness is important as the variance affects the calculated volume of displaced fluid as previously described. The volume and the change in volume of the fluid film adhered to the surface to the pore volume is expressed in Equations 5.14 and

5.15 respectively. The relationship between sample size, expressed in pore volume, and the relative volume of fluid adhered to the surface of the sample is shown in Figure 5.9.

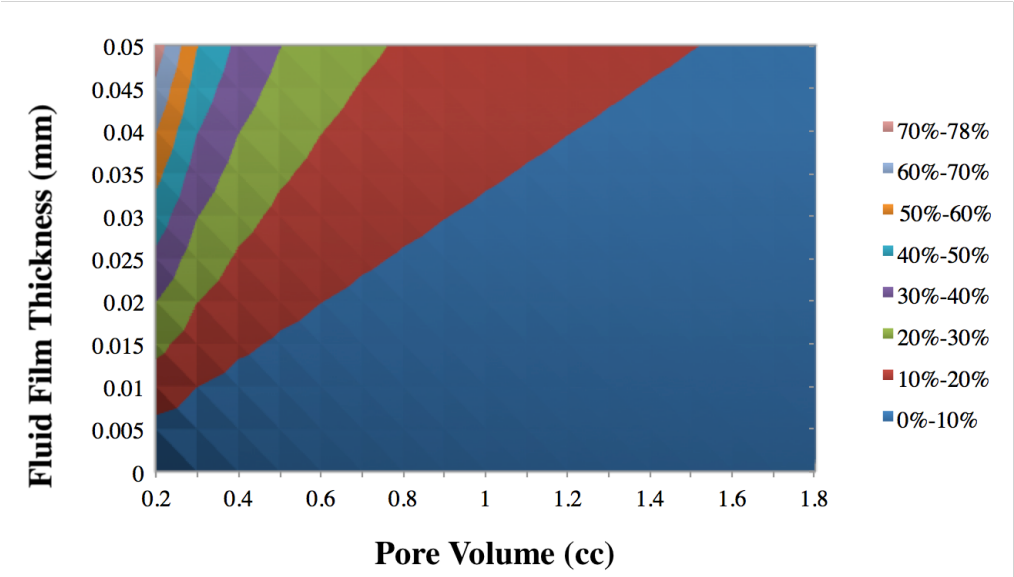

Figure 5.9: Contour plot of percent Volume of pore volume of fluid film as function of thickness of film and length of 1-inch diameter by 1-inch long core plug.

Figure 5.9, demonstrates that it is important to choose a sample size large enough that the relative volume of fluid on the surface is less than the volume of adhered surface fluid. Though the total volume of surface fluid is accounted for in the weight change, the variance between measurements can have a significant impact. This thickness can vary by up to nearly 10 microns or 0.01 millimeters. This variance as shown in Figure 5.8 can create a large error if the pore volume is too small.

Due to this sensitivity to both measurements, this is an ideal graphical metric for examining if the fluid measurements can be trusted to be representative of the true mass change. If the plot of $\Delta W_{\text{surface fluid}}(t)$ exhibits any time dependent increase, then the fluid

measurements are consistently less than the air weight measurements. If the fluid weight measurements are representative of the sample, then $\Delta W_{\text{surface fluid}}(t)$ will vary a small amount but will not exhibit time dependent increase.

5.2.2 Fluid Weight Precision and Volume Change of Sample

Though the first metric allows for a graphical analysis of swelling, the change in volume of the sample can be directly calculated using Archimedes method. Though this calculated volume change, is not decoupled from the variance in air weight measurements previously described. For the fluid measurements to be representative of the change in mass due to spontaneous imbibition, a consistent increase in volume must be visible. This calculation has a large amount of error due to the propagation of uncertainty in measurement, which is further compounded by the variance in the thickness of the fluid film in the air weight measurements.

The volume of the sample calculated from Archimedes principle is a function of the density of the fluid, and the air and fluid weight measurements as shown in Equation 5.16. It is important to recall that the weight or change in weight of the surface fluid cannot be directly measured and will be neglected in the following equations though it is still coupled to the measured air weight. The change in volume and relative change in volume are represented in 5.17 and 5.18 accordingly.

It is important to recall in the case of a constant volume sample that the change in air and fluid weight measurements are equivalent, symbolically represented as

$V_{sample}(t) = V_{sample}^{intial}$ and $\Delta W_{air}(t) = \Delta W_{fluid}(t)$ respectively. Equation 5.18 can be simplified to Equation 5.19 in the case of sample that does not undergo swelling. As the weight or change in weight of the fluid film cannot be measured it will be neglected, in the following calculations.

$$V_{sample}(t) = \frac{W_{air}(t) - W_{surface\ fluid}(t) - W_{fluid}(t)}{\rho_{fluid}} \quad \text{.....(5.16)}$$

$$\%\Delta V_{sample}(t) = \frac{\Delta W_{air}(t) - \Delta W_{fluid}(t)}{\rho_{fluid} V_{pore}} \quad \text{.....(5.17)}$$

$$\%\Delta V_{sample}(t) = \frac{\Delta W_{air}(t) - \Delta W_{fluid}(t)}{\rho_{fluid} V_{sample}^{intial}} \quad \text{.....(5.18)}$$

$$\%\Delta V_{sample}(t) = \frac{\Delta W_{surface\ fluid}(t)}{\rho_{fluid} V_{sample}^{intial}} = \frac{\Delta V_{surface\ fluid}(t)}{\rho_{fluid} V_{sample}^{intial}} \quad \text{.....(5.19)}$$

Equitation 5.19 implies that even in the case of a constant volume sample, the calculated change in volume will be sensitive to variance in the thickness of the fluid film. As such any plot of the change in volume of the sample where the percent change is within the range of the error caused by the changing thickness the adhered surface fluid can be assumed to have minimal to no swelling. The values for the calculated change in volume as a function of pore volume (Equation 5.17) of the example Bakken shale sample is shown in Figure 5.10. Figure 5.10 demonstrates little to no positive correlation with time, and as a result the volume of swelling can be assumed to be minimal.

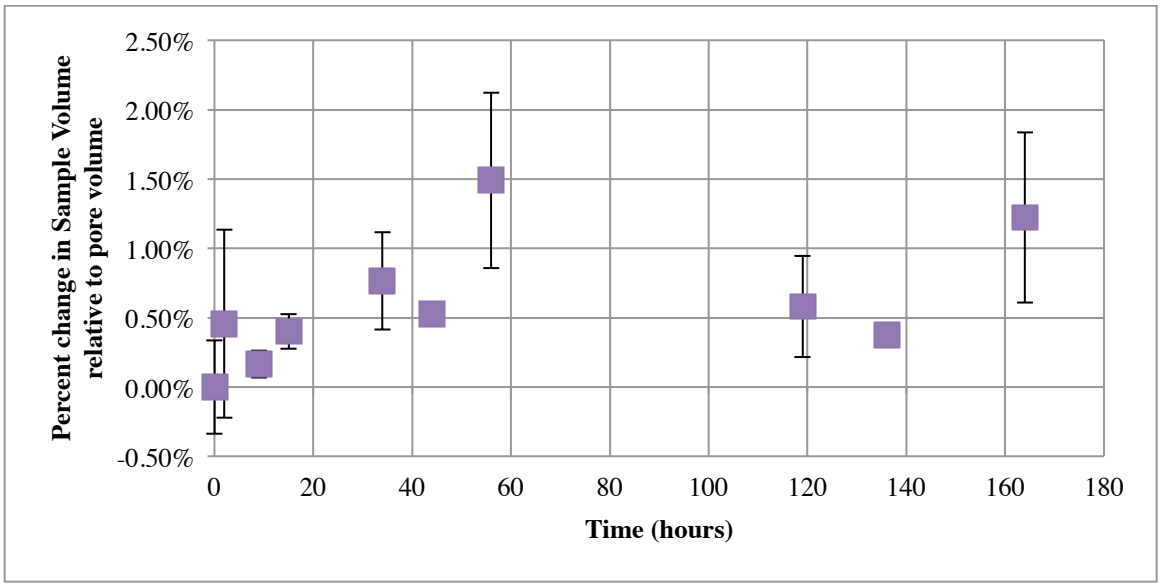

Figure 5.10: Percent change of thin fluid film relative to pore volume of example Bakken sample.

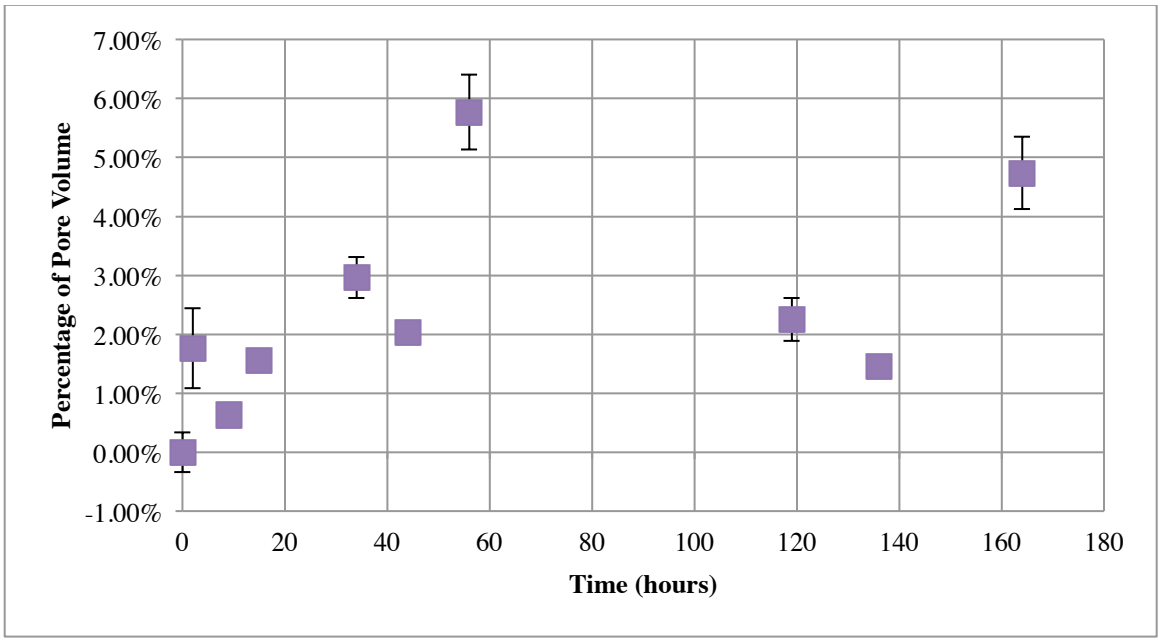

Figure 5.11: Error in displaced pore volume due to variance in thickness of fluid film on the example Bakken sample.

$$\%\Delta V^{\text{Error}}_{\text{Displaced pore fluid}}(t) = \frac{\Delta W_{\text{air}}(t) - \Delta W_{\text{fluid}}(t)}{\left(\rho_{\text{fluid}} - \rho_{\text{pore fluid}}\right)V_{\text{pore}}} \quad \text{.....(5.20)}$$

This figure is quite useful in determining the quality of the data set. The lack of equivalence between the change in air weight, and change fluid weight could be due two factors: a changing volume of adhered surface fluid affecting the air measurements, or due to an change in the volume in the sample affecting the displacement of fluid and consequently the measured fluid weight. An ideal plot of this equation all the data points would be zero or near zero. Any variance from ideal is likely caused due to one of the following reasons: an increase or decrease in the volume of adhered surface fluid, swelling of the sample, or shrinking of the sample. The effects of the different types of error upon this figure are summarized in Table 5.3.

Table 5.3: Individual effects of different types of error upon coupled error analysis figures.

Type of Error	**Figure response**
Increase in adhered surface fluid	Positive error
Decrease in adhered surface fluid	Negative error
Swelling of sample	Positive error
Shrinking of sample	Negative error

This variance can have a significant impact upon the calculated volume of imbibition when only the air measurements are used as shown in Figure 5.11. The percentage of pore volume is calculated using Equation 5.16. The change volume of fluid adhered to the surface has a significant impact upon the calculated volume of displaced fluid as a

percentage of pore volume. The variation in this case causes an error of five percent in the percentage of displaced fluid volume. For this reason it is imperative to minimize the use of the air weight measurements. However, the air weight measurements are needed to ensure that the fluid measurements are accurate, and quantify swelling. The above analysis however can be also be used to examine if the fluid weight measurements are accurate. As $\Delta W_{\text{surface fluid}}(t)$ is calculated from the difference of the weight gain in the fluid and air weight measurements, it is sensitive to both the changing volume of surface fluid and any changes in buoyancy due to swelling effects as shown in Equation 5.12. Figures such as Figure 5.11, and Equation 5.20 are the most useful tools in determining the validity of the data set, as the calculated volume of adhered surface fluid, or calculated change in volume of the sample, because the individual sources of error in the air and fluid measurements cannot be decoupled.

5.2.4 Spontaneous Imbibition: Volume of Displaced Pore Fluid

Once all the metrics have been examined, and passed then the sample's fluid weight measurements can be believed as real. This change in mass is fundamental as this is the sign that imbibition is occurring in the sample, when the volume remains constant. This change in mass and consequently density, equations 4.10 and 4.11, is directly proportional to the volume of fluid imbibed, and consequently the volume of fluid displaced by spontaneous imbibition.

The volume of displaced pore fluid is defined in equations 4.13 and 4.20, which are functions of the change in air and fluid weight of the shale sample respectively. The results for the Bakken brine shale sample are shown in Figure 5.12. The volume of total imbibition is relatively small compared to the total volume of the Bakken brine shale sample, 10.16 cc, however this is a reasonable value as the total porosity of the Bakken samples received was measured to be 10.07% through NMR and the actual effective porosity is likely to be much lower.

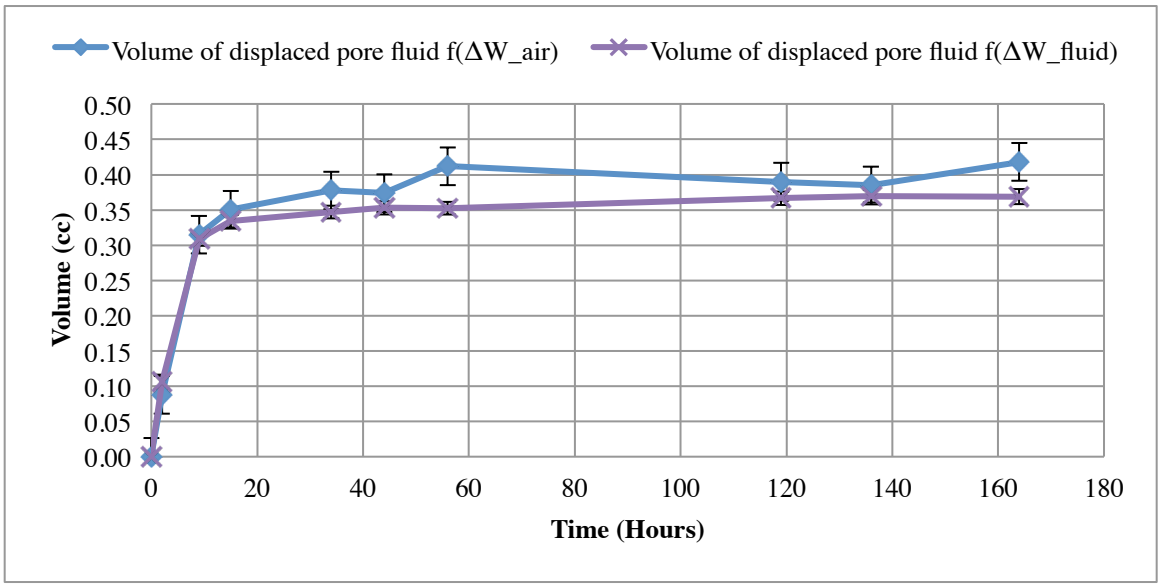

Figure 5.12: Volume of displaced pore fluid in the example Bakken sample.

Figure 5.12 is a very useful figure for determining the total volume displaced pore fluid from the shale sample, but it is not independent of the volume of the shale sample or the pore space of the shale sample. Figure 5.13 solves this problem by plotting the percent volume of displaced pore fluid relative to the pore volume of the sample. This

allows for the comparison of imbibition between different samples of varying volumes and porosities.

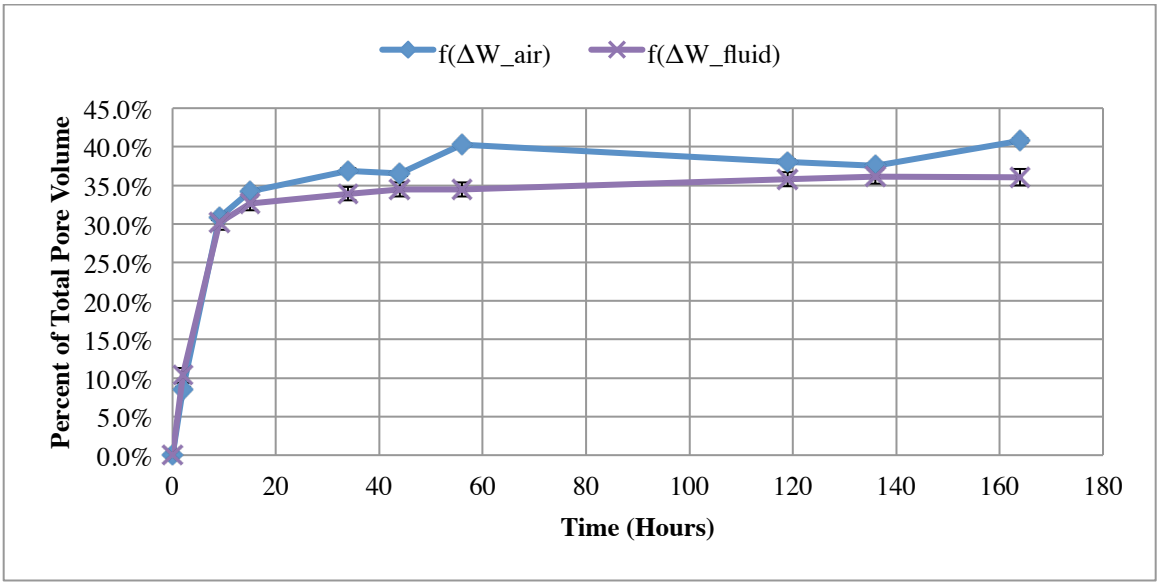

Figure 5.13: Displaced pore fluid as percent of total pore volume of the example Bakken sample.

Neither Figure 5.12 nor Figure 5.13 account for the exposed surface area of the shale sample, which affects the rate of imbibition. To account for the relative surface available for imbibition, time is divided by the square of characteristic length from the dimensionless time defined by Ma (1996), as described in equation 2.4, and shown in again in Equation 5.20.

While the time scaling factor in Equation 5.20 allows for the comparison of samples with different surface areas. Equation 5.20 defined as dimensionless time contains values for permeability, viscosity, and interfacial tension are not known for the following shale samples. As such these terms are neglected as the dimensionless time,

and Equation 5.20 is simplified to Equation 5.21, as dimensionless time is proportional to time divided by the square of characteristic length, Equation 5.22. Figure 5.14 plots the percent volume of displaced pore volume relative to the total pore volume against this dimensionless time.

$$t_D = \sqrt{\frac{k}{\phi}} \frac{\sigma}{\sqrt{\mu_o \mu_w}} \frac{t}{L_C^2} \quad \text{.....(5.20)}$$

$$t_D = \frac{t}{L_C^2} \quad \text{.....(5.21)}$$

$$L_C = \frac{Ld}{2\sqrt{d^2 + 2L^2}} \quad \text{.....(5.22)}$$

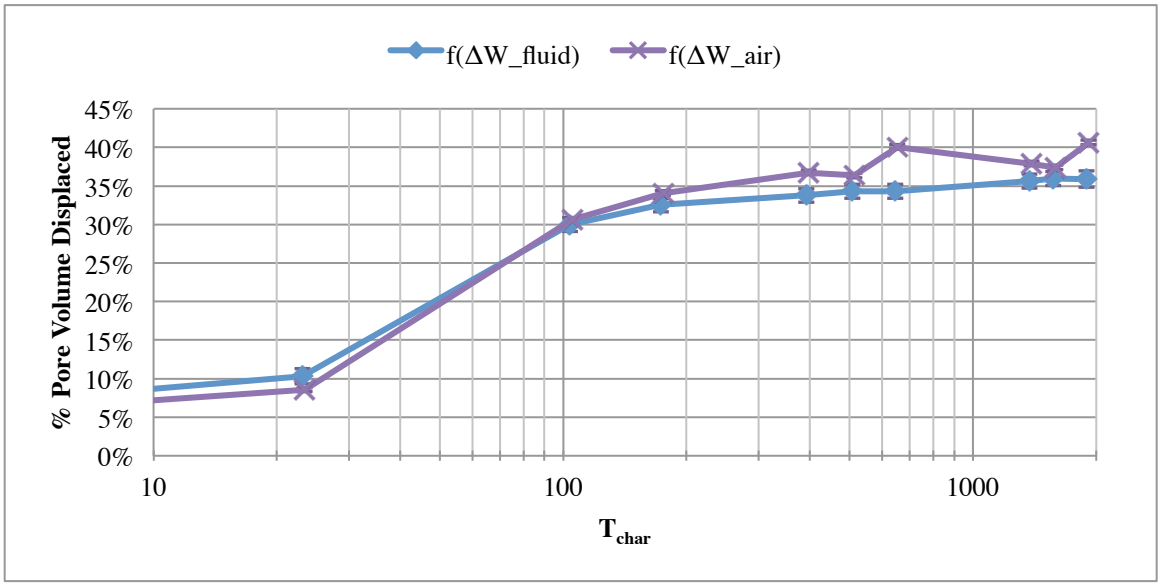

Figure 5.14: Displaced pore fluid as percent of total pore volume of the example Bakken sample in characteristic time.

This relative displacement of pore fluid is more useful than the absolute volume of the fluid displaced, as it does not require any previous knowledge about the shale samples in question in order to evaluate the imbibition. As the true form of dimensionless time is not being used, the time divided by the characteristic length will be referred to as characteristic time.

Though the imbibition time is also important as it gives a scale of how quickly imbibition occurs. Figures 5.13 and 5.14 of pore volume displacement in imbibition time, and characteristic time respectively are simply the volume of the pore fluid displaced divided by the total pore volume of the sample. As a result this plot is ideal for understanding the scale and rate of imbibition within in a single sample, and is a valuable metric for comparing the amount and rate of imbibition occurring in various different samples within a single Figure.

The theory and assumptions described in this and the proceeding Chapter are supported by the single set of experimental data presented, but by no means is this an exhaustive study concluding that this experimental method is a valid approach for the measure of spontaneous imbibition and specifically in regards to measuring the spontaneous imbibition in shale samples. The experimental design was focused primarily on measuring the small mass changes as a result of the exchange of small volumes of differing density fluids during spontaneous imbibition. The following section will discuss further experimental results from this experiment.

5.3 Analysis of Experimental Results

The following section demonstrates the effectiveness of the gravimetric measurement spontaneous imbibition experiments through the use of three discrete data sets containing the Bakken and Utica shale. Each experimental data set consists of four companion plug shale samples and four different imbibition fluids. These companion plugs are selected in such a manner as to have similar mineralogical properties. The imbibition fluids tested in each data consist of control brine selected for that rock type, and three different surfactant mixtures made from that brine. Each surfactant mixture differs in type and concentration of surfactant.

The properties of the brine, type of surfactants, and concentrations were provided by the sponsors of this research. The selection, optimization, and detailed study of wettability modification of the selected surfactants were not within the scope of this project, and consequently the mechanics of the surfactant interaction and wettability modification will not be discussed. All of the following experiments made use of the same surfactants and concentrations dissolved in the appropriate brine for the shale sample. Each surfactant was given a designation for the formulation that, for ease of reference, can be found in Table 5.4.

The evaluation of the experimental results mirrors the format of the preceding section introducing the results of the experiment in the example Bakken sample; however, differing in that not all of the plots discussed will be examined. Each data set will be

examined to evaluate the precision and accuracy of the measurements because of the adhered surface fluid, as well as any swelling of the sample.

Table 5.4: Surfactant designations and formulations.

Imbibition fluid	Surfactant Concentration by Weight Percent
A	0.5% Petrostep R-1
B	0.25% Biosoft and 0.25% Petrostep S-2
C	0.25% Biosoft and 0.25% Petrostep R-1
Brine	None

If the data set demonstrates an absence of swelling effects, then the fluid weight measurements will be used to calculate the displaced pore fluid. However, if the data set does not meet the requirements for the constant volume assumption, then the noisier air weight measurement values are used to compute the volume of the displaced pore fluid.

5.3.1 Bakken Shale Spontaneous Imbibition Experiments

A total of eight preserved Bakken shale samples were tested in two experiments. Though both experiments used the same surfactant formulations, one was performed using filtered field brine, and the other was performed using laboratory-produced artificial field brine. The concentrations of the ions in both in the brines used in each experiment were identical and are listed in Table 5.5.

All of the Bakken samples were prepared from Bakken preserved plugs. The porosity was determined through NMR measurement of a single neighboring plug, and

was found to have an absolute porosity of 10.07%. This value of porosity was used for all Bakken samples in the following project, and to estimate fluid saturations for all the following Bakken sample computations.

Table 5.5: Produced Bakken brine fluid properties, 7.2 pH.

Ions	Concentration (mg/L)
Barium	2.78
Bicarbonate	244
Boron	143
Calcium	244
Chloride	10600
Iron	0.370
Lithium	43.6
Maganese	1.87
Magnesium	40.0
Potassium	5290
Sodium	60700

5.3.1.1 Bakken Experiment 1

The first experiment of two involving the Bakken shale described in this project will simply be referred to throughout as "Bakken Experiment 1" for reasons of conciseness and clarity. This experiment began as described in the procedure above with the measurement of the fluid and shale sample properties (with slight variations coming into effect later that are described and explained below). The shale, sample, and fluid properties measured and calculated are shown in table 5.6, where they are organized according to which imbibition fluid they were exposed. The shale sample and fluid

properties are fundamental in calculating the rate of spontaneous imbibition, as well as the total amount of spontaneous imbibition. The measured fluid and shale properties shown in table 5.6 are within the range expected for the Bakken shale.

Table 5.6: Bakken experiment 1— Shale sample and fluid properties.

Imbibition fluid	**A**	**B**	**C**	**Brine**
$W_{air}^{initial}$	9.0543 g ± 5.00E-5 g	8.9993 g ± 5.00E-5 g	9.1548 g ± 5.00E-5 g	9.1762 g ± 5.00E-5 g
$W_{fluid}^{initial}$	5.0671 g ± 5.00E-5 g	5.0164 g ± 5.00E-5 g	5.1261 g ± 5.00E-5 g	5.1553 g ± 5.00E-5 g
ρ_{fluid}	1.128 g/cc ± 5.00E-4 g/cc	1.128 g/cc ± 5.00E-4 g/cc	1.128 g/cc ± 5.00E-4 g/cc	1.127 g/cc ± 5.00E-4 g/cc
$\rho_{pore\ fluid}$	0.823 g/cc ± 5.00E-4 g/cc	0.823 g/cc ± 5.00E-4 g/cc	0.823 g/cc ± 5.00E-4 g/cc	0.823 g/cc ± 5.00E-4 g/cc
$V_{sample}^{initial}$	3.574 cc ± 2.24E-3 cc	3.576 cc ± 2.24E-3 cc	3.600 cc ± 2.20E-3 cc	3.598 cc ± 2.20E-3 cc
ρ_{bulk}^{intial}	2.533 g/cc ± 1.59E-3 g/cc	2.517 g/cc ± 1.58E-3 g/cc	2.543 g/cc ± 1.55E-3 g/cc	2.550 g/cc ± 1.56E-3 g/cc
ϕ_{Total}	10.07% ± 0.005%	10.07% ± 0.005%	10.07% ± 0.005%	10.07% ± 0.005%
$V_{Pore\ Total}$	0.3599 cc ± 4.30E-4 cc	0.3601 cc ± 4.30E-4 cc	0.3625 cc ± 4.24E-4 cc	0.3623 cc ± 4.24E-4 cc
d	2.41 cm ± 5.00E-5 cm	2.41 cm ± 5.00E-5 cm	2.41 cm ± 5.00E-4 cm	2.41 cm ± 5.00E-5 cm
L	0.797 cm ± 5.00E-5 cm	0.801 cm ± 5.00E-5 cm	0.805 cm ± 5.00E-4 cm	0.803 cm ± 5.00E-5 cm
L_c	0.163 ± 1.39E-5	0.164 ± 1.39E-5	0.165 ± 1.39E-4	0.164 ± 1.39E-5

The experimental procedure differed slightly from procedure described in Chapter 3. This experiment was the first successful test of the complete experimental setup and measurement procedures. Because of the novel nature of this experiment, there were

some minor differences in the experimental procedure, as not all aspects of the procedure had not yet been concretely defined.

The shale preparation and handling procedure was followed as previously described for shale samples preserved in mineral oil, and was carried out at room temperature. Other notable departures between the previously stated procedure include the difference in the volume of the shale samples used, the time measurement steps, and the brine used. The bulk volumes of the shale samples used in this data set were only on the order of 3.5 cubic centimeters. This volume is much smaller than the approximately 10 cubic centimeter samples described in the previous procedure. Filtered field brine was used to make the various imbibition fluids.

It is important to note that samples B and C have a lower density than that of A and Brine. This density difference could be caused by a number of factors ranging from a different porosity, geologic properties, or different levels of preservation and saturation. These cores were received as sealed plugs and it is possible that there are varying levels of preservation as there may have been cracks in the sealing wax.

The quality of the constant volume assumption must be evaluated before the rate or the volume of imbibition can be calculated for any of the shale samples in this experiment. As the equivalence of the change in measured weight of the shale sample in air and in the imbibition fluid can only be compared for a single shale sample at a time, the shale samples in this experiment are broken up into two groups to ease the visual comparison.

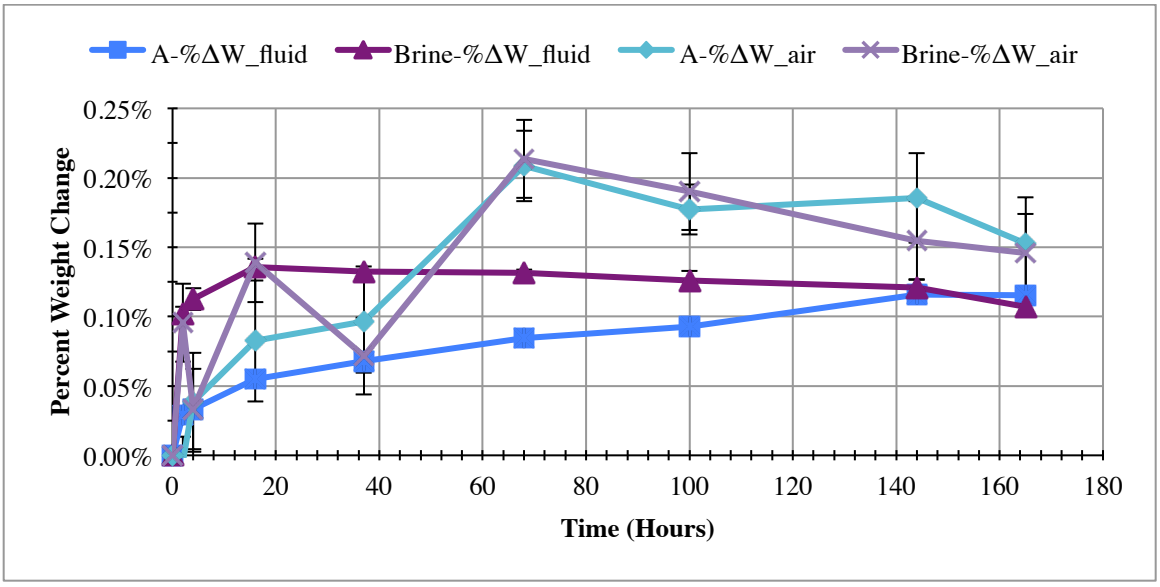

Figure 5.15: Bakken Experiment 1—Change in measured air and fluid weight for Bakken shale samples A and brine.

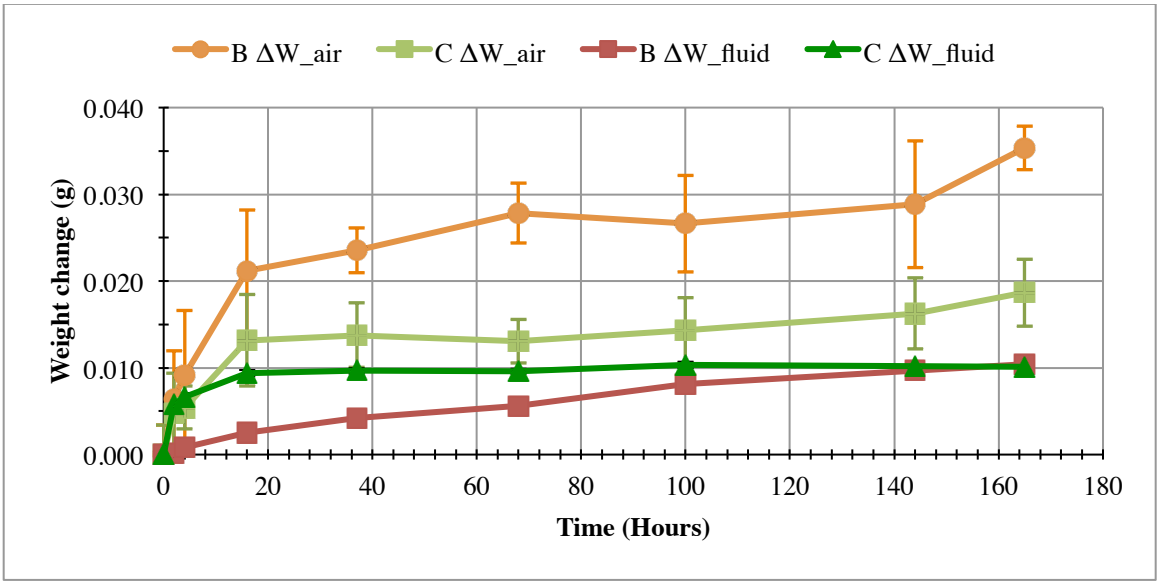

Figure 5.16: Bakken Experiment 1—Change in measured air and fluid weight for Bakken shale samples B and C.

The choice of what samples to use to form the two subsets of the weight changes of the shale samples is determined by pairing which measurements will minimize the overlapping data points. The subsets created to compare the weight change as a result of spontaneous imbibition for Bakken Experiment 1 are the A and Brine samples, and the B and C samples. These plots of these two subsets are shown in Figure 5.15 and 5.16, respectively.

The results of Bakken Experiment 1 shown in Figure 5.15 and 5.16, do not adequate agreement with the anticipated equivalence for a sample undergoing zero swelling. The non-equivalence of the change in air and fluid weight measurements implies that, as shown in the example case, the volume of fluid on the surface is not ideal and fluctuates with time. However, with sample B there does seem to be some time-dependent effects as the differences increase with respect to time showing that swelling is likely occurring, as the volume of adhered surface fluid should remain somewhat constant. This error must be quantified before any conclusive arguments can be made.

The errors affecting the constant volume assumption are the variance in volume of adhered surface fluid, and shale swelling cannot be decoupled, as each error is unique to the measurement method. Though these errors cannot be decoupled using the current experimental procedure, this error must be examined in order to determine the validity of the constant volume assumption, and the overall quality of the data. This coupled error in terms of the percentage of pore volume of the sample the calculated using equation 5.20

as shown previously, and repeated below. The results of this coupled error analysis for this data set is presented in Figure 5.17.

$$\%\Delta V^{\text{Error}}_{\text{Displaced pore fluid}}(t) = \frac{\Delta W_{\text{air}}(t) - \Delta W_{\text{fluid}}(t)}{\left(\rho_{\text{fluid}} - \rho_{\text{pore fluid}}\right) V_{\text{pore}}} \quad \text{.....(5.20)}$$

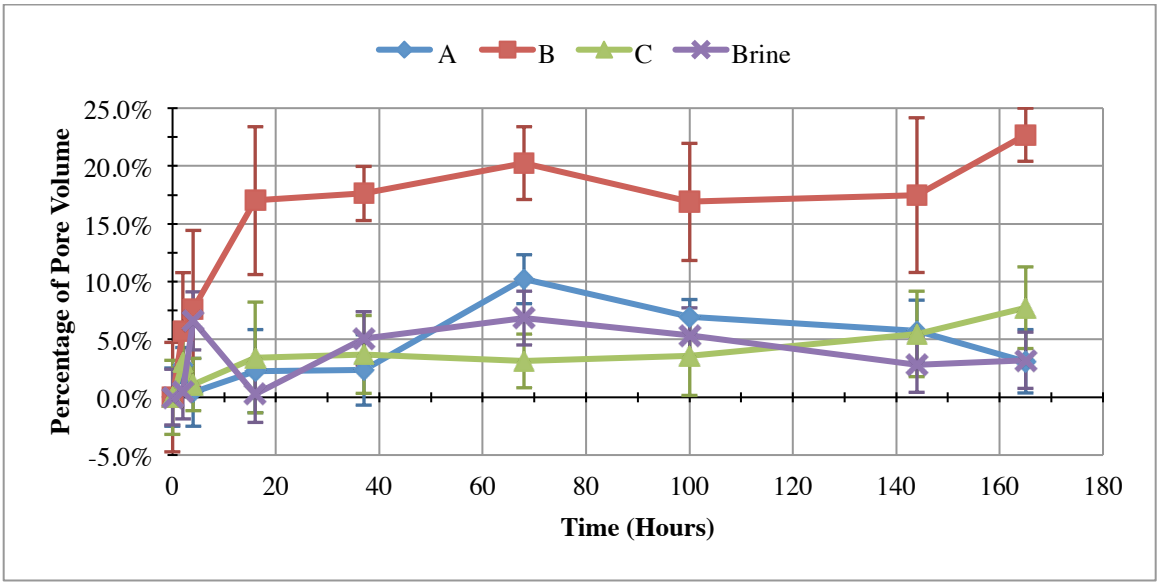

Figure 5.17: Bakken experiment 1— Variance in displaced pore volume between air and fluid measurements resulting from variance in thickness of fluid film and/or swelling from Equation 5.20.

As previously discussed in an ideal plot, all the values of the above figure would be equal to zero. The lack of equivalence between the change in air weight, and change fluid weight is likely due one, or a combination of the following factors: a changing volume of adhered surface fluid affecting the air measurements, or due to an change in the volume in the sample affecting the displacement of fluid and consequently the measured fluid weight. The variance from ideal is significant for this data set especially

for sample B. Consequently sample B must either be swelling or the volume of fluid adhered to the surface increased over time.

Error cannot be avoided in the measurement of physical phenomena, but it must fall within an acceptable limit. Ideally this error should fall within less than 1% of the quantity of which you are attempting to measure. None of the samples fall within this ideal limit, but in order to draw a conclusion from this data set a higher limit of less than 10% error will be used. Consequently only samples A, C and Brine can be considered valid, and though sample B will be included to demonstrate the significance of this error and how it can lead to false conclusions. The error in measurement in sample B in could be caused by factors, such as wettability modification of the surface of the shale sample causing the thin film volume of adhering fluid to increase, or due to swelling causing a decrease in the measured fluid weight due to the increase in displacement.

The shale samples used in this experiment were nearly one-third the weight and roughly one-fourth the volume of the example used to demonstrate the theory in the previous section. As a result of this lower mass and volume, the air weight measurements are much more sensitive to the fluctuation of fluid adhering to the surface of the sample. This sensitivity, and the consequent error is due to a poor choice in sample size.

Table 5.7 displays the estimated fluid mass, and volume of the fluid adhering to the surface of the sample, calculated by calculating the difference between the measured air weight and the air weight calculated by using Archimedes method as shown in

Equations 5.1 and 5.3. This relative amount of surface fluid mass implies that the thickness of the fluid layer is between 0.025 and 0.03 mm thick which is reasonable.

Table 5.7: Bakken experiment 1—Estimated amounts and error of fluid adhering to surface of shale sample during air weight measurements.

Imbibition fluid	$\overline{W_{\text{surface fluid}}(t)}$	$\overline{\frac{W_{\text{surface fluid}}(t)}{W_{\text{air}}^{\text{intial}}}}$	$\overline{V_{\text{Surface fluid}}(t)}$	$\overline{\left(\frac{V_{\text{Surface fluid}}(t)}{V_{\text{sample}}^{\text{intial}}}\right)}$	**Thickness of Fluid Film**
A	0.0469 g ± 0.0043 g	0.52% ± 0.048%	0.0416 cc ± 0.0038 cc	1.164% ± 0.1076%	0.0274 mm ± 0.0080 mm
B	0.0350 g ± 0.0083 g	0.39% ± 0.093%	0.0311 cc ± 0.0074 cc	0.869% ± 0.2069%	0.0204 mm ± 0.0154 mm
C	0.0464 g ± 0.0042 g	0.51% ± 0.046%	0.0411 cc ± 0.0037 cc	1.143% ± 0.1029%	0.0270 mm ± 0.0768 mm
Brine	0.0655 g ± 0.0050 g	0.71% ± 0.055%	0.0581 cc ± 0.0045 cc	1.615% ± 0.1244%	0.0382 mm ± 0.0930 mm

It is rather conclusive after examining the change in densities that sample B is indeed swelling at some rate, as this is the only possible explanation for the data thus far presented. As a result, fluid measurements cannot be used to measure the relative weight change for this sample. Though all the other samples pass the quantitative metrics previously stated, but the data is quite noisy and some of the samples appear to lose weight as time goes in in the fluid, which is an indicator of swelling, as the resulting change in measured weight must be do to an increase in buoyancy. Figures 5.18 and 5.19, show the final results of imbibition testing using air weight measurements and Figures 5.20 and 5.21 using the fluid weight measurements.

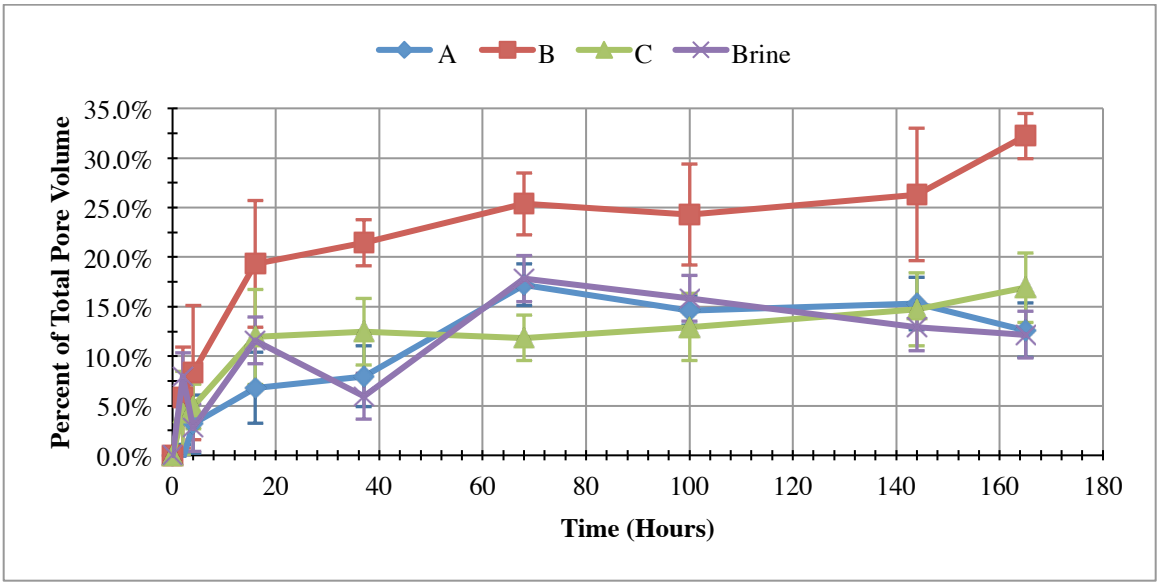

Figure 5.18: Bakken experiment 1—Percent displaced pore fluid of total pore fluid of shale samples calculated only from air weight measurements.

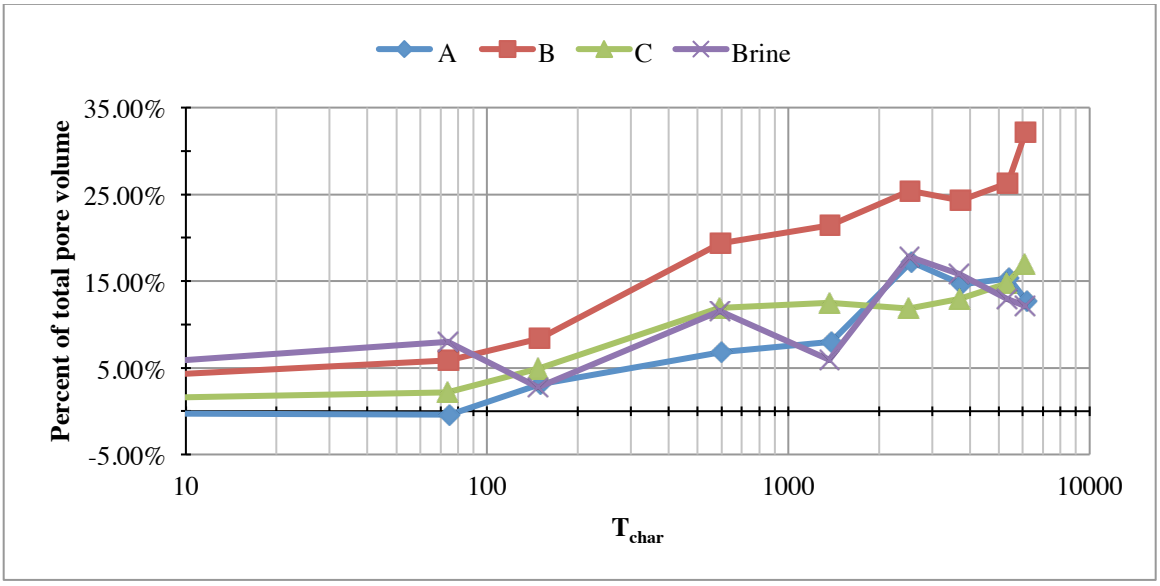

Figure 5.19: Bakken experiment 1—Percent displaced pore fluid of total pore fluid of shale samples calculated only from air weight measurements in characteristic time.

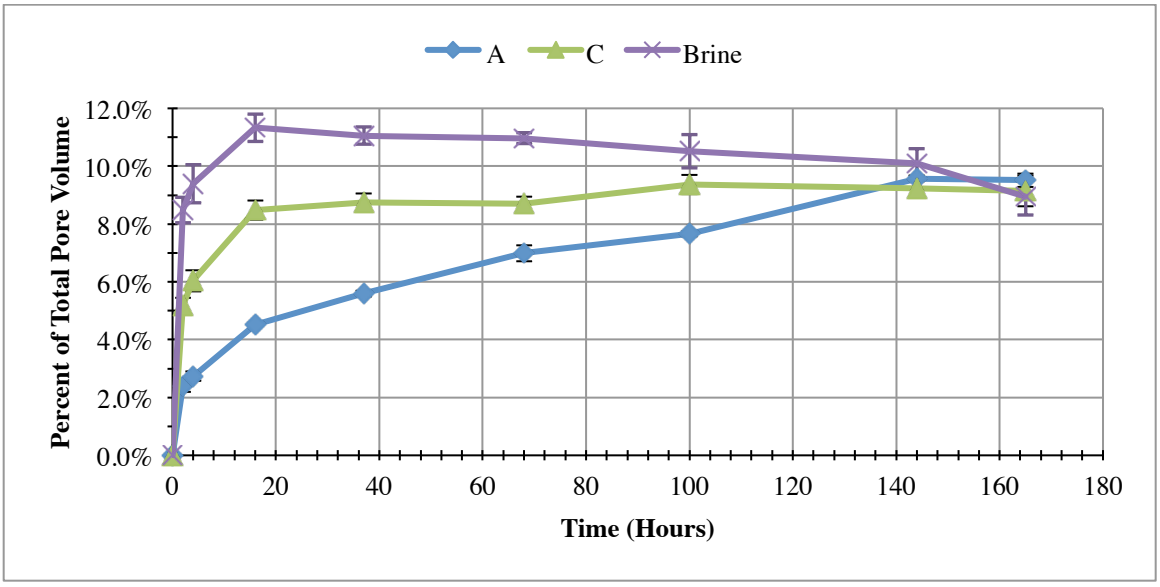

Figure 5.20: Bakken experiment 1—Percent displaced pore fluid of total pore fluid of shale samples calculated only from fluid weight measurements.

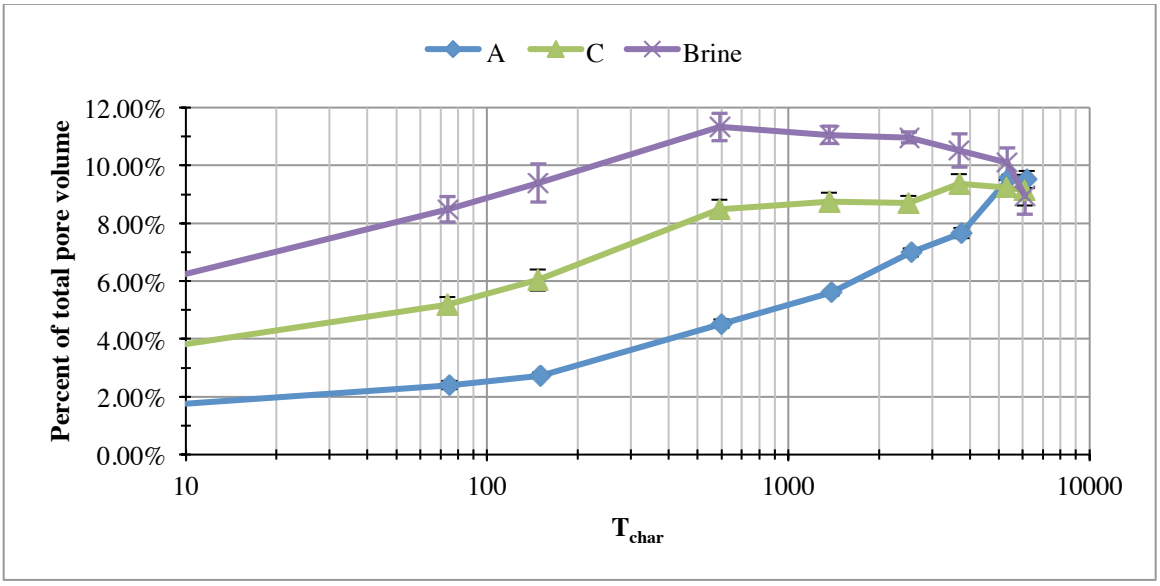

Figure 5.21: Bakken experiment 1—Percent displaced pore fluid of total pore fluid of shale samples calculated only from fluid weight measurements in characteristic time.

From examining the final results it is possible to note that imbibition is indeed occurring, however the volume of imbibition that is occurring compared to swelling becomes unclear once the percent of displaced pore fluid—calculated from fluid weight measurements—are examined. They converge at a single point, which implies that each sample had the same amount of swelling occurring. For this reason, we can use the calculation of the pore fluid displaced by air weight measurements, but it cannot be concluded that this weight gain is a result of swelling alone, rather than imbibition.

The amount of relative error, along with the heightened sensitivity to this error because of the smaller physical volume, push this data set to the point where it may not be valid or valuable for making meaningful conclusions about the volume and/or rate of imbibition occurring within the samples. The volume of the samples is far too small to draw any significant conclusions. This, however, was an incredibly important learning experience and helped us to establish the best possible procedure for future tests.

5.3.1.2 Bakken Experiment 2

Table 5.8: Bakken Experiment 2—Shale sample and fluid properties.

Imbibition fluid	A	B	C	Brine
$W_{air}^{initial}$	27.9484 g ± 5.00E-5 g	25.7862 g ± 5.00E-5 g	27.9050 g ± 5.00E-5 g	26.9534 g ± 5.00E-5 g
$W_{fluid}^{initial}$	16.2696 g ± 5.00E-5 g	15.0109 g ± 5.00E-5 g	16.1938 g ± 5.00E-5 g	15.6299 g ± 5.00E-5 g
ρ_{fluid}	1.110 g/cc ± 5.00E-4 g/cc	1.110 g/cc ± 5.00E-4 g/cc	1.110 g/cc ± 5.00E-4 g/cc	1.110 g/cc ± 5.00E-4 g/cc
$\rho_{pore\ fluid}$	0.823 g/cc ± 5.00E-4 g/cc	0.823 g/cc ± 5.00E-4 g/cc	0.823 g/cc ± 5.00E-4 g/cc	0.823 g/cc ± 5.00E-4 g/cc
$V_{sample}^{initial}$	10.521 cc ± 4.74E-3 cc	9.707 cc ± 4.37E-3 cc	10.551 cc ± 4.75E-3 cc	10.212 cc ± 4.60E-3 cc
ϕ_{Total}	10.07% ± 0.005%	10.07% ± 0.005%	10.07% ± 0.005%	10.07% ± 0.005%
$V_{Pore\ Total}$	1.0595 cc ± 1.56E-3 cc	0.9775 cc ± 1.38E-3 cc	1.0625 cc ± 1.56E-3 cc	1.0284 cc ± 1.49E-3 cc
ρ_{bulk}^{intial}	2.656 g/cc ± 1.20E-3 g/cc	2.656 g/cc ± 1.20E-3 g/cc	2.645 g/cc ± 1.19E-3 g/cc	2.639 g/cc ± 1.19E-3 g/cc
d	2.43 cm ± 5.00E-5 cm	2.43 cm ± 5.00E-5 cm	2.41 cm ± 5.00E-5 cm	2.41 cm ± 5.00E-5 cm
L	2.320 cm ± 5.00E-5 cm	2.160 cm ± 5.00E-5 cm	2.270 cm ± 5.00E-5 cm	2.240 cm ± 5.00E-5 cm
L_c	0.293 ± 1.32E-5	0.296 ± 1.40E-5	0.294 ± 1.34E-5	0.294 ± 1.36E-5

Bakken experiment 2 was performed according to the procedure for a shale sample that has not been exposed to mineral oil. The samples were cut using an air-cooled saw. The measured shale sample and fluid properties are shown below in table 5.8. The shale samples used in this experiment were significantly larger than in Bakken Experiment 1 in both volume and mass as previously described. The densities of the brine

solutions used in Bakken experiment 1 and 2 are noticeably different but this is because of Experiment 2's use of laboratory-prepared artificial brine. The porosity was assumed to be the same as the measured value used in Experiment 1 and agrees with literature values Table 5.9 quantifies the weight of the fluid adhering to the surface of the sample through the use of Archimedes weight as discussed previously.

Table 5.9: Bakken Experiment 2— Estimated amounts and error of fluid adhering to surface of shale sample during air weight measurements.

Imbibition Fluid	$\overline{W_{\text{surface fluid}}(t)}$	$\overline{\frac{W_{\text{surface fluid}}(t)}{W_{\text{air}}^{\text{intial}}}}$	$\overline{V_{\text{Surface fluid}}(t)}$	$\overline{\left(\frac{V_{\text{Surface fluid}}(t)}{V_{\text{sample}}^{\text{intial}}}\right)}$	**Thickness of Fluid Film**
A	0.0643 g ± 0.0079 g	0.23% ± 0.028%	0.0580 cc ± 0.0071 cc	0.551% ± 0.0676%	0.0229 mm ± 0.0887 mm
B	0.0571 g ± 0.0072 g	0.22% ± 0.028%	0.0515 cc ± 0.0064 cc	0.530% ± 0.0664%	0.0234 mm ± 0.0927 mm
C	0.0613 g ± 0.0081 g	0.22% ± 0.029%	0.0552 cc ± 0.0073 cc	0.523% ± 0.0693%	0.0227 mm ± 0.0952 mm
Brine	0.0502 g ± 0.0077 g	0.19% ± 0.029%	0.0452 cc ± 0.0070 cc	0.443% ± 0.0681%	0.0191 mm ± 0.0930 mm

As seen by Examining Figures 5.22 and 5.23, all of the samples in Bakken Experiment 2 show a very close relationship between the relative change in air and fluid weight measurements for each sample. The difference between the fluid measurements, and the air measurements for each sample appears to be very small graphically. This difference is much smaller than the samples observed in the first Bakken experiment. Though this may appear trivial, it is an implication that the error due to swelling and/or variance in the volume of adhered surface fluid may be minimal. Despite the apparent minimal difference, further investigation into the error must be drawn before any

conclusions can be drawn about this data set. The bulk density of the samples are not identical, and, as with Experiment 1, this difference in bulk density is likely the result of a difference in mineralogical content, porosity, or initial saturation. Despite this difference, the difference between the fluid and air measurements for both samples is extremely small.

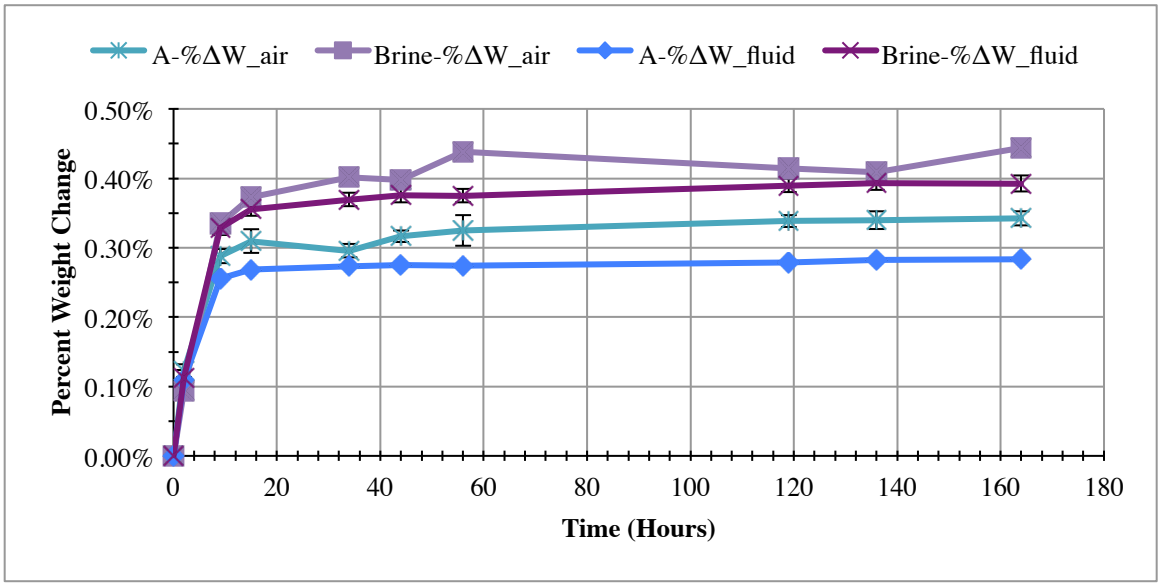

Figure 5.22: Bakken Experiment 2—Change in measured air and fluid weight for Bakken shale samples A and Brine.

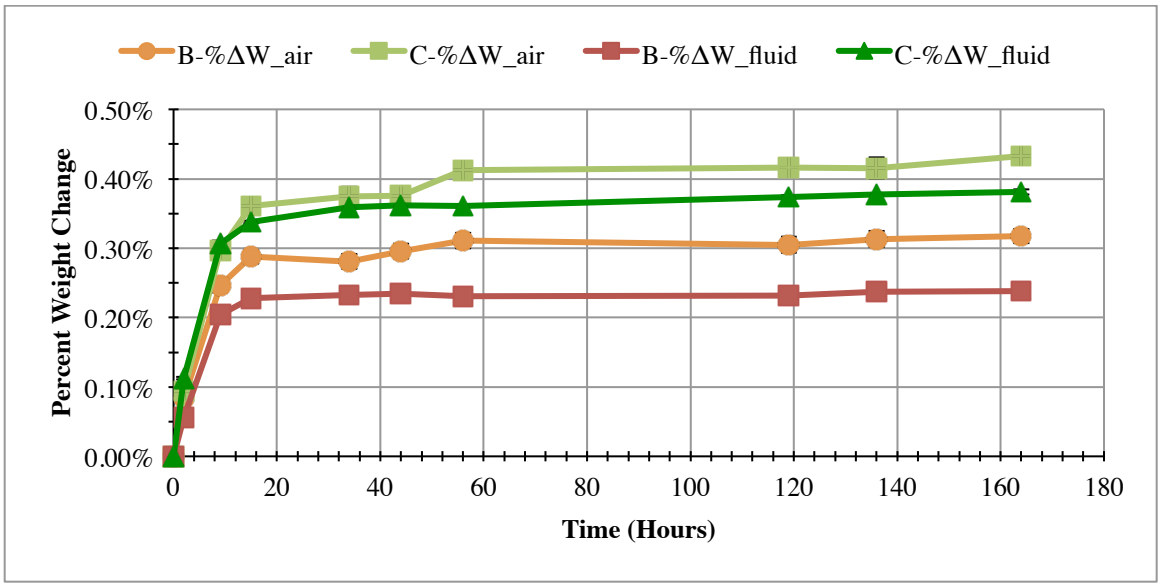

Figure 5.23: Bakken Experiment 2—Change in measured air and fluid weight for Bakken shale samples B and C.

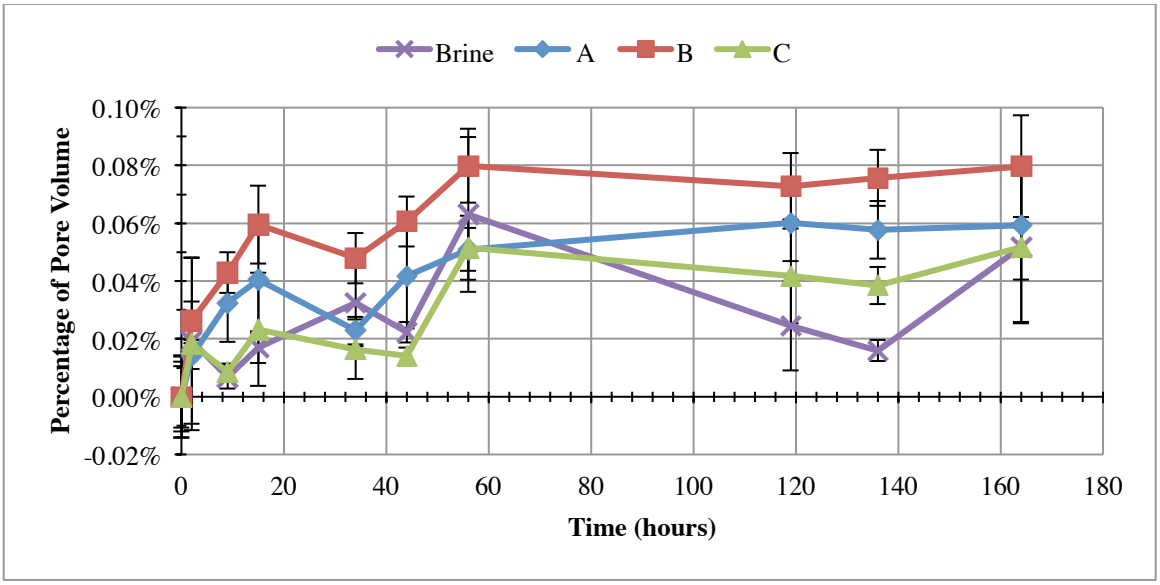

Figure 5.24: Bakken Experiment 2— Variance in displaced pore volume between air and fluid measurements due to variance in thickness of fluid film and/or swelling from Equation 5.20.

The difference between $\Delta W_{\text{fluid}}(t)$ and $\Delta W_{\text{air}}(t)$ is within the range of acceptable error previously stated of less than 1 percent of the total pore volume. The time-dependence of the difference in the increases in weight is present, but again, it is not conclusive to claim that this trend that seems somewhat pervasive across all the samples is a result of swelling. As this effect could have something to do with the surface chemistry of the rock changing, that could cause an increase in the volume of the thin film fluid adherence to the surface. Additionally, the velocity of removal of the sample is not known—or even consistent—so some variation in the relative thin film of fluid adhering to the surface of the sample would result from removal velocity.

From this error analysis it is possible to conclude that the samples undergo a level of swelling, and/or change in adhered surface fluid that is well below the tolerance of the measurement of change in weight in the fluid. This allows for the use of the fluid weight measurements to calculate the rate and volume of spontaneous imbibition. For good measure the percent displaced pore fluid calculated air weight measurements, Figure 5.25, is included for comparison to the fluid weight measurements. The percent of total pore fluid displaced of the pore volume calculated from fluid measurements is shown in Figures 2.26 and 2.27 in imbibition time and characteristic time respectively.

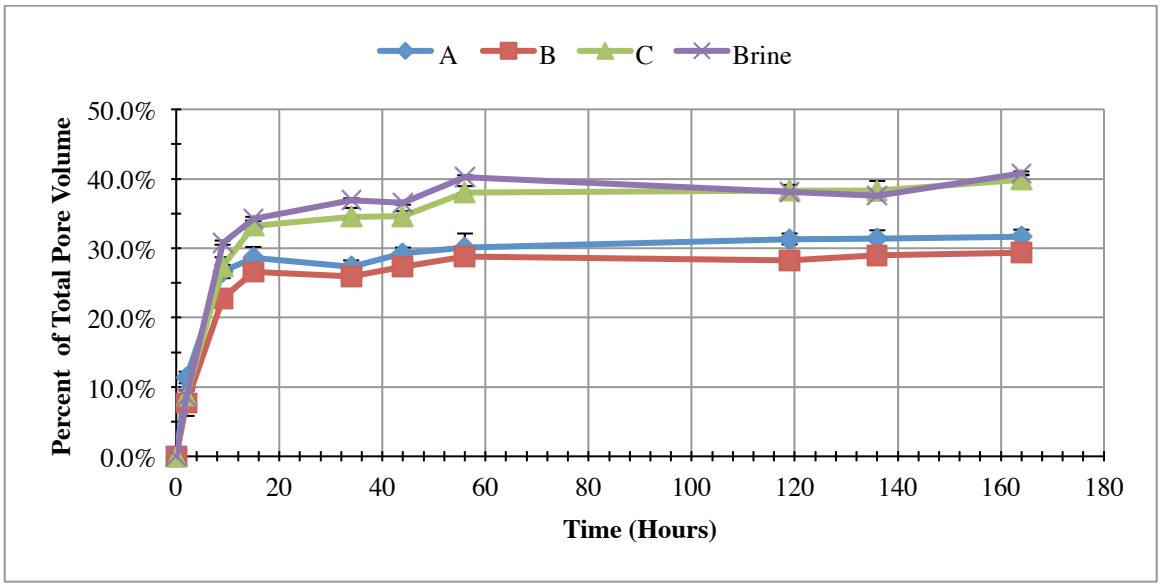

Figure 5.25: Bakken Experiment 2—Percent displaced pore fluid of total pore fluid shale samples calculated only from air weight measurements.

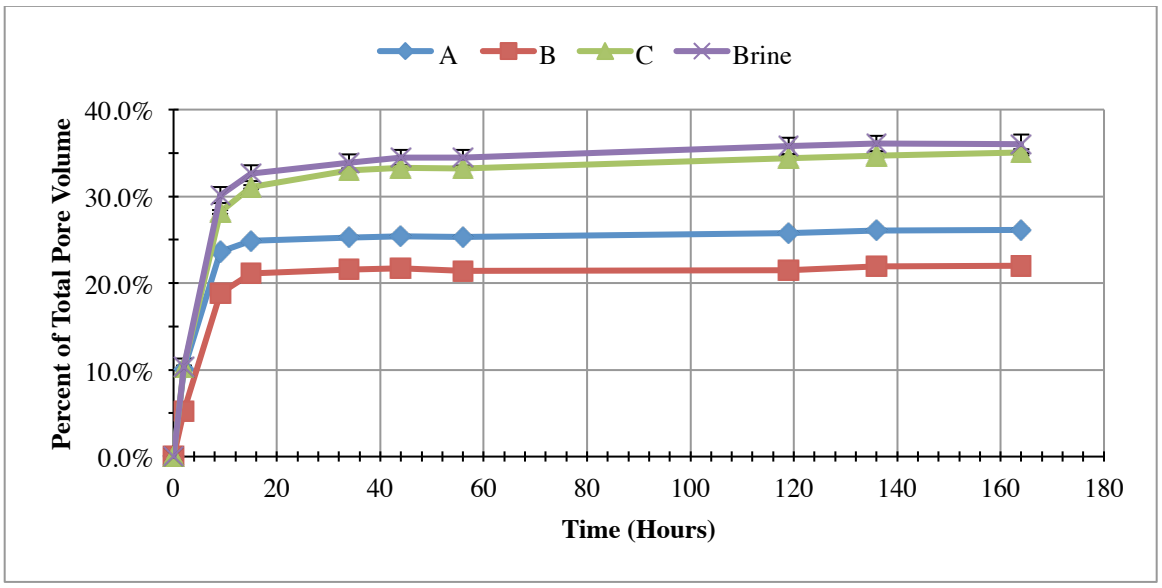

Figure 5.26: Bakken Experiment 2—Percent displaced pore fluid of total pore fluid of shale samples calculated only from fluid weight measurements.

Though the performance of A and B at first seem far lower than C and Brine, this might not be the case as the actual porosity of the samples are not known and this is highly likely as the bulk density is higher for these samples than C and Brine. However what is clear is that with a sufficient sample size the rate of imbibition can be measured and has two distinct flow regimes. One slope that rises rapidly in less than 20 hours and another slope that increases slowly. This is clear that sign there is imbibition occurring within the shale sample. The two different flow regimes are even more apparent in characteristic time, shown in Figure 5.27.

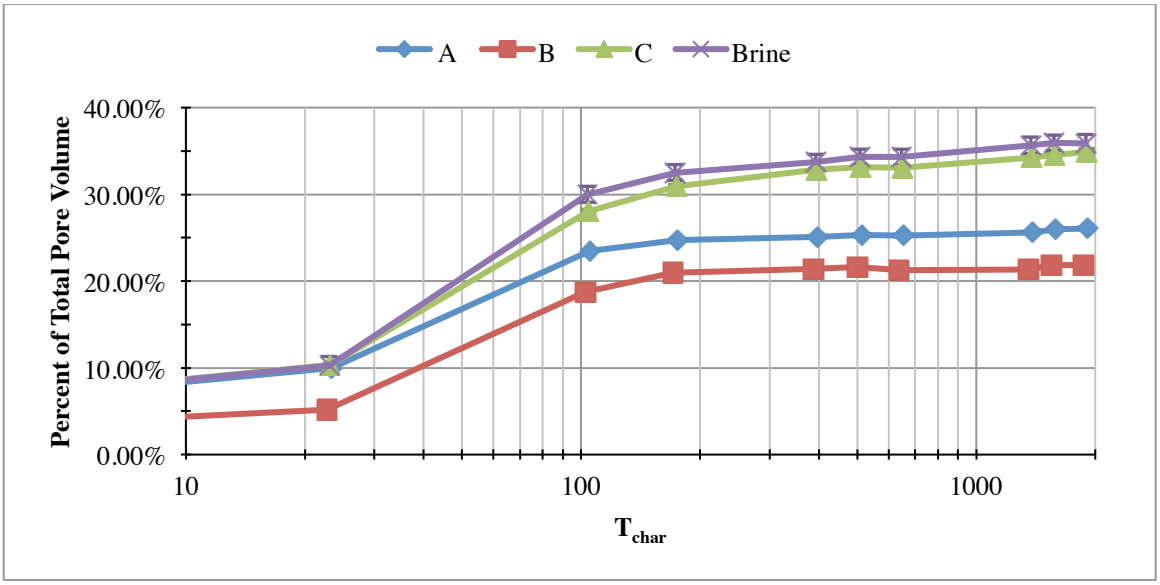

Figure 5.27: Bakken Experiment 2—Percent displaced pore fluid of total pore fluid of shale samples calculated only from fluid weight measurements.

A likely explanation for the dual flow regimes visible in Figure 5.26 and 5.27, is the initial imbibition front reaching the end of the sample or the other imbibition fronts. The speed at which the fluid is imbibed is likely because of the capillary pressure of the

laminar organ pores that the Bakken shale posses (Sarg, 2011). While a true conclusion of which surfactant is the best for enhancing spontaneous imbibition cannot be made, the test is obviously successful in samples of sufficient size.

5.3.2 Utica Spontaneous Imbibition Experiment

Table 5.10: Utica experiment— Utica Brine (6.07 pH).

Parameters	Concentration (mg/L)
TDS	142,960
Sodium	59,934
Potassium	693
Magnesium	526
Calcium	7,068
Strontium	1,048
Barium	120
Iron	29
Zinc	0
Lead	1
Manganese	19
Chloride	108,000
Sulfate	58
Bicarbonate	35

The Utica spontaneous imbibition experiment was carried out in accordance with the procedure for samples stored in mineral oil. The Utica samples were larger than the samples used in Bakken Experiment 1, but smaller than the samples used in Bakken Experiment 2—as seen below in Table 5.11. The samples did vary from perfectly cylindrical as during the cutting process some pieces sheared along the bedding plane, but all measurements were taken after shearing. In this experiment there are two additional assumptions beyond the assumptions made in Bakken experiments one and two. These two assumptions are assumed values for the total porosity of the Utica shale samples, and density of the saturation fluid.

The densities of the pore fluid were assumed to be 0.8 g/cc as a sample of the pore saturating fluid was not available or provided by the research sponsor as with the Bakken samples. The porosity for these samples was assumed to be equal to 5 percent, which is a median value of the literature values porosity for the Utica. Additionally, the ion concentrations seen in table 5.10, and the densities of the imbibition fluids were equivalent with the exception of the brine, which was one thousandth of a gram per cubic centimeter more than the other samples.

Table 5.11: Utica experiment—Shale sample and fluid properties.

Imbibition fluid	**A**	**B**	**C**	**Brine**
$W_{air}^{initial}$	19.4353 g ± 5.00E-5 g	17.8686 g ± 5.00E-5 g	22.4984 g ± 5.00E-5 g	23.2398 g ± 5.00E-5 g
$W_{fluid}^{initial}$	11.3003 g ± 5.00E-5 g	10.3880 g ± 5.00E-5 g	13.0746 g ± 5.00E-5 g	13.4862 g ± 5.00E-5 g
ρ_{fluid}	1.106 g/cc ± 5.00E-4 g/cc	1.106 g/cc ± 5.00E-4 g/cc	1.106 g/cc ± 5.00E-4 g/cc	1.107 g/cc ± 5.00E-4 g/cc
$\rho_{pore\ fluid}$	0.800 g/cc ± 5.00E-4 g/cc	0.800 g/cc ± 5.00E-4 g/cc	0.800 g/cc ± 5.00E-4 g/cc	0.800 g/cc ± 5.00E-4 g/cc
$V_{sample}^{initial}$	7.355 cc ± 3.33E-3 cc	6.764 cc ± 3.06E-3 cc	8.521 cc ± 3.85E-3 cc	8.811 cc ± 3.98E-3 cc
ρ_{bulk}^{intial}	2.642 g/cc ± 1.19E-3 g/cc	2.642 g/cc ± 1.19E-3 g/cc	2.640 g/cc ± 1.19E-3 g/cc	2.638 g/cc ± 1.19E-3 g/cc
ϕ_{Total}	5.00% ± 0.005%	5.00% ± 0.005%	5.00% ± 0.005%	5.00% ± 0.005%
$V_{Pore\ Total}$	0.3678 cc ± 4.58E-4 cc	0.3382 cc ± 4.05E-4 cc	0.4260 cc ± 5.70E-4 cc	0.4405 cc ± 5.99E-4 cc
d	2.53 cm ± 5.00E-5 cm	2.34 cm ± 5.00E-5 cm	2.53 cm ± 5.00E-5 cm	2.54 cm ± 5.00E-5 cm
L	1.485 cm ± 5.00E-5 cm	1.480 cm ± 5.00E-5 cm	1.765 cm ± 5.00E-5 cm	1.770 cm ± 5.00E-5 cm
L_c	0.264 ± 1.54E-5	0.276 ± 1.67E-5	0.288 ± 1.52E-5	0.287 ± 1.51E-5

In Figures 5.28 and 5.29, the measured weight changes in the air and in the fluid are plotted against time, as previously described. However unlike the previous cases there is significantly more deviation between the two measurements. This is an obvious implication that there is swelling going or a significant amount of fluid adhering to the surface of the sample. Additional analysis is required, and the error must be examined before any conclusions can be drawn.

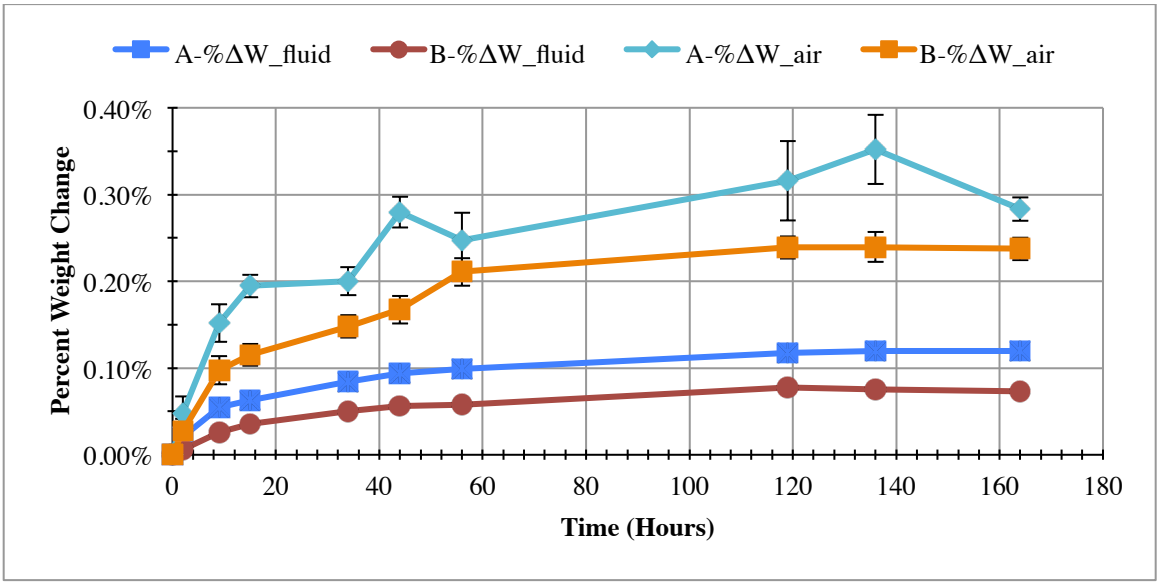

Figure 5.28: Utica experiment—Change in measured air and fluid weight of Utica shale samples A and B.

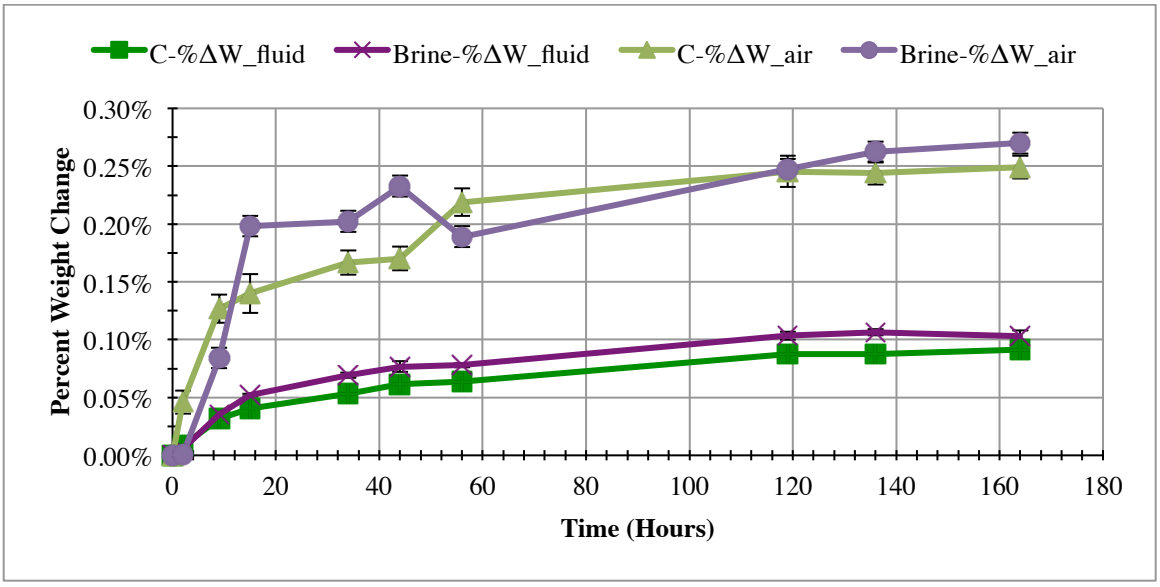

Figure 5.29: Utica experiment—Change in measured air and fluid weight of Utica shale samples C and Brine.

Table 5.12: Utica experiment—Estimated amounts and error of fluid adhering to surface of shale sample during air weight measurements.

Imbibition fluid	$\overline{W_{\text{surface fluid}}(t)}$	$\overline{\frac{W_{\text{surface fluid}}(t)}{W^{\text{intial}}_{\text{air}}}}$	$\overline{V_{\text{Surface fluid}}(t)}$	$\overline{\left(\frac{V_{\text{Surface fluid}}(t)}{V^{\text{intial}}_{\text{sample}}}\right)}$	**Thickness of Fluid Film**
A	0.1061 g ± 0.0143 g	0.55% ± 0.074%	0.0960 cc ± 0.0129 cc	1.305% ± 0.1756%	0.0439 mm ± 0.1869 mm
B	0.1019 g ± 0.0107 g	0.57% ± 0.060%	0.0921 cc ± 0.0097 cc	1.362% ± 0.1433%	0.0474 mm ± 0.0158 mm
C	0.1071 g ± 0.0122 g	0.48% ± 0.054%	0.0969 cc ± 0.0110 cc	1.137% ± 0.1294%	0.0403 mm ± 0.0145 mm
Brine	0.1089 g ± 0.0154 g	0.47% ± 0.066%	0.0984 cc ± 0.0139 cc	1.117% ± 0.1575%	0.0406 mm ± 0.0181 mm

The values of the estimated fluid on the surface of the shale sample are shown in Table 5.12. Despite having a similar surface area to the Bakken samples, the calculated value of the mass of the relative volume of thin film fluid adhering to the surface of the

Utica samples is significantly higher than either of the Bakken values, but the relative weight of this mass is equal to the relative mass of the adhering surface water in Bakken Experiment 1.

This relative value is what is most important, as the porosity value assumed for the Utica (5.0%) is roughly half of the value for porosity of the Bakken samples (10.07%). Porosity is directly related to the total volume of spontaneous imbibition, and consequently weight change in the sample. This higher value of relative weight, with a lower porosity is not ideal, as the total weight changes from spontaneous imbibition at its maximum is only roughly 60% of the weight of the fluid adhering to the surface of the sample during air weight measurements.

This increase in the weight of the adhered surface fluid is also observed in the error analysis shown in Figure 5.30. The error for every sample is greater 10% after only eight hours of exposure to the brine mixture. The Utica samples demonstrate greater error than the absolute maximum amount of error established in Experiment 1 and all approach a final value of approximately 30% of the pore volume. This error means any displacement of pore fluid calculated using the fluid mixture has an error of plus or minus 30% of the total pore volume. As this is on the order of the volume of displaced volume of pore fluid measured, this is not a quality data set. It is possible to use the air weight measurements to calculate the volume of displaced pore fluid, however it is impossible to determine any effect the volume of fluid adhered to the surface may be having upon the measurements.

The measured error in Figure 5.30 demonstrates time dependence, and appears to follow a logarithmic trend. This time dependent logarithmic trend likely implies the presence of swelling. Though this is impossible to determine conclusively as the time dependent increase in error could be due to an increase in the adhered surface fluid volume.

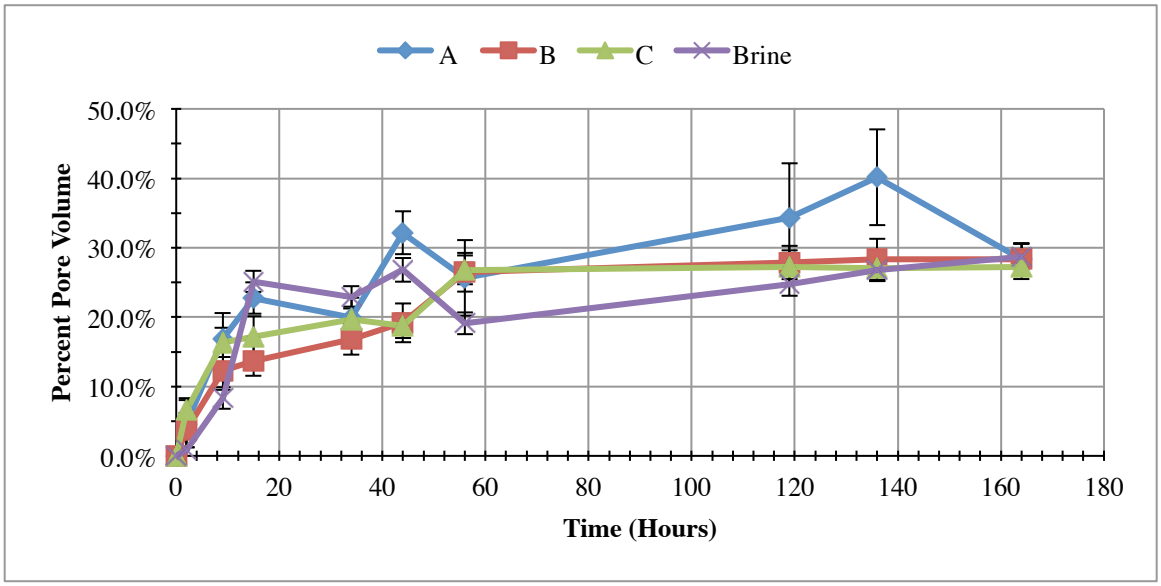

Figure 5.30: Utica experiment —Variance in displaced pore volume between air and fluid measurements due to variance in thickness of fluid film and/or swelling from Equation 5.20.

This trend of time-dependence of the change in the fluid weight measurements is further supported by Figure 5.31, as the calculated volume of displaced fluid follows the same logarithmic trend observed in the Figure 5.30. As a result, swelling is likely occurring in the samples and fluid measurements cannot be relied upon to accurately be representative of the mass gain in the sample resulting from spontaneous imbibition. Utica likely has a significant amount more clay, as shown in Chapter 2. These clays are

most likely causing the swelling. However Figure 5.31 cannot be used to make any meaningful conclusions about the rate, or volume of fluid imbibed by the sample as the amount of possible error due to swelling is on the order of the magnitude of the error, shown in Figure 5.30.

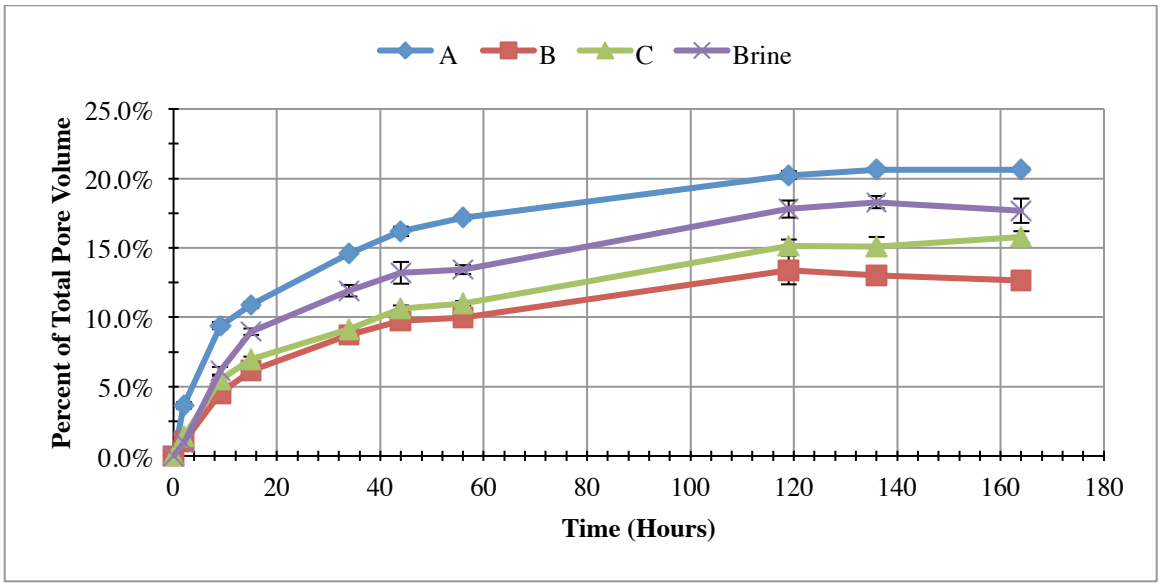

Figure 5.31: Percent displaced pore fluid of total pore fluid of Utica experiment shale samples calculated only from fluid weight measurements.

The conclusion that the fluid measurements are not a reliable data source of the change in weight in the sample doesn't imply that the air weight measurements are an accurate data source. The amount of error in the measurements used to calculate displaced volume of pore fluid shown in Figure 5.32 and Figure 5.33, is unknown. The apparent fluid displacement could be due to many other factors in addition imbibition, such as a time dependent increase in the volume adhered surface fluid to the samples.

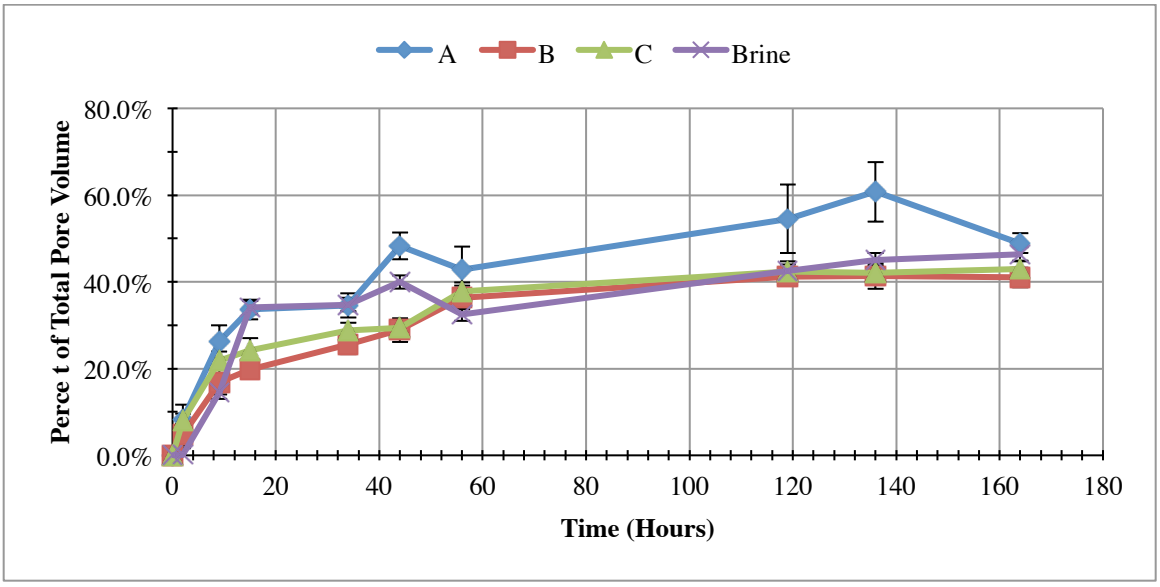

Figure 5.32: Percent displaced pore fluid of total pore fluid of Utica experiment shale samples calculated only from air weight measurements.

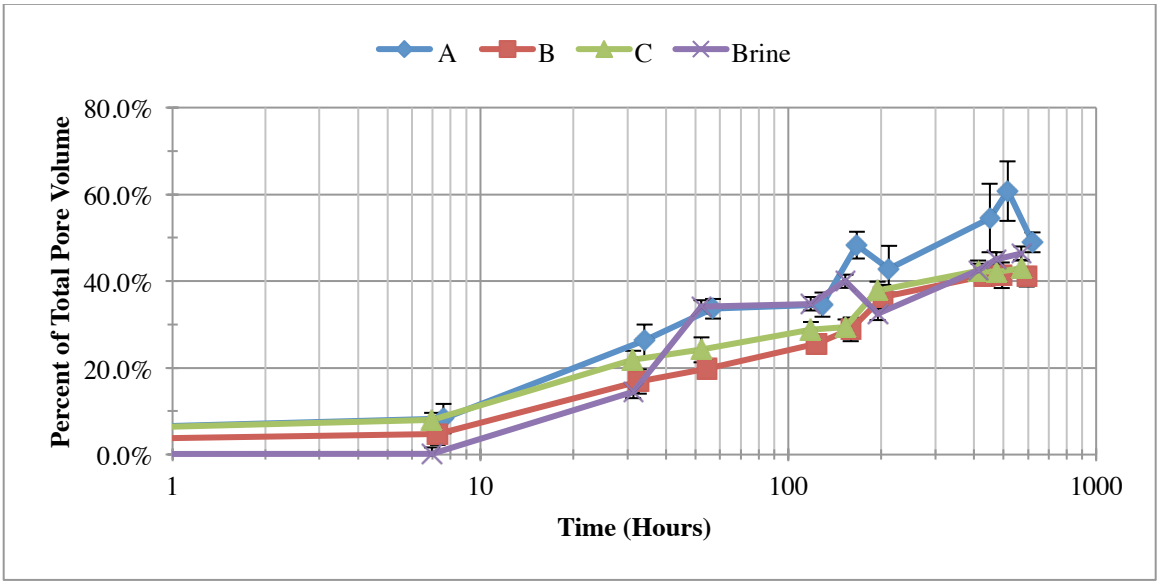

Figure 5.33: Percent displaced pore fluid of total pore fluid of Utica experiment shale samples calculated only from air weight measurements.

Due to the inability to quantify the error of the measurement, a conclusion cannot be made about the volume of displaced pore fluid. However, if the error in the measurement is indeed small and not affected by any external factors then all the samples behave similarly in the volume of imbibed fluid. The values are significantly higher than the Bakken samples, though this could be due to an error in the assumptions of the saturation fluid density or due to an incorrect value of porosity. Again as with the Bakken samples there is not a clear effect from the surfactants used. A more detailed comparison of the Bakken and Utica and over all results will be discussed in the concluding chapter, Chapter 6.

Chapter 6: Conclusions and Future Work

6.1 Conclusions

Measuring spontaneous imbibition through weight change is a well-documented experimental method and can successfully be applied to shale, though additional considerations must bed made as shale can swell depending upon the fluid contact. For this reason, measurements need to be made both in the air and in the fluid. Additional consideration must be made in the context of measuring imbibition in shale gravimetrically regarding the sample size and the relative volume of fluid adhered to the surface. To this end, it is important to determine both the amount of swelling that the shale undergoes because of fluid exposure as well as the fluid imbibed. Chenevert (2001) proposed a plot to examine the relative volume of fluid absorbed versus the amount of swelling. This same plot can repurposed for examining the relative amount of swelling versus imbibition occurring within shale measured through gravimetric experimental methods as purposed in this thesis.

The results of this experiment are shown in Figure 6.1. Chenevert (2001) first used this figure to examine the relative volumes of swelling and imbibition of samples. The experimental results are grouped together by both the shale type and sample size. Conclusions cannot be drawn about which samples or surfactants perform best overall or for each shale, as the plot is not independent of pore size or sample size. However, there is a clear trend of larger volumes of imbibition occurring than swelling when the volume

of fluid imbibed was equivalent to the volume of swelling. If this is the case, then all the data points would lie along the black line of slope equals one.

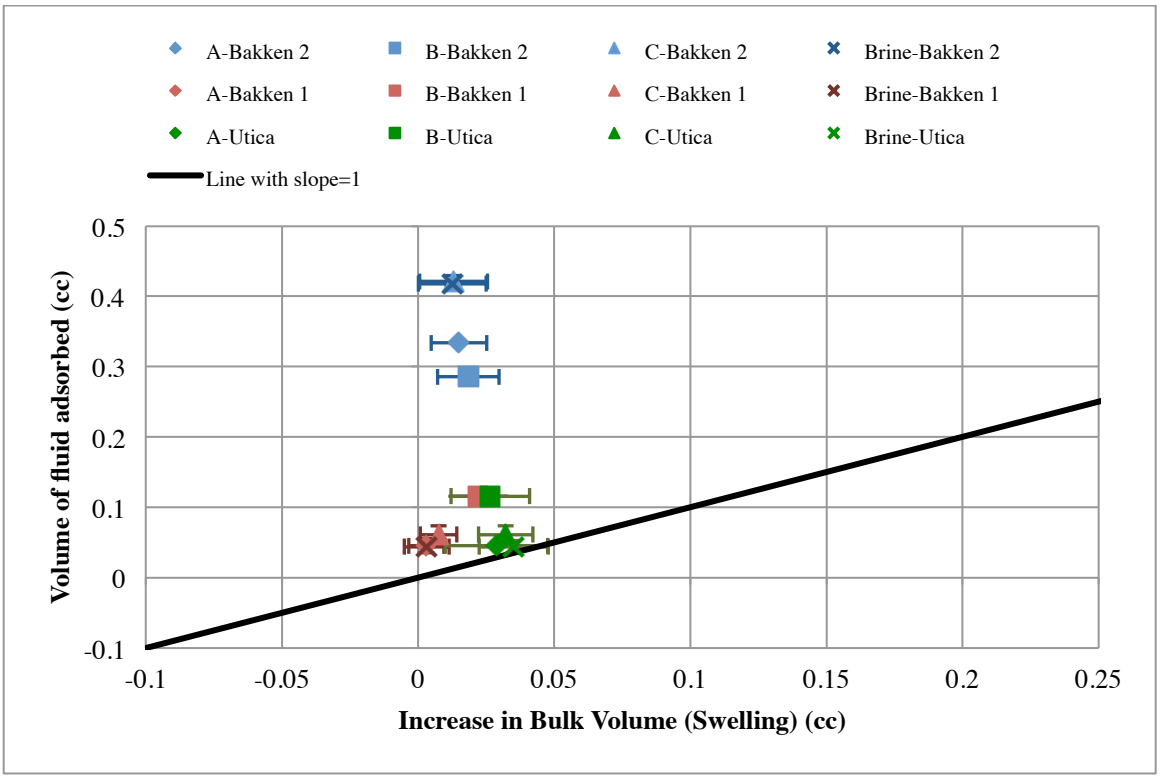

Figure 6.1: Volume of adsorbed fluid of samples versus Increase in Bulk Volume.

It is clear that this experimental method is a valid approach for measuring spontaneous imbibition in shale, as it has not only been proven in other rocks, but the addition of measuring the shale in and out of the fluid allows for a basic analysis of the relative amount of swelling. Additional experiments must be run in order to conclude that this experiment is the best method for measuring imbibition in shale.

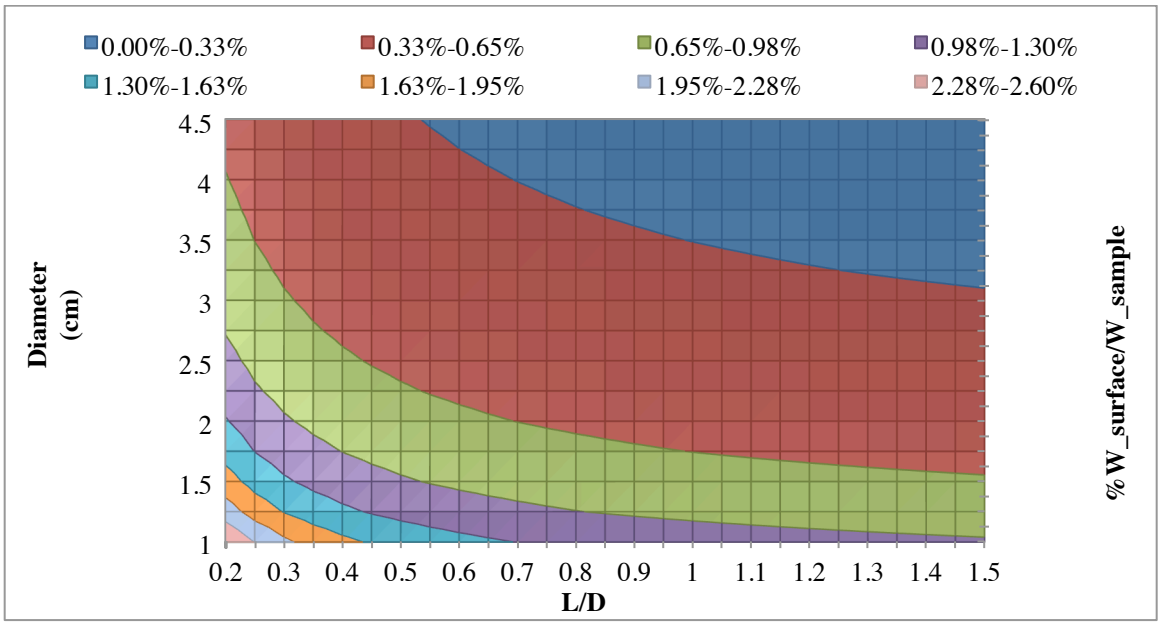

Figure 6.2: Contour plot of relative weight of 0.05 mm thin fluid layer of density 1.0 g/cc adhered to surface of cylindrical shale sample with a bulk density of 2.65 g/cc.

This experiment is very effective in comparing relative imbibition rates and the effect that various surfactants can have on different kinds of shale. The quality of the air measurements is highly dependent upon the relative volume and weight of the thin film of fluid relative to the total bulk volume. Figures 6.2 demonstrates this effect by illustrative the relative weight of a 0.05 mm fluid film as a function of sample size. The overall trend is that the larger the samples size the better. An ideal sample size must be established in order to best balance out the total volume amount of preserved shale used compared to the error caused in air measurements compared to the fluid film. Ideally the measured change in weight due to imbibition should be significantly more than the variation due to the fluid film on the surface of the sample on the order of a few percent. Though as sample size increases the time for imbibition to fully occur also increases as

well as the total difference in weight change as shown in figure 6.3. Additionally the thin film of fluid may be increase or decrease as a function of time due to the modification of the contact angle between the shale sample and the fluid, as stipulated by the studies involving dip coating have shown.

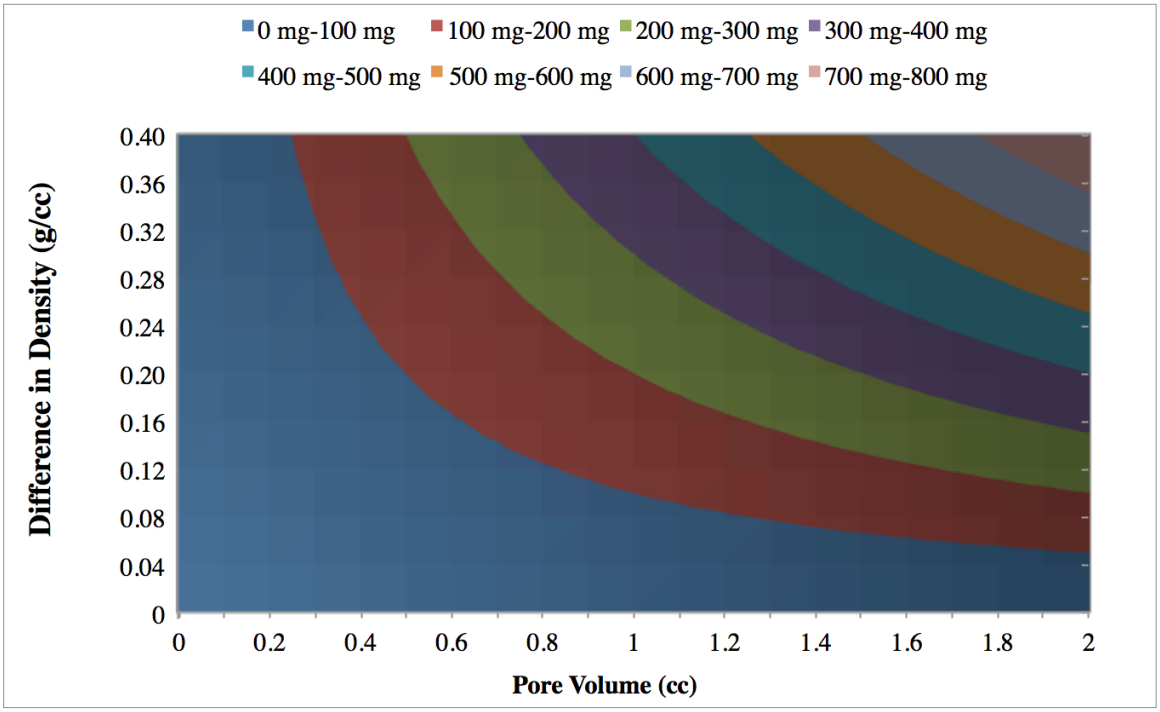

Figure 6.3: Change in measured weight of sample as a function of pore volume and difference between saturation fluid density and imbibition fluid density.

The Bakken had as much larger pore volume relative to the Utica, and as a result much more imbibition occurred. The rate of imbibition was also much slower in the Utica than the Bakken and did not demonstrate the classical two stage imbibition fronts. The first rate observed in the Bakken is dominated by spontaneous imbibition dominated by capillary pressure, which is a function of pore size. The first rate of imbibition dominated

by capillary pressure collapses when the imbibition front displacing the pore fluid reaches a no flow boundary or when it contacts another imbibition front. This was clearly observed in the Bakken and appeared to follow a trend proportional to a power of time as shown in the Chapter 5.

Permeability is a well-documented rate-limiting factor in spontaneous imbibition and this trend was demonstrated as well in this experimental study. The Utica according to the literature has a much lower permeability as well as a smaller median pore size. While the Bakken and Utica both have pores measuring as small 2 nanometers. The typical pore size of the Bakken is 20 nm with a range of 2 nm to 100 nm (Ramakrishna, 2010) while the Utica covers about the same range (2 – 200 nm) the median is only 5 nm (Bohacs, 2013). The Bakken is also considered to have a much higher permeability than the Utica depending upon the member of the Bakken being tested.

Capillary pressure is a function of pore size and pore throat radius, and increases as the pore size decreases. However the same effects documented at the micrometer level cannot be expected to continue at the nanometer scale. As the size of the pores decrease, the interaction of individual molecules has a larger effect. What happens at this scale is just beginning to be studies, however it has been shown that the rate of spontaneous imbibition of nanometer scale capillary tubes obeys a modified Washburn equation after with a factors to account for a dynamic contact angle and non zero fluid velocity at the wall of the tube known as slip flow (Supple, 2004; Dimitrov, 2007). The unmodified Washburn equation is shown in equation 6.1 where r is the radius of the capillary tube, L

is the length traveled by the fluid, gamma is the interfacial tension or surface tension, eta is the dynamic viscosity, and t is time.

$$L = \left(\frac{r\gamma}{2\eta} \right)^{1/2} \sqrt{t} \quad \text{..... (6.1)}$$

Though the behavior of a fluid in a capillary tube still follows this equation overall the phenomena in pores is not well documented in pores. Many authors including Dimitrov (2007), Stukan (2012) note that the contact angle at this scale becomes dynamic and is no longer a constant, which may complicate the interaction with surfactant. Dimitrov (2007) has shown through simulations that surfactants still work at the nanoscale, but further research is needed to experimentally prove how effective they are at modifying the contact angle at the nanometer scale.

Despite the concerns of what the behavior of surfactant will be in the nanopores in shale, it is important to determine if they have an effect. There was no discernable difference or measured increase in effectiveness with the use of the surfactant in the experiments preformed. However that is most likely due to the actual behavior of the surfactant and the fluid and rocks involved not properly being formulated.

Overall this experiment was effective in measuring the weight change of shale samples as they underwent spontaneous imbibition and is an effective test for measuring the rate of imbibition of an unconfined organic-rich shale sample in a very detailed range, while maintaining the ability to measure the relative amount of swelling to ensure that spontaneous imbibition is occurring rather than swelling in an unconfined sample.

6.2 FUTURE WORK

Further experiments need to be preformed in order to completely verify this experimental method. While it is clear that this method is a viable option for rock and shale samples that exhibit little to no fluid sensitivity, many shales are highly sensitive to fluids and do not have the cohesion required to satisfy the assumptions made in this experimental method. If the variations of the thin film of surface fluid can be further restrained through experimental procedure changes, the volume of swelling can be calculated with less error through using Archimedes method. This may be accomplished through the better selection of sample size and perhaps a modification of the sample shape. The effect of surfactants have upon this fluid film also needs to be considered.

Additional work still needs to be done to confirm the assumptions about the density of the saturation fluid, and the imbibition fluid. The initial saturation, porosity, mineralogy and permeability of the samples need to be fully quantified to allow for the true comparison of the rates of imbibition. The total amount of organic content is a good indicator of porosity, oil, and gas in shale and should be investigated in relation to the wettability of shale samples. Several methods such as x-ray computed tomography and nuclear magnetic resonance methods could be combined with this experiment to evaluate the relative penetration and displacement of the imbibition fluid. The effect reservoir temperatures and pressures have upon spontaneous imbibition should also be investigated.

A surfactant formulation study to evaluate what surfactant or mix of surfactants in combination can reduce the contact angle to very water wet levels while maintaining the interfacial tension must be done to further evaluate effect of surfactant in shale. Organic-rich shale creates presents a unique challenge as there are multiple pore structures within the sample most likely have unique contact angles. It is unlikely that organic pores have the same wettability as an intergranular pore.

Appendix

A.1 Measured Air and Fluid Weights

Table A.1: Bakken Experiment 1 Measured Data: Imbibition Fluids A and B.

Imbibition Fluid	**A**				**B**			
Time (hours)	$W_{air}(t)$ (g)	Error (±g)	$W_{fluid}(t)$ (g)	Error (±g)	$W_{air}(t)$ (g)	Error (±g)	$W_{fluid}(t)$ (g)	Error (±g)
0	9.1426	1.2014 E-03	5.0671	0.0000 E+00	9.0694	2.4007 E-03	5.0164	0.0000 E+00
2	9.1421	1.1240 E-03	5.0697	2.3094 E-04	9.0758	5.0521 E-03	5.0166	1.5275 E-04
4	9.1460	3.0006 E-03	5.0701	1.7321 E-04	9.0786	7.0378 E-03	5.0172	1.0000 E-04
16	9.1500	3.7634 E-03	5.0721	5.7735 E-05	9.0906	6.6010 E-03	5.0189	1.5275 E-04
37	9.1513	3.1321 E-03	5.0732	1.1547 E-04	9.0930	9.0738 E-04	5.0206	1.0000 E-04
68	9.1614	1.9630 E-03	5.0748	3.0551 E-04	9.0973	2.4583 E-03	5.0220	1.5275 E-04
100	9.1586	1.1000 E-03	5.0755	1.0000 E-04	9.0961	5.0292 E-03	5.0245	2.0000 E-04
144	9.1594	2.6652 E-03	5.0776	1.0000 E-04	9.0983	6.9217 E-03	5.0261	1.0000 E-04
165	9.1564	2.7514 E-03	5.0775	2.5166 E-04	9.1048	7.2342 E-04	5.0268	3.2146 E-04
Average (g)	**9.1532**	**2.4375 E-03**	**5.0738**	**1.6681E-04**	**9.0918**	**4.3414 E-03**	**5.0216**	**1.5996 E-04**
Standard Deviation (g)	**6.8938 E-03**	**9.5971 E-04**	**3.0649 E-03**	**8.7872E-05**	**9.9310E-03**	**2.6306 E-03**	**3.9468E-03**	**7.4283 E-05**

Table A.2: Bakken Experiment 1 Measured Data: Imbibition Fluids C and Brine.

Imbibition fluid	**C**				**Brine**			
Time (hours)	$W_{air}(t)$ (g)	Error (±g)	$W_{fluid}(t)$ (g)	Error (±g)	$W_{air}(t)$ (g)	Error (±g)	$W_{fluid}(t)$ (g)	Error (±g)
0	9.2302	2.4249 E-03	5.1261	2.6458 E-04	9.2748	2.5423 E-03	5.1553	1.7321 E-04
2	9.2326	1.1547 E-04	5.1318	5.7735 E-05	9.2836	3.7242 E-03	5.1646	4.5092 E-04
4	9.2356	4.9329 E-04	5.1328	3.0551 E-04	9.2779	7.2381 E-03	5.1656	7.0238 E-04
16	9.2434	4.6876 E-03	5.1355	2.5166 E-04	9.2876	5.0639 E-03	5.1678	4.9329 E-04
37	9.2440	2.8006 E-03	5.1358	2.0817 E-04	9.2814	1.4799 E-03	5.1675	2.8868 E-04
68	9.2433	7.5056 E-04	5.1357	1.0000 E-04	9.2944	3.7448 E-03	5.1674	1.1547 E-04
100	9.2445	2.8827 E-03	5.1364	2.5166 E-04	9.2923	5.8595 E-04	5.1669	6.1101 E-04
144	9.2465	3.2868 E-03	5.1363	1.0000 E-04	9.2890	4.6694 E-03	5.1664	5.2915 E-04
165	9.2489	3.0089 E-03	5.1362	5.2915 E-04	9.2882	4.7508 E-03	5.1651	6.6583 E-04
Average (g)	**9.1532**	**2.4000 E-03**	**5.0738**	**2.0000 E-04**	**9.0918**	**4.3000 E-03**	**5.0216**	**2.0000 E-04**
Standard Deviation (g)	**6.9000 E-03**	**1.0000 E-03**	**3.1000 E-03**	**1.0000 E-04**	**9.9000 E-03**	**2.6000 E-03**	**3.9000 E-03**	**1.0000 E-04**

Table A.3: Bakken Experiment 2 Measured Data: Imbibition Fluids A and B.

Imbibition Fluid	**A**				**B**			
Time (hours)	$W_{air}(t)$ (g)	Error (±g)	$W_{fluid}(t)$ (g)	Error (±g)	$W_{air}(t)$ (g)	Error (±g)	$W_{fluid}(t)$ (g)	Error (±g)
0.01	27.9961	2.3180 E-03	16.2696	0.0000 E+00	25.8228	2.4440 E-03	15.0109	3.6056 E-04
2	28.0304	1.0149 E-03	16.2999	2.8868 E-04	25.8441	4.5398 E-03	15.0255	1.1547 E-04
9	28.0766	1.7156 E-03	16.3410	3.0000 E-04	25.8863	1.2583 E-03	15.0634	2.6458 E-04
15	28.0826	4.1243 E-03	16.3448	1.5275 E-04	25.8969	3.5119 E-04	15.0697	2.0000 E-04
34	28.0788	1.5631 E-03	16.3458	3.5119 E-04	25.8952	1.3051 E-03	15.0709	2.5166 E-04
44	28.0846	6.9282 E-04	16.3464	3.4641 E-04	25.8990	1.3317 E-03	15.0715	4.6188 E-04
56	28.0869	5.7073 E-03	16.3462	1.5275 E-04	25.9030	1.6258 E-03	15.0705	1.7321 E-04
119	28.0908	7.5056 E-04	16.3474	0.0000 E+00	25.9014	1.6862 E-03	15.0707	1.5275 E-04
136	28.0911	2.7006 E-03	16.3484	2.0000 E-04	25.9035	1.6523 E-03	15.0721	7.8102 E-04
164	28.0918	1.7088 E-03	16.3487	2.0817 E-04	25.9046	9.2376 E-04	15.0722	1.0000 E-04
Average (g)	**28.0710**	**2.2296 E-03**	**16.3338**	**1.9999 E-04**	**25.8857**	**1.7118 E-03**	**15.0597**	**2.8611 E-04**
Standard Deviation (g)	**0.0319**	**1.5958 E-03**	**0.0269**	**1.2767 E-04**	**0.0285**	**1.1320 E-03**	**0.0223**	**2.0676 E-04**

Table A.4: Bakken Experiment 2 Measured Data: Imbibition Fluids C and Brine.

Imbibition Fluid	**C**				**Brine**			
Time (hours)	$W_{air}(t)$ (g)	Error (±g)	$W_{fluid}(t)$ (g)	Error (±g)	$W_{air}(t)$ (g)	Error (±g)	$W_{fluid}(t)$ (g)	Error (±g)
0.01	27.9604	2.0421 E-03	16.1938	4.0415 E-04	27.0101	7.3711 E-04	15.6299	2.6006 E-03
2	27.9867	1.5620 E-03	16.2252	2.0817 E-04	27.0352	3.7099 E-03	15.6603	1.2124 E-03
9	28.0434	3.3081 E-03	16.2791	4.1633 E-04	27.1004	2.9366 E-03	15.7184	6.1101 E-04
15	28.0611	2.0000 E-04	16.2880	2.0817 E-04	27.1105	6.4291 E-04	15.7258	2.3094 E-04
34	28.0650	3.2083 E-03	16.2938	1.5275 E-04	27.1183	1.0583 E-03	15.7294	2.3094 E-04
44	28.0652	1.3317 E-03	16.2946	1.0000 E-04	27.1172	3.8354 E-03	15.7311	5.1316 E-04
56	28.0755	2.1517 E-03	16.2945	1.7321 E-04	27.1281	2.0207 E-03	15.7310	1.0000 E-04
119	28.0764	1.3077 E-03	16.2981	5.5678 E-04	27.1218	3.3710 E-03	15.7350	7.8102 E-04
136	28.0763	3.6501 E-03	16.2990	3.0551 E-04	27.1203	2.0000 E-04	15.7359	1.5275 E-04
164	28.0811	8.0208 E-04	16.3001	8.9629 E-04	27.1298	2.9445 E-03	15.7357	1.6523 E-03
Average (g)	**28.0491**	**1.9564 E-03**	**16.2766**	**3.4213 E-04**	**27.0992**	**2.1456 E-03**	**15.7132**	**8.0852 E-04**
Standard Deviation (g)	**0.0417**	**1.1398 E-03**	**0.0367**	**2.4101 E-04**	**0.0416**	**1.3862 E-03**	**0.0370**	**8.0367 E-04**

Table A.5: Utica Experiment Measured Data: Imbibition Fluids A and B.

Imbibition Fluid	**A**				**B**			
Time (hours)	$W_{air}(t)$ (g)	Error (±g)	$W_{fluid}(t)$ (g)	Error (±g)	$W_{air}(t)$ (g)	Error (±g)	$W_{fluid}(t)$ (g)	Error (±g)
0.001	19.5161	2.4987 E-03	11.3003	0.0000 E+00	17.9522	2.2338 E-03	10.3880	0.0000 E+00
2	19.5255	2.8711 E-03	11.3044	2.6458 E-04	17.9571	1.3051 E-03	10.3891	1.1547 E-04
9	19.5457	3.4020 E-03	11.3109	2.8868 E-04	17.9696	1.8330 E-03	10.3927	1.1547 E-04
15	19.5540	4.5092 E-04	11.3125	2.0817 E-04	17.9727	2.5166 E-04	10.3944	5.7735 E-05
34	19.5550	1.8771 E-03	11.3167	7.2111 E-05	17.9786	5.7735 E-04	10.3970	1.5275 E-04
44	19.5705	2.4249 E-03	11.3185	3.6056 E-04	17.9821	1.8193 E-03	10.3981	5.7735 E-05
56	19.5643	5.5824 E-03	11.3196	1.7321 E-04	17.9899	1.7954 E-03	10.3983	1.0000 E-04
119	19.5775	8.5247 E-03	11.3231	3.0551 E-04	17.9949	4.0000 E-04	10.4019	1.0693 E-03
136	19.5845	7.3582 E-03	11.3235	1.0000 E-04	17.9950	2.0809 E-03	10.4015	3.7859 E-04
164	19.5712	8.1854 E-04	11.3235	1.5275 E-04	17.9946	6.4291 E-04	10.4011	1.5275 E-04
Average (g)	**19.5564**	**3.5808 E-03**	**11.3153**	**1.9255 E-04**	**17.9787**	**1.2939 E-03**	**10.3962**	**2.1998 E-04**
Standard Deviation (g)	**0.0222**	**2.7098 E-03**	**0.0081**	**1.1439 E-04**	**0.0157**	**7.5599 E-04**	**0.0050**	**3.1495 E-04**

Table A.6: Utica Experiment Measured Data: Imbibition Fluids C and Brine.

Imbibition Fluid	**C**				**Brine**			
Time (hours)	$W_{air}(t)$ (g)	Error (±g)	$W_{fluid}(t)$ (g)	Error (±g)	$W_{air}(t)$ (g)	Error (±g)	$W_{fluid}(t)$ (g)	Error (±g)
0.001	22.5810	2.2234 E-03	13.0744	1.5275 E-04	23.3242	2.0785 E-03	13.4862	2.5166 E-04
2	22.5914	4.7258 E-04	13.0763	2.0817 E-04	23.3243	2.9297 E-03	13.4875	3.0000 E-04
9	22.6095	1.5885 E-03	13.0816	3.4641 E-04	23.3438	1.1269 E-03	13.4945	3.0551 E-04
15	22.6125	3.0665 E-03	13.0835	1.7321 E-04	23.3703	1.8248 E-03	13.4983	1.5275 E-04
34	22.6186	8.5049 E-04	13.0864	2.5166 E-04	23.3712	5.3926 E-03	13.5023	5.1316 E-04
44	22.6193	6.6583 E-04	13.0883	2.0000 E-04	23.3783	5.5073 E-03	13.5041	1.0214 E-03
56	22.6303	1.5308 E-03	13.0888	1.5275 E-04	23.3681	1.1930 E-03	13.5044	3.5119 E-04
119	22.6363	2.0306 E-03	13.0942	5.6862 E-04	23.3817	3.8786 E-03	13.5103	7.9373 E-04
136	22.6360	4.1633 E-04	13.0941	8.5049 E-04	23.3851	3.2347 E-03	13.5110	5.5076 E-04
164	22.6371	2.8868 E-04	13.0950	5.2915 E-04	23.3869	5.1627 E-03	13.5101	1.1846 E-03
Average (g)	**22.6172**	**1.3134 E-03**	**13.0863**	**3.4332 E-04**	**23.3634**	**3.2329 E-03**	**13.5009**	**5.4248 E-04**
Standard Deviation (g)	**0.0193**	**9.2701 E-04**	**0.0073**	**2.3364 E-04**	**0.0239**	**1.6991 E-03**	**0.0091**	**3.4862 E-04**

Glossary

Arch W_air—calculated value of $W_{\text{air}}(t)$ using Archimedes principle from equation 1.

Bight—a slack portion of line between any two ends of a line.

Bulk volume—the total volume of a porous media, includes both the physical and void volume.

Clay—minerals or particles less than 5 microns.

Detrital—partials orginating from a preexisting rock, many grains in shales are detrital grains.

Devonian—sub period of geologic timescale ranging from 419.2 to 358.9 million years ago.

Effective pore volume—volume of interconnected pore space.

Fracing—see hydraulic fracturing.

Hydraulic fracturing—a well stimulation technique accomplished by the fracturing of a rock by a pressurized liquid.

Imbibition—the displacement of one fluid by another immiscible fluid.

Interfacial tension—see surface tension.

Overhand knot—a knot tied by creating a loop and push the working end through the loop with your thumb.

Mississipian —subperiod of geologic time scale spanning from 358.9 to 323. 2 million years ago.

Mudstone—a sedimentary rock classified as having grains smaller than 62.5 microns.

Mudrock—see mudstone.

Overhand loop—a overhand knot where a loop of line is used as the working end.

Pore space—the void volume of a porous media.

Pore volume—volume of pore space: see total pore volume and effective pore volume.

ρ_{fluid}—the density of the brine solution imbibing into the shale sample. Measured experimentally using balance and density kit as described in procedure chapter.

$\rho_{\text{pore fluid}}$—the density of the fluid saturating the pore space of the shale sample, shale sample is assumed to be completely oil saturated.

$\rho_{\text{sample}}^{\text{intial}}$—density of the preserved shale sample before exposure to the brine solution.

$\rho_{\text{sample}}(t)$—density of the shale sample at time t after exposure to the brine solution.

$\Delta\rho_{\text{sample}}(t)$—change in density of the shale sample at time t after exposure to the brine solution.

Standing end—the load-bearing portion between the overhand loop and the shale sample and in general the part of the line that is not active in the knot tying.

Surface tension—the bulk phenomena of liquids that is a result of the cohesive properties of the molecules that make up the fluid; often represented with the symbol γ.

Surfactant—a compound that is both hydrophobic and hydrophilic that lowers surface tension or interfacial tension.

Total pore volume—volume of the absolute pore space of a sample. Contains interconnected and separated pores.

Unconventional hydrocarbon resources

$V_{\text{pore fluid}}^{\text{displaced}}(t)$ —volume of saturating fluid, oil if sample completely oil saturated, displaced from sample due to spontaneous imbibition.

$V_{\text{Pore Total}}$ —the total void space volume or pore volume of a porous media sample includes void or pore space that is not interconnected, calculated using equation A.1.

$V_{\text{sample}}^{\text{initial}}$ —volume of the preserved shale sample before spontaneous imbibition occurs

$V_{\text{sample}}(t)$ —volume of the shale sample at time t after spontaneous imbibition begins.

$\Delta V_{\text{drops}}(t)$ —apparent increase in volume of sample during fluid measurements due to displacement of oil droplets adhered to surface of shale sample during fluid measurements. Equal to zero if discussing true volume of shale in air.

$\Delta V_{\text{swell}}(t)$ —change in volume of shale sample due to swelling from brine solution exposure.

$W_{\text{air}}^{\text{initial}}$ —the initial measured air weight of the preserved shale sample.

$W_{\text{air}}(t)$ —the measured air weight of the shale sample at time t.

$\Delta W_{\text{air}}(t)$ —the change in the measured air weight of the sample in air from time 0 to time t.

$W_{\text{fluid}}^{\text{initial}}$ —the initial measured weight of the preserved shale sample immersed in the imbibition fluid.

$W_{\text{fluid}}(t)$ —the measured weight of the shale sample immersed in the imbibition fluid at time t.

$\Delta W_{\text{fluid}}(t)$ — the change in the measured weight of the shale sample immersed in the imbibition fluid from time 0 to time t.

Working end—the part of the line that is active in the knot tying and is the excess portion of the knot that is trimmed in this project.

References

Agboada, D.K., Ahmadi, M. 2013. Production Decline and Numerical Simulation Model Analysis of the Eagle Ford Shale Oil Play. SPE Western Regional & AAPG Pacific Section Meeting, 2013 Joint Technical Conferenceheld in Monterey, California, USA, 19–25 April 2013.

Al-Bazali, T.M. 2005. Experimental study of the membrane behavior of shale during interaction with water-based muds. PhD dissertation, The University of Texas at Austin, Austin, Texas, USA.

Al-Bazali, T.M., J. Zhang, M.E. Chenevert, and M.M. Sharma. 2005. Measurement of the sealing capacity of shale caprocks. SPE 96100 presented at the SPE Annual Technical Conference and Exhibition held in Dallas, Texas, USA, 9 – 12 October, 2005.

Al-Menjeni, R., Arora, S., Cherukupalli, P. et al. 2011. Has the time come for EOR?. Oilfield Review, Winter 2010/2011: 22, no 4. http://www.slb.com/~/media/Files/resources/oilfield_review/ors10/win10/eor.pdf

Allix, P.; Burnham, A.; Fowler, T.; Herron, M.; Kleinberg, R., Symington, B. 2010, Coaxing oil from shale, Winter 2010/2011: 22, no. 4: p. 4-15.

Amott, E. Observations Relating to Wettability of Porous Rock. Trans., AIME (1959) 216, 156-162.

Anderson, W.G. 1986. Wettability Literature Survey-part I: Rock/oil/brine Interactions and the Effects of Core Handling on Wettability. Journal of Petroleum Technology, 38(1986a) pages1125-1144.

Anderson, W.G. 1986. Wettability Literature Survey-part II: Wettability Measurement. Journal of Petroleum Technology, 38, 1246-1262.

Austad, T. and Milter, J. 1997. Spontaneous Imbibition of Water Into Low Permeable Chalk at Different Wettabilities Using Surfactants. Paper SPE 37236 presented at the International Symposium for oilfield chemistry, Houston, Texas, 18-21 February 1997.

Bates, R. L. 1984. Dictionary of Geological Terms, third edition. New York: Anchor Books.

Barford, N. C., 1985. Experimental measurements: Precision, error, and truth. John Wiley and Sons, New York, 159 pp.

Birger, J. 2011. EOG'S BIG GAMBLE ON SHALE OIL. Fortune, 164(3), 94-100.

Bohacs, K. M., Grawbowski, G. J., Carroll, A. R., Mankeiwitz, P. J., Miskell-Gerhardt, K. J., Schwalbach, J. R., Wegner, M. B., Simo, J. A. 2005. Production, Destruction, and Dilution – the Many Paths to Source-Rock Development, SEPM Special Publication 82, p. 61-101.

Borysenko, A., Sedev, R., Ralston, J. *et al*. 2009. MONITORING OF FLUID SATURATION AND OIL-WATER DISPLACEMENT USING DIELECTRIC AND NMR MEASURMENTS. Conference Paper SPWLA-2009-33373 presented at 21-24 June 2009.Bourbiaux, B.J., Kalaydjian, F.J. 1990. Experimental study of co- current and countercurrent flows in natural porous media. Soc. Pet. Eng. Res. Eng. 5, 361–368.

Bourgoyne, A.T., Millheim, K.K., Chenevert, M.E., Young, F.S. 1986. Applied Drilling Engineering, Richardson, Texas: Society of Petroleum Engineers.

Boyer, C.; Kieschnick, J.; Suarez-Rivera, R.; Lewis, R., and G. Waters, 2006, Producing gas from its source, Oilfield Review, Autumn 2006, p. 36 – 49.

Bourrel, M. and Schechter, R.S., 1988, Microemulsions and Related Systems, Marcel Dekker, Inc., New York, NY, 1988.

Carman, P.S.,Lant, K.S. 2010. Making the Case for Shale Clay Stabilization. Paper SPE 139030 presented at the SPE Eastern Regional Meeting held in Morgantown, West Virginia, USA, 12–14 October 2010.

Chauvet, F., Geoffroy, S., Hamoumi, A. et al. 2012. Nanobubbles and gas dynamics during capillary filling of nanochannels. Presented at The 16th International Conference on Miniaturized Systems for Chemistry and Life Sciences. October 28 - November 1, 2012, Okinawa, Japan.

Chenevert, M.E. and Sharma, A.K. 1992. Permeability and Effective Pore Pressure of Shales. Paper SPE 21918 presented at the International Association of Drilling Contractors, Amsterdam, Netherlands, 11-14 March.

Chenevert, M.E. and Sharma, A.K. 1993. Permeability and Effective Pore Pressure of Shales. SPE Drill & Compl 8 (1): 28–34; Trans, AIME, 295. SPE-21918-PA.

Chenevert, M. 1970. Shale Alteration by Water Adsorption. Paper SPE 2401 presented at SPE Fourth Conference on Drilling and Rock Mechanics, Austin, Texas, 14-15 January 1969.

Chenevert, M.E., Amanullah, M. 2001. Shale Preservation and Testing Techniques for Borehole-Stability Studies. SPE Drill & Compl.16 (3): 146 – 149. SPE-73191-PA.

Clark, A.J. 2009. Determination of Recovery Factor in the Bakken Formation, Mountrail County, ND. SPE International Student Paper Contest at the SPE Annual Technical Conference and Exhibition held in New Orleans, Louisiana, USA, 4–7 October 2009. SPE-133719-MS.

Clarkson, C.R., Pederson, P. K. 2011. Production Analysis of Western Canadian Unconventional Light Oil Plays. CSUG/SPE 149005 presented at the Canadian Unconventional Resources Conference, Calgary, CA, 15-17 November, 2011.

Cil, M., Reis, J.C., Miller, Mark M.A., Misra, D. 1998. An Examination of Countercurrent Capillary Imbibition Recovery from Single Matrix Blocks and Recovery Predictions by Analytical Matrix/Fracture Transfer Functions. SPE 49005 Presented at SPE Annual Technical Conference and Exhibition, 27-30 September 1998, New Orleans, Louisiana

Cil, M., Reis, J. 1996. A multi-dimensional, analytical model for counter-current water imbibition into gas-saturated matrix blocks. Journal of Petroleum Science and Engineering, Volume 16, Issues 1–3, September 1996, Pages 61-69

Cuiec, L.E. 1991. Evaluation of Reservoir Wettability and Its Effects on Oil Recovery. Interfacial Phenomena in Oil Recovery, N.R. Morrow, ed., Marcel Dekker, Inc., New York City (1991), 319-375.

Cuiec, L.E., Bourbiaux, B. and Kalaydjian, F. 1994. Oil Recovery by Imbibition in Low-Permeability Chalk, SPE formation Evaluation, 9 1994: 200-208

Dechongkit, P., Prasad, M. 2011. Recovery Factor and Reserves Estimation in the Bakken Petroleum System (Analysis of the Antelope, Sanish and Parshall fields). Paper SPE- CSUG/SPE 149471-MS presented at Canadian Unconventional Resources Conference held in Calgary, Alberta, Canada, 15–17 November 2011.

Economides, M.J., Hill, A.D. and Ehlig-Economides, C. 1994. Petroleum Production Systems. Upper Saddle River, NJ: Prentice Hall.

Elgmati, M., Zhang, H., Bai, B., Flori, R., & Qu, Q. 2011. Submicron-pore characterization of shale gas plays. In North American Unconventional Gas Conference and Exhibition. June.

Elijah, O., Carl, S., Chandra, R. 2011. An NMR Study on Shale Wettability. Paper SPE 147371 presented at the Canadian Unconventional Resources Conference, Calgary, Alberta, Canada, 15–17 November.

Flores, 2011. Economics and Technology Drive Development of Unconventional Oil and Gas Reservoirs - Lessons learned in the United States

Gamero-Diaz, H., Miller, C. 2013. sCore: A Mineralogy Based Classification Scheme for Organic Mudstones. Paper SPE 166284 presented at SPE Annual Technical Conference and Exhibition held in New Orleans, Louisiana, USA, 30 September–2 October 2013.

Gaswirth, S.B., Marra, K.R., Cook, T.A, Charpentier, R.R., Gautier, D.L., Higley, D.K., Klett, T.R., Lewan, M.D., Lillis, P.G., Schenk, C.J., Tennyson, M.E., and Whidden, K.J., 2013, Assessment of undiscovered oil resources in the Bakken and Three Forks Formations, Williston Basin Province, Montana, North Dakota, and South Dakota, 2013: U.S. Geological Survey Fact Sheet 2013–3013, 4 p., http://pubs.usgs.gov/fs/2013/3013/.

Guidry, F. K., Luffel, D. L., Curtis, J. B. 1996. Development of Laboratory and Petrophysical Techniques for Evaluating Shale Reservoirs, Gas Research Institute. GRI-5/0496.

Ground Water Protection Council and ALL Consulting. 2009. Modern Shale Gas Development in the United States: A Primer, prepared for the U.S. Department of Energy, Office of Fossil Energy, and the National Energy Technology Laboratory.

Harper, J.A. 2011. Activity and Potential of the Utica Shale in Pennsylvania. Retrieved from http://www.dcnr.state.pa.us/cs/groups/public/documents/document/dcnr_008947.pdf

Hamon, G. and Vidal, J., 1986. Scaling-Up the Capillary Imbibition Process From Laboratory Experiments on Homogeneous and Heterogeneous Samples. Paper SPE 15852 presented at the SPE European Petroleum Conference, London, 20-22 October.

Hirasaki, G.J., Zhang, G.Q., and Huang, C.-C. 2000. Interpretation Of Wettability In Sandstones With Nmr Analysis. SPWLA-2000-v41n3a1. PetroPhysics, 41(3), (2000).

Hurlbut, C.S. 1988. Dana's Manual of Mineralogy. 4th edition New York: John Wiley & Sons, Inc.

Iffly, R., Rousselet, D.C. and Vermeulen, J.L., 1972. Fundamental Study of Imbibition in Fissured Oil Fields. Paper SPE 1072 presented at the SPE Annual Fall Meeting, San Antonio, Texas, 8-11 October 1972.

Jung, C.M., Zhou, J., Chenevert, M., Sharma, M., 2013. The Impact of Shale Preservation on the Petrophysical Properties of Organic-Rich Shales. Paper SPE 166419 presented at SPE Annual Technical Conference and Exhibition held in New Orleans, Louisiana, USA, 30 September–2 October 2013.

King, G.E. 2010. Thirty Years of Gas Shale Fracturing: What Have We Learned. Paper SPE 133456 presented at the SPE Annual Technical Conference and Exhibition, Florence, Italy, 19-22 September.

Kirschbaum, M.A., Schenk, C.J., Cook, T.A., Ryder, R.T., Charpentier, R.R., Klett, T.R., Gaswirth, S.B., Tennyson, M.E., and Whidden, K.J., 2012, Assessment of undiscovered oil and gas resources of the Ordovician Utica Shale of the Appalachian Basin Province, 2012: U.S. Geological Survey Fact Sheet 2012–3116, 6 p.

Krechetnikov, R., Homsy, G.M. 2005. Experimental study of substrate roughness and surfactant effects on the Landau-Levich law. Citation: Physics of Fluids 17, 102108.

Lakatos, I., Szabó, JL. 2009. Role of Conventional and Unconventional Hydrocarbons in the 21st Century: Comparison of Resources, Reserves, Recovery Factors and Technologies. EUROPEC/EAGE Conference and Exhibition, 8-11 June 2009, Amsterdam, The Netherlands.

Landau, L., Levich, B. 1942. Dragging of a liquid by a moving plate. Acta Physicochim. (USSR) 17, 42–54.

Loucks, R. 2011. Origin and Classification of Pores in Mudstones from Shale-Gas Systems. Proc., AAPG International Conference and Exhibition, Milan, Italy, 23-26 October.

Loucks, R.G., Reed, R.M., Ruppel, S.C., Hammes, U. 2012. Spectrum of pore types and networks in mudrocks and a descriptive classification for matrix-related mudrock pores. The American Association of Petroleum Geologists Bulletin, v. 96, no. 6 (June 2012), pp. 1071–1098.

Luffel, D. L., Guidry, F. K. and Curtis, J. B. 1992. Evaluation of Devonian shale with new core and log analysis methods. SPE 21297, Journal of Petroleum Technology, November 1992, pp. 1192-1197.

Ma, S., Zhang, X., and Morrow, N.R. 1999. Influence of Fluid Viscosity On Mass Transfer Between Rock Matrix And Fractures. PETSOC-99-07-02. Journal of Canadian Petroleum Technology, 38(7), (1999).

Macquaker, J and A. Adams, 2003, Maximizing information from fine-grained sedimentary rocks: an inclusive nomenclature for mudstones, Journal of Sedimentary Research, v. 73 (5): 753-744p.

Makhanov, K., Dehghanpour, H., and Kuru, E. 2012. An Experimental Study of Spontaneous Imbibition in Horn River Shales. Conference Paper SPE-162650-MS presented at SPE Canadian Unconventional Resources Conference, Calgary, Alberta, Canada, 30 October-1 November 2012.

Makhanov, K., Dehghanpour, H., and Kuru, E. 2012. An Experimental Study of Spontaneous Imbibition in Horn River Shales. Conference Paper SPE-162650-MS presented at SPE Canadian Unconventional Resources Conference, Calgary, Alberta, Canada, 30 October-1 November 2012.

Makhanov, K., Kuru, E., and Dehghanpour, H. 2013. Measuring Liquid Uptake of Organic Shales: A Workflow to Estimate Water Loss During Shut-in Periods. Conference Paper SPE-167157-MS presented at SPE Unconventional Resources Conference - Canada, Calgary, Alberta, Canada, November 05 - 07, 2013 2013.

Makhanov, K., Kuru, E., and Dehghanpour, H. 2013. Measuring Liquid Uptake of Organic Shales: A Workflow to Estimate Water Loss During Shut-in Periods. Conference Paper SPE-167157-MS presented at SPE Unconventional Resources Conference - Canada, Calgary, Alberta, Canada, November 05 - 07, 2013 2013.

Mohanty, K., & Kathel, P. 2013. EOR in Tight Oil Reservoirs through Wettability Alteration. In SPE Annual Technical Conference and Exhibition. September.

Morey, F. C. 1940. Thickness of a liquid film adhering to surface slowly withdrawn from the liquid. Natl Bur. Stan. J. Res, 25, 385-393.

Morsy, S., Sheng, J., and Soliman, M. 2013. Waterflooding in the Eagle Ford Shale Formation: Experimental and Simulation Study. Conference Paper SPE-167056-MS presented at 2013 SPE Unconventional Resources Conference & Exhibition - Asia Pacific, Brisbane, Australia, 11-13 Nov 2013.

Morsy, S., Sheng, J., and Soliman, M. 2013. Waterflooding in the Eagle Ford Shale Formation: Experimental and Simulation Study. Conference Paper SPE-167056-MS presented at 2013 SPE Unconventional Resources Conference & Exhibition - Asia Pacific, Brisbane, Australia, 11-13 Nov 2013.

Morsy, S., Sheng, J.J., and Ezewu, R.O. 2013. Potential of Waterflooding in Shale Formations. Conference Paper SPE-167510-MS presented at Nigeria Annual International Conference and Exhibition, Lagos, Nigeria, 30 July - 1 August 2013.

Morsy, S., Sheng, J.J., and Ezewu, R.O. 2013. Potential of Waterflooding in Shale Formations. Conference Paper SPE-167510-MS presented at Nigeria Annual International Conference and Exhibition, Lagos, Nigeria, 30 July - 1 August 2013.

Murphy, E. Warner, M. 2013. A Workflow to Evaluate Porosity, Mineralogy, and TOC in the Utica- Pleasant Shale Play. Paper SPE 165682 presented at SPE Eastern Regional Meeting held in Pittsburgh, Pennsylvania, USA, 20–22 August 2013.

Morrow, N.R. 1990. Wettability and Its Effect on Oil Recovery. J. Pet. Tech. (December 1990) 1476-1484.

Nes, O., Horsrud, P., Skjetne, T. 1993. Shale Porosities As Determined By NMR. Paper presented at 1993 SEG Annual Meeting, September 26 - 30, 1993 , Washington, DC.

Neuendorf, K, Mehl, P., Jackson, A. eds. 2005. Glossary of Geology (5th ed.). Alexandria, VA: American Geological Institute. ISBN 0-922152-76-4.

Nyahay, R. 2011, Vertical Utica Shale wells in Otsego and surrounding counties, New York State and its baseline water quality data, in Taking a deeper look at shales: Geology and potential of the Upper Ordovician Utica Shale in the Appalachian basin. Petroleum Technology Transfer Council, Ohio Geological Survey, and Ohio Geological Society, June 21, 2011, New Philadelphia, OH.

NPC. 2007a. UNCONVENTIONAL GAS In Facing the Hard Truths about Energy, TOPIC PAPER #29, 1-52. (2007a). Washington, DC (July, 2007).

OECD. 2013. World Energy Outlook 2013, OECD Publishing.

Passey, Q., Bohacs, K., Esch, W., Klimentidi, R., and Sinha, S. 2010. From Oil-Prone Source Rock to Gas-Producing Shale Reservoir - Geologic and Petrophysical Characterization of Unconventional Shale Gas Reservoirs. SPE 131350, 1-29.

Passey, Q. R.; Bohacs, K. M.; Esch, W. L., Klimentidis, R., and S. Sinha, 2012. My source rock is now my reservoir – Geologic and Petrophysical characterization of shale-gas reservoirs, search and discovery article. #80231, 47p.

Power, J. H., Morrison, W. L., Zeringue, J. 1991. Determining the mass, volume, density, and weight in water of small zooplankters. Marine Biology,110(2), 267-271.

Power, J. H. 1996. Errors associated with using Archimedes' principle to determine mass and volume of small aquatic organisms. Hydrobiologia, 335(2), 141-145.

Roychaudhuri B., Tsotsis T., Jessen K. 2011. An Experimental Investigation of Spontaneous Imbibition in Gas Shales, SPE Annual Technical Conference and Exhibition held in Denver, Colorado, USA, 30 October–2 November 2011

Ruppel, S. 2012. Shale Gas/Oil Systems. Oral presentation given at the University of Texas at Austin, Austin, TX, 4 December 2012.

Peters, E. J., Jessen F. W. 2009. Advanced Petrophysics. University of Texas At Austin.

Sarg, J. 2011. The Bakken - An Unconventional Petroleum and Reservoir System. doi:10.2172/1084030

Scriven, L. E. 1988. Physics and Applications of DIP Coating and Spin Coating. MRS Proceedings, 121, 717 doi:10.1557/PROC-121-717.

Sondergeld, C. H., Newsham, K. E., Comisky, J. T., Rice, M. C., and Rai, C. S. 2010. Petrophysical Considerations in Evaluating and Producing Shale Gas Resources. Paper SPE 131768 presented at SPE Unconventional Gas Conference, Pittsburgh, Pennsylvania 23-25, 2010.

Spears, R.W., D. Dudus, A. Foulds, Q. Passey, S. Sinha, and W.L. Esch, 2011, Shale gas core analysis: strategies for normalizing between laboratories and a clear need for standard materials: 52nd Annual SPWLA Logging Symposium Transactions, Paper A, 11 p.

Spears, R. W. and Jackson, S. L., 2009. Development of a predictive tool for estimating well performance in horizontal shale gas wells in the Barnett Shale, North Texas, USA. Petrophysics, Vol 58, no. 1, p.19-31.

Srodoń, J., Drits, V., McCarty, D.K., Hseih J.C.C.m Eberl, D.D., 2001. Quantitative X-Ray Diffraction Analysis of Clay-Bearing Rock From Random Preparations. Clays and Clay Minerals, Vol. 49, No. 6, 514-528, 2001.

Standnes D.C., Austad, T. 2006. Wettability Alteration in Chalk 2: Mechanism for Wettability Alteration from Oil-Wet to Water-wet using Surfactants, Journal of Petroleum Science and Engineering, 28(2000): 123-143.

Stephen A.H. 2013. Unconventional oil and gas resource development – Let's do it right, Journal of Unconventional Oil and Gas Resources, Volumes 1–2, June 2013, Pages 2-8, ISSN 2213-3976.

Stukan, M. R., Ligneul, P., & Boek, E. S. (2012). Molecular Dynamics Simulation of Spontaneous Imbibition in Nanopores and Recovery of Asphaltenic Crude Oils Using Surfactants for EOR Applications. Oil & Gas Science and Technology–Revue d'IFP Energies nouvelles, 67(5), 737-742.

Sulucarnain, I.D., Sondergeld, C.H., and Rai, C.S. 2012. An NMR Study of Shale Wettability and Effective Surface Relaxivity. Conference Paper SPE-162236-MS presented at SPE Canadian Unconventional Resources Conference, Calgary, Alberta, Canada, 30 October-1 November 2012.

Supple, S., & Quirke, N. 2004. Molecular dynamics of transient oil flows in nanopores I: Imbibition speeds for single wall carbon nanotubes. The Journal of chemical physics, 121, 8571.

Takahashi, S., and Kovscek, A.R. 2009. Spontaneous Countercurrent Imbibition and Forced Displacement Characteristics of Low-Permeability, Siliceous Shale Rocks. Conference Paper SPE-121354-MS presented at SPE Western Regional Meeting, San Jose, California, 24-26 March 2009.

Toumelin, E., Torres-Verdin, C., Sun, B. et al. 2004. A Numerical Assessment of Modern Borehole NMR Interpretation Techniques. Conference Paper 00090539 presented at SPE Annual Technical Conference and Exhibition, Houston, Texas, 26-29 September 2004.

Taylor, J. R. 1982. An Introduction to Error Analysis, Univ. Sci., Mill Valley, Calif.

US Energy Information Administration (EIA). 2013a. Annual Energy Outlook 2013, http://www.eia.gov/forecasts/aeo/er/ (accessed 1 November 2013)

US Energy Information Administration (EIA). 2013b. International Energy Outlook 2013, http://www.eia.gov/forecasts/aeo/er/ (accessed 1 November 2013)

van Olfen, H. 1953. Interlayer Forces in Bentonite. Proc., Second National Conference on Clays and Clay Minerals, Washington D.C., Vol. 327, 418-438.

Wang, D., Butler, R., Liu, H. et al. 2010. Flow Rate Behavior and Imbibition in Shale. Conference Paper SPE-138521-MS presented at SPE Eastern Regional Meeting, Morgantown, West Virginia, USA, 12-14 October 2010.

Wang, D., Butler, R., Liu, H. et al. 2011. Flow-Rate Behavior and Imbibition in Shale. SPE-138521-PA. SPE Reservoir Evaluation & Engineering, 14(4), pp. 485-492 (2011).

Wang, D., Butler, R., Zhang, J.Seright, R. 2012. Wettability Survey in Bakken Shale With Surfactant-Formulation Imbibition. December 2012 SPE Reservoir Evaluation & Engineering: 695-705

Wang, D., Zhang, J., and Butler, R. 2013. Optimal Salinity Study to Support Surfactant Imbibition into the Bakken Shale. Conference Paper SPE-167142-MS presented at SPE Unconventional Resources Conference - Canada, Calgary, Alberta, Canada, November 05 - 07, 2013 2013.

West, D., Harkrider, J., Besler, M., Barham, M., Mahrer, K., 2013. Optimized Production in the Bakken Shale: South Antelope Case Study. Paper SPE 167168 presented at Unconventional Resources Conference-Canada held in Calgary, Alberta, Canada, 5–7 November 2013.

Whitby, M., & Quirke, N. (2007). Fluid flow in carbon nanotubes and nanopipes. Nature Nanotechnology, 2(2), 87-94.

Winston, P.W., Bates, D.H. 1960. Saturated Solutions for the Control of Humidity in Biological Research. Ecology. 41: 232 – 237.

Wood T. and Milne B. 2011. Waterflood potential could unlock billions of barrels: Crescent Point Energy. http://www.investorvillage.com/uploads/44821/files/CPGdundee.pdf (accessed Oct 2013).

Yang, Y., and Aplin, A.C. 2009. A Permeability-porosity Relationship for Mudstones, Marine and Petroleum Geology, Marine and Petroleum Geology, 27(8), 1692-1697.

Zhang, J. 2005. The Impact of Shale Properties on Wellbore Stability. PhD dissertation, University of Texas at Austin, Austin, Texas (August 2005)

Zhang, J., Al-Bazali, T., Chenevert, M.E., Sharma, M.M. 2004. A New Gravimetri-Swelling Test for Evaluating Water and Ion Uptake in Shales. SPE 89831 presented at the SPE Annual Technical Conference and Exhibition held in Houston, Texas, USA, 26 – 29 September, 2004.

Zhang, J., Al-Bazali, T.M., Chenevert, M.E., Sharma, M.M., Clark, D.E., Benaissa, S., Ong, S. 2006. Compressive Strength and Acoustic Properties Changes in Shale with Exposure to Water-Based Fluids. ARMA/USRMS 06-900 paper presented at Golden Rocks 2006, the 41st U.S. Symposium on Rock Mechanics (USRMS): "50 Years of Rock Mechanics – Landmarks and Future Challenges.", held in Golden, Colorado, June 17 – 21, 2006.

Zhang, J., Clark, D., Al-Bazali, T., Chenevert, M.E., Sharma, M.M., Rojas, J.C., 2006. Laboratory Technique to Control Wellbore Stability. AADE-06-DF-HO-37 paper presented at AADE 2006 Fluids Conference held at the Wyndam Greenspoint Hotel in Houston, Texas, April 11-12, 2006

Zhang, X., Morrow, N.R., and Ma, S. 1996. Experimental Verification of a Modified Scaling Group for Spontaneous Imbibition. 00030762. SPE Reservoir Engineering, 11(4), 280-285 (1996). Mattax, C.C., Kyte, J.R. 1962. Imbibition Oil Recovery from Fractured, Water-Driven reservoirs, SPEJ, 2(1962): 177-184.

Zhou, D., L. Jia, J. Kamath, Kovscek, A. R. 2002. Scaling of Counter-Current Imbibition Processes in Low-Permeability Porous Media. „Journal of Petroleum Science and Engineering, 33(1-3), 61-74.

Zhou, J., Jung, C.M., Chenevert, M., Sharma, M.M. 2013. A Systematic Approach to Petrophysical Characterization of Organic- Rich Shales in Barnett and Eagle Ford Formations. Paper SPE 168792 / URTeC 1581323 presented at Unconventional Resources Technology Conference held in Denver, Colorado, USA, 12-14 August 2013.

Zhou, J., Jung, C.M., Chenevert, M., Pedlow, J.W., Sharma, M.M. 2013. A New Standardized Laboratory Protocol to Study the Interaction of Organic-Rich Shales with Drilling and Fracturing Fluids. Paper SPE 166216 preseneted at SPE Annual Technical Conference and Exhibition held in New Orleans, Louisiana, USA, 30 September–2 October 2013.

Zhou, X., Morrow, N.R. and Ma, S.M. 2000. Interrelationship of Wettability, Initial Water Saturation, Aging Time, and Oil Recovery by Spontaneous Imbibition and Waterflooding. SPE Journal, 5(2): 199-207

Zhou, Z., 1995. Construction and Application of Clay-Swelling Diagrams by Use of XRD methods. Journal of Petroleum Technology, Volume 47, Number 4 April 1995.

Zhou, Z. , Gunter, W.D., B. Kadatz, Cameron, S. 1997. Clay Swelling Diagrams: Their Applications in Formation Damage Control. SPE Journal Volume 2, Number 2 99-106.